THE UNIVERSITY OF CHICAGO

EVOLUTION OF NEURAL COMPUTATION IN COLOR VISION CIRCUITS

A DISSERTATION SUBMITTED TO
THE FACULTY OF THE DIVISION OF THE BIOLOGICAL SCIENCES
AND THE PRITZKER SCHOOL OF MEDICINE
IN CANDIDACY FOR THE DEGREE OF
DOCTOR OF PHILOSOPHY

COMMITTEE ON NEUROBIOLOGY

BY
NATHAN PAUL BUERKLE

CHICAGO, ILLINOIS
MARCH 2020

TABLE OF CONTENTS

LIST OF FIGURES

LIST OF TABLES

ACKNOWLEDGMENTS

I would first like to thank my advisor, Stephanie Palmer, whose support and guidance over the past six years has played an important role in my growth both as a scientist and as a person. Her unwavering enthusiasm for my projects and confidence in me was integral to my success.

I would also like to thank our close collaborator, Marcus Kronforst, whose support of me and my projects was equally important to completing my thesis. His curiosity and intelligence was enormously helpful in guiding my experiments and the way I think about science.

I owe a special thanks to Michiyo Kinoshita, who welcomed me into her lab for 3 months and was willing to train me in everything she knows about butterfly behavior and physiology. Without her training and mentoring, my experiments would have been immeasurably more difficult and frustrating.

I would also like to thank the members of the Palmer lab for creating a great environment and community for my years of thesis work. In particular, Joe Lombardo, Jared Salisbury, and Vaughn Spurrier were around for the majority of my Ph.D. and were always available for scientific discussions, puzzles, and breaks from work.

Finally, I would like to thank the rest of my committee including Dan Margoliash, Steve Shevell, and Melina Hale. Their time and support were invaluable for helping my projects progress.

ABSTRACT

The observable diversity in animal behaviors and perceptions evolves as adaptive responses to various ecological pressures. In order to evolve these diverse behavioral phenotypes, genetic mutations need to occur that alter the connectivity and activity of neural circuits that represent the proximate cause of behavior. My thesis work consisted of two complementary projects that examined how evolution shapes the functional connectivity of neural circuits related to color vision. For my first project, I conducted a series of experiments characterizing the organization of the eye in closely related *Heliconius* butterflies where males exhibit different mate preferences for females with either white or yellow wing patterns. Both wing color and mate preference are genetically simple traits, which allowed for a targeted examination of how natural genetic variation gives rise to different behaviors. Results revealed a surprising amount of diversity in eye organization across species and sex, with one feature in particular correlated with male mate preference. This feature was a signature of differences in photoreceptor synaptic connectivity, with evidence for inhibition of UV photoreceptors by long wavelength sensitive photoreceptors present in males that prefer yellow females but not in males that prefer white females. My second project used a theoretical, machine learning approach to simulate the evolution of tetrachromatic color vision from a trichromatic ancestor. The results of my simulations showed that the learning trajectories and specific computational mechanisms used for color vision in these circuits were predictable and depended on the specific network architecture of the original trichromatic network. Together, my results show how an evolutionary perspective and approach can lead to insights into how neural circuits are organized and function to produce adaptive behaviors.

CHAPTER 1

INTRODUCTION

1.1 Background

Animals exhibit a rich diversity of behaviors and perceptual capacities that can be both divergent among closely related species and convergent between distantly related species. These diverse behaviors evolve as an adaptive response to ecological pressures in order to survive and navigate complex natural environments. However, the evolutionary processes that give rise to behavioral variability do not occur in isolation and are not *de novo* searches for globally optimal solutions [1, 2]. Instead, factors such as phylogenetic history [3], development [4], and evolvability [5] have the capacity to constrain and bias evolutionary trajectories. Accounting for these constraints and studying the mechanistic basis of adaptation has been invaluable for better understanding evolutionary patterns in morphological traits [6], protein sequences [7], and gene regulatory networks [8]. Direct application of these concepts to behavior, in contrast, have been relatively limited (but see [9, 10, 11, 12, 13]). Because behavior is the product of a complex nervous system interacting with a dynamic environment, data broadly indicate that behavioral evolution is subject to especially strong constraints [14, 15, 16]. Investigating how these constraints influence evolution by studying the mechanisms underlying behavioral adaptation could yield a deeper understanding of how and why animals, including humans, behave the way they do.

The proximate cause of diverse animal behaviors is the functional output of neural circuits comprised of individual neurons acting in concert [17, 18]. Because modifying behavior requires modifying the output of these circuits, many have suggested that neural circuits and the computations they implement represent the biological substrate upon which natural selection directly acts [9, 15, 16]. However, the inherently complex and highly integrated organization of neural circuits potentially limits innovation and resists modification, making evolution of the brain and behavior conservative [14, 19, 20]. Circuits and cells can be multi-

functional, so adaptive changes to physiology in one context can easily be disruptive to other functions. Additionally, circuits must interface with both upstream and downstream processing areas. Even small changes to local circuit function could conceivably have large and deleterious effects on how large scale sensory-motor circuits function to generate observable behavior.

Constraints on circuit evolution do not necessarily strictly prohibit particular evolutionary trajectories, but rather bias evolution into more accessible and plastic pathways [4, 21]. Different brain regions and aspects of circuit organization can vary in the degree of evolutionary plasticity they exhibit [9, 22]. The gross anatomical organization of the brain appears to be rigidly constrained and varies little across deep phylogenetic relationships [23, 24], but notable counter-examples exist in the mushroom bodies and visual systems of insects [25, 26, 27]. Cell types and the genes regulating their development are also highly conserved, including homology of telencephalon neurons in birds and mammals [28] or Pax6 regulating eye development in insects and vertebrates [29]. Ciliary and rhabdomeric photoreceptors are also homologous between insects and vertebrates, but substantial functional differences highlight the need to examine these basic homologies at the level of circuits [30].

Other features of brain organization are more plastic and are regularly co-opted for adaptive evolution. Neuromodulatory systems are one system regularly implicated as targets for evolutionary change [14, 22]. Acting through G-protein coupled receptors, these systems are modular and diverse, which can allow for a large amount of flexibility. For example, swimming behavior in a closely related pair of nudibranchs use homologous motor circuits, but serotonin modulates the circuit in one species to produce a novel swim pattern [31]. Additionally, rather than directly altering the core synaptic connections across the brain, these systems can often act more subtly in ways such as varying the overall excitability of a circuit. A classical example of this situation is modulation of the ventral pallidum by differential expression of the vasopressin 1A receptor causing differences in reproductive behavior and pair bonding in mammals [32].

A second aspect of brain organization that appears to be disproportionately targeted for evolutionary change, and the focus of my thesis work, are peripheral sensory systems [22]. Examples of rapid peripheral evolution can be found across numerous taxa and sensory systems including chemosensation [33], audition [34], and vision [35]. Animal behaviors are triggered and regulated by environmental cues, so modifications to the response properties of the receptors directly interacting with the environment provides a direct way for animals to adapt to diverse habitats. Peripheral sensory systems also benefit from being relatively independent, modular, and feed forward [9]. These aspects of peripheral sensory systems allows for behavior to evolve without requiring changes to complex circuits and can minimize deleterious, pleiotropic effects. However, because these changes are relatively simple, evolution of sensory reception can only influence behavior to a potentially limited degree. Shifts in sensory reception adapt animals to the statistics of the natural environment, including co-evolution of signal-receiver dynamics for conspecific communication [36]. Radical shifts in a behavioral repertoire, in contrast, would likely require changing how sensory information is processed in complex circuits, although exceptions do exist [37, 38, 39].

Understanding how the brain and behavior evolves and functions requires an integrated approach linking different levels of nervous system analysis [9]. First, the goal of the nervous system is to produce adaptive behaviors that allow an animal to successfully interact with its natural environment. Clear and complete descriptions of these behavioral repertoires and how they vary between species is a necessary component of understanding how the nervous system might function to implement the observable behavior. Behavioral evolution also necessarily includes a genetic component, as genetic mutation is the core mechanism responsible for generating phenotypic diversity. Interactions between genes, development, and circuits are particularly important as a major source of phylogenetic constraint. These complementary top-down and bottom-up approaches to understanding the neural basis and evolution of behavior converge on and are linked by the functional organization of neural circuits.

My thesis work consists of two projects exploring how neural circuits related to color vision evolve. In particular, both projects are related to understanding how differences in the sensory periphery might contribute to the evolution of behavior and perception. The first project takes a bottom-up approach examining how genetic variability affects the functional organization of the eye in *Heliconius* butterflies that have different mate choice preferences based on wing color. The second project uses a top-down, theoretical approach to neural circuit evolution, focusing on how phylogenetic history might constrain neural computation associated with trichromatic and tetrachromatic color vision. Common to both of these projects is that changes in the visual periphery are associated with behavioral evolution. However, both projects also find that relatively simple shifts in spectral sensitivity are insufficient, and behavioral evolution requires more substantial changes to neural computation.

1.2 Genetic basis of behavior

Most, if not all, animal behaviors have a genetic component that describes some amount of variability between species or individuals within a population [40, 41]. As genetic methods have become increasingly sophisticated and affordable, mapping behaviors to specific regions ranging from entire chromosomes to single mutations has also become increasingly common. Studies in model organisms such as rodents, *Drosophila*, and humans broadly confirm intuitions that the genetic architecture responsible for behavioral variation is complex [22]. Most behaviors are associated with numerous epistatic genetic loci with exponentially distributed effect sizes. Although progress is being made, the complexity of these multi-gene behaviors, in general, limits the ability to link genes and behavior at the level of neural circuits.

A growing number of studies, including the experimental portion of my thesis, have identified behaviors with simpler and tractable genetic origins. Typically these studies involve pairs of sister taxa exhibiting different behaviors such as pair bonding in mammals [32] or burrowing in *Peromyscus* mice [42, 43]. Despite the fundamentally different behavioral phenotypes in species pairs, these complex sensory-motor behaviors can often be described by

a surprisingly small number of genetic loci that each have large effect sizes. Identification of the specific genes located within these loci can further lead to functional studies examining how patterns of gene expression affect the behavior of interest. Genetic methods that allow for experimenters to manipulate when and where candidate genes are expressed are a powerful way to better understand the genetic and molecular basis for behavior.

Further analysis of how this genetic variability directly changes neural circuit function and computation is often difficult or impossible to achieve. Behaviors such as pair bonding involve complex sensory-motor transformations that engage circuits potentially spanning the entire brain. Studying the effect of the vasopressin 1A receptor on local circuits in the ventral pallidum is relatively straightforward [32], but this brain region is just one node in a larger circuit. Understanding how this localized change in activity propagates to downstream targets that are not fully described is then an enormous task. However, assessing how specific evolutionary changes integrate into the functional organization of an entire neural circuits is an important aspect for understanding behavioral evolution. These insights could reveal broader evolutionary patterns that describe why particular genes or brain regions are targeted for modification.

My thesis work on male mate preference in *Heliconius* butterflies overcomes many of the challenges that can prevent in-depth, circuit focused studies on behavioral evolution. Assortative mating in these butterflies is a vision dominated behavior that appears to have a genetically simple origin. In particular, males preferentially court females with conspecific wing patterns, meaning that evolutionary changes are likely confined to circuits strictly involved in visual processing. My experiments characterizing the organization of the eye in butterflies with different mate preferences identified a potential difference in the synaptic connections of photoreceptors that may explain mate choice preferences. Importantly, the courtship circuit of insects is thought to be genetically specified by a specific transcription factor, making the entire sensory-motor circuit tractable. This courtship circuit has already allowed for several studies into courtship differences between species of *Drosophila* and can

facilitate future investigations into how the circuit differences I uncovered integrate into the full circuit.

1.3 Comparative physiology

Complementary to mapping the genetic basis of behavior are comparative studies examining circuit function in species with varying degrees of shared phylogenetic history and behavioral similarities. This comparative approach provides snapshots into the diversity of neural systems structure and function [3], which can give insights into how rigidly constrained or plastic neural systems are. One important result using these methods has been the realization that cell types [44, 45], gross morphology [23, 24], and genes regulating development [46, 47] share deep homologies that can span taxa as distantly related as insects and vertebrates. This conservation broadly supports notions about brain evolution being slow, conservative, and constrained. However, conserved features of the nervous system can have vastly different functions across taxa [30]. Functional comparisons of these identified homologous features can subsequently be mapped onto phylogenetic trees that can lead to inferences about when and where major evolutionary events may have occurred [3].

Parallel to studies examining how homologous circuits diverge in function are comparisons of the circuits underlying convergent behaviors in relatively unrelated taxa. These studies are important because they lend insights into the extent to which neural circuits can find alternative solutions to similar computational problems. Interestingly, circuits that perform similar tasks often share similar organizational schemes and implement similar computations, such as the olfactory and visual systems of vertebrates and insects [48, 49, 50]. These structures are not necessarily homologous, but instead represent convergent mechanisms for convergent behaviors. A clear example of homologous computation in non-homologous brain regions comes from distantly related *Gymnotiform* and *Mormyrid* fish that independently evolved electro-sensation. The circuit computations associated with this novel sensory system appear to be highly similar between these two groups, but the specific anatomical regions

of the brain are distinct [51]. An open question that emerges from these observations is why circuits often converge on similar organizations. One possibility is that circuits may be plastic and flexible enough to find and implement computations that are optimal solutions for a behavior. Alternatively, matching the deep homologies of cell types and gene networks, basic principles guiding circuit structure and function may have emerged in the earliest stages of nervous system evolution that constrain and bias nervous system structure and function.

Examining the potential conflict between optimality and constraint in neural computation would benefit from a system that is relatively simple, tractable, and well-studied. For the second project in my thesis, I have identified color perception as such a system. Motivated by the diversity in photoreceptor spectral tuning across butterflies, I used a machine learning approach to simulate the evolution of tetrachromatic vision from trichromatic ancestors. Although the neural implementation of color computations may be complex in a real biological system, the theoretical basis for color vision is well-described and relatively simple, and my neural networks broadly conformed to these theoretical expectations. Evolution of the network 'eye' had minimal negative effects on color vision, but also was insufficient to improve color vision. Allowing the circuits to evolve led to improved color vision that followed predictable learning trajectories that were constrained by the specific parameters of the original trichromatic network. Overall, the results from this theoretical study suggest that considering the phylogenetic history of an animal is important for understanding how its neural circuits are designed to produce observable behavior.

CHAPTER 2

EVOLUTION OF DIVERGENT MATE CHOICE PREFERENCES IN *HELICONIUS CYDNO* BUTTERFLIES

2.1 Abstract

Heliconius butterflies mate assortatively, with males across this species rich genus preferentially courting females with conspecific wing patterns. In the cydno clade of *Heliconius* butterflies, white vs. yellow wing color is a Mendelian trait that correlates with male mate preferences. Males that are homozygous at the wing color locus preferentially court females of the same color, while heterozygotes show no color preference. The candidate mate choice gene, sens2, is differentially expressed in the eyes of white and yellow males, suggesting the hypothesis that differences in eye organization contribute to differences in male courtship preferences. Here, I conducted a series of experiments using electrophysiology, eyeshine, and antibody staining to characterize the functional organization of the *Heliconius cydno* eye. Eye organization was surprisingly variable across species and sex, with one feature correlated with male mate preference. This feature suggests that males preferring yellow females have UV photoreceptors that receive synaptic inhibition from green sensitive photoreceptors. The effect on unknown, downstream circuits is unclear, but differences in synaptic connectivity between photoreceptors has the potential to have large, non-linear effects on male perception and behavior.

2.2 Introduction

2.2.1 Background

Heliconius butterflies are a diverse group of neotropical species that have been an influential model in the study of ecology, evolution, and behavior since the time of Darwin [52, 53]. A relatively recent adaptive radiation of this genus has led to 42 identified species, but the true diversity lies in the numerous subspecies and more than 400 described color patterns [54]. A major ecological factor driving the evolution of this diversity is predator avoidance, as these colorful wing patterns serve as conspicuous and honest warning signals that these chemically defended animals are unpalatable. Distantly related pairs of sympatric species often converge on similar phenotypes that can co-vary across wide geographic ranges [55, 56, 57]. Potential avian predators learn to avoid the locally abundant morphs, which results in strong purifying selection against hybrid or novel phenotypes [58, 59].

Wing patterns that diverge between closely related species and converge between distantly related co-mimetic species has made *Heliconius* a valuable model system for studying the genetic and molecular basis for phenotypic evolution [55, 60]. Paired with genus-wide diversity in wing pattern, this combination of convergence and divergence allows for comparative studies that can potentially uncover larger evolutionary patterns linking genotype to phenotype [61]. Additionally, much of the diversity can be attributed to a small number of unlinked Mendelian loci [62, 63, 64, 65, 66] that further allows for in-depth studies on how variability in specific genes results in different wing patterns. Genetic mapping of a few of these Mendelian loci has revealed that the same genes and even the same regulatory regions are often used repeatedly to generate similar phenotypes, such as the role of optix in making red wings and WntA in melanic patterning [67, 68, 69, 70].

In addition to a role in aposematic signaling, diverse wing patterns also function as an important pre-mating reproductive barrier [71]. Many sympatric species are interfertile, but hybridization rates are estimated to be very low in natural settings [72, 73, 74]. Although the

courtship ritual itself is an elaborate and multimodal behavior with many potential factors contributing to pre-mating reproductive isolation [75, 76], visual perception of color patterns is the dominant cue mediating preference [63, 71, 77]. In particular, males preferentially approach and court females with conspecific wing patterns compared to the wing patterns of hybrids or closely related species [57, 63, 73, 74, 78, 79]. Further, male preference for conspecific wing patterns has a genetic basis that is often genetically linked to the Mendelian loci controlling wing pattern [57, 63, 80, 81]. Together, the association between wing color and mate preference has the potential to play a significant role in reproductive isolation and speciation [60, 71].

The correlation between wing pattern and mate choice behavior makes *Heliconius* butterflies an excellent model system for studying the evolution of neural computation. Genetic linkage between wing and behavioral phenotypes suggests this complex behavioral decision is also controlled by a limited number of genetic loci. Genetic mapping of male mate preference has confirmed this expectation for two pairs of species, including the butterflies examined here (Fig. 2.1) [63, 81]. Thus, consistent with other studies into the genetic basis of natural, species-specific behaviors (see chapter 1 for details), limited amounts of genetic variability can lead to radically different behaviors. Because both the mate choice behavior and the underlying genetics appear to be relatively straightforward and tractable, this system has the potential for detailed examinations of how genetic and behavioral variability converge at the level of neural circuits.

Behavioral details such as the sequence of the courtship ritual and female choice are undoubtedly important and interesting aspects of the mating behavior, but they also are not directly related to male preference [71]. Instead, the behavior of interest is specifically about perception and preference for specific wing patterns, which suggests that behaviorally relevant circuit differences will be confined to brain areas involved in visual processing. Identification and localization of the specific genes responsible for behavioral differences can further narrow and guide the search for where neural circuits change. The behaviorally

relevant stimulus is also well-defined, as wings can be easily parameterized into patterns and reflectance spectra. Thus, visual stimuli can be precisely controlled and tailored to better understand how neural circuits process natural stimuli.

Finally, data from other insects, primarily but not exclusively *Drosophila*, suggests that the entire sensory-motor courtship circuit of a male insect is genetically specified by the transcription factor fruitless [82, 83]. If this is also true for butterflies, access to this clearly defined circuit would allow for a complete and detailed study of butterfly courtship. Overlap of candidate mate choice genes and fruitless would allow for highly targeted investigations of neurons likely involved in wing pattern perception and preference. Importantly, it would also allow for future studies aimed at understanding how differences at one node in a circuit propagate throughout the system to influence behavioral output. This capacity to gain a broader view of the circuit could lead to insights into evolutionary patterns about why particular parts of a circuit are modified compared to others. Overall, courtship in *Heliconius* overcomes many of the barriers preventing detailed circuit analysis of other systems that have clear links between genes and behavior, which can potentially lead to greater insights into how the neural circuits directly responsible for behavior evolve.

2.2.2 Study system

This study focuses on male courtship preferences in a small group of closely related butterflies in the cydno clade of *Heliconius* that are distinguished by a forewing color band that appears to humans as either white or yellow (Fig. 2.1). *Heliconius cydno galanthus* and *H. pachinus* are parapatric species from opposite coasts of Costa Rica that are monomorphic for white and yellow wings, respectively [63]. A second cydno subspecies, *H.c. alithea*, is found in Ecuador and is polymorphic with individuals that are either white or yellow [57]. Like many *Heliconius* color patterns, wing color in these butterflies is inherited as a Mendelian trait with white dominant to yellow. A recent genome wide association study (GWAS) identified single nucleotide polymorphisms (SNPs) in the regulatory regions of the gene aristaless1 that

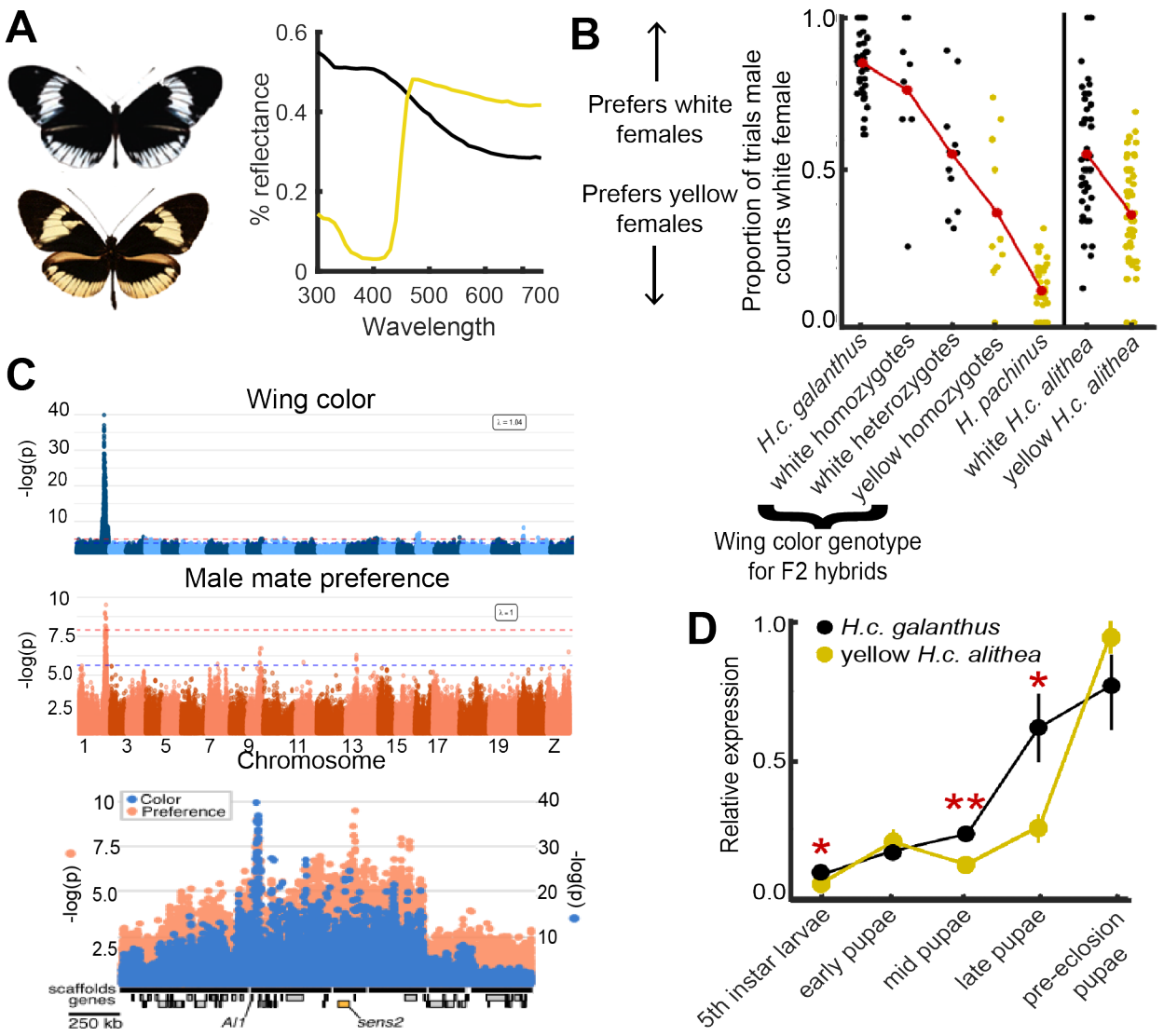

Figure 2.1: Study system
A) Color patterns and wing reflectance of butterflies used in this study.
B) Males were repeatedly given the choice to court either a white or yellow female over the course of days. Data shows the proportion of trials a male chose the white female. For *H.c. galanthus* and *H. pachinus*, wing color genotype predicts male preference. For *H.c. alithea*, yellow males preferentially court yellow females, while white males show no preference.
C) A GWAS was used to identify SNPs associated with either wing color (top) or mate preference (middle). The bottom panel shows a zoomed in overlay of the color and preference SNPs. Note different scales on y-axis. Single peaks of significantly associated SNPs 200 kb apart are consistent with genetically linked Mendelian traits.
D) qPCR for the candidate mate choice gene, sens2, in whole heads of developing butterflies shows differential expression in late pupal stages.
All data in this figure was provided to me by Nick VanKuren and Marcus Kronforst.

were perfectly associated with color. CRISPR knockouts of aristaless1 have confirmed its role in white and yellow patterning [84].

This Mendelian wing color phenotype correlates with male courtship preferences. When given a choice to court either a white or yellow female, white *H.c. galanthus* and yellow *H. pachinus* males preferentially court females of the same color (Fig. 2.1) [63, 85]. Controlled breeding experiments generating hybrids between these two species allowed for an examination of the genetics underlying this preference [63]. First generation hybrids (F1 hybrids) have an *H.c. galanthus* allele and an *H. pachinus* allele for the entire genome. In contrast to the parent species, F1 males have no color preference and instead court white and yellow females with equal frequency. Because of genetic recombination, each genetic locus for second generation hybrids (F2 hybrids) is independently either homozygous for the *H.c. galanthus* allele, homozygous for the *H. pachinus* allele, or heterozygous. F2 males exhibited a wide range of female color preferences, and these preferences can largely be explained by the genotype at the wing color locus (Fig. 2.1). Males homozygous for the white allele prefer white females, males homozygous for the yellow allele prefer yellow females, and white heterozygotes have no preference.

Similar behavioral experiments in the polymorphic *H.c. alithea* allowed for fine scale genetic mapping of preference and the identification of a candidate gene (Fig. 2.1). Matching *H. pachinus* behavior, yellow *H.c. alithea* males that are homozygous for the yellow allele preferentially court yellow females [57]. White males with unknown wing color genotypes, in contrast, have no color preference on average. Genetic mapping of *H.c. alithea* preference using a GWAS identified SNPs approximately 200 kb from the wing color locus that were significantly associated with preference for white or yellow females (Fig. 2.1). These SNPs explain nearly 20% of the variability in male mate preference and are in linkage disequilibrium with the wing color locus. The candidate mate choice gene that emerged from the GWAS is a transcription factor called senseless2 (sens2), with the significant SNPs located in regulatory regions rather than the coding sequence. Although little is known about the cellular and

molecular function of sens2, its paralog senseless is known to be involved in the development of all peripheral sensory structures [86, 87, 88].

Differential expression of sens2 in developing white and yellow butterflies further supported a role of this gene in male courtship preference. qPCR was first used to measure the relative expression levels of sens2 mRNA in whole heads of butterflies across several developmental times (Fig. 2.1D). During early pupal development, sens2 was expressed at low levels in both white and yellow butterflies. Expression remained low for yellow butterflies in the late pupal stages of development, but white butterflies showed a significant increase in sens2 expression. Around the time of eclosion, yellow butterflies then increase expression to match white butterflies. This differential expression could reflect delayed expression in the same brain regions of yellow butterflies compared to white. Alternatively, differential expression could be specific to one brain region, with the later, equal expression localized to a different brain region with functions unrelated to courtship preference.

To localize the source of sens2 expression, butterfly eyes and brains were stained with antibodies specific to sens2 at two time points. Early in development, sens2 expression is found in the R9 photoreceptors of both white and yellow butterflies (data not shown). Matching qPCR, there was no evidence for differential expression at this early stage of development in these photoreceptors that are potentially non-functional in adults (see below for details). For newly eclosed butterflies, however, only white *H.c. galanthus* males and all females showed strong sens2 expression in the eye (Fig. 2.2). Yellow *H.c. alithea* males, in contrast, had either limited or no sens2 expression (Fig. 2.2). This expression appeared spatially homogeneous and only in the proximal 2/3 of the eye. Precise identification of which cell types expressed sens2 was not possible, but the staining pattern did point towards expression in the R3-R8 photoreceptors that express a long wavelength sensitive opsin (see below for details). Because qPCR showed equal expression in white and yellow butterflies at the time of eclosion, additional expression in the central brain is also likely. Results from ongoing staining experiments are inconclusive at this time, but data from a single study in

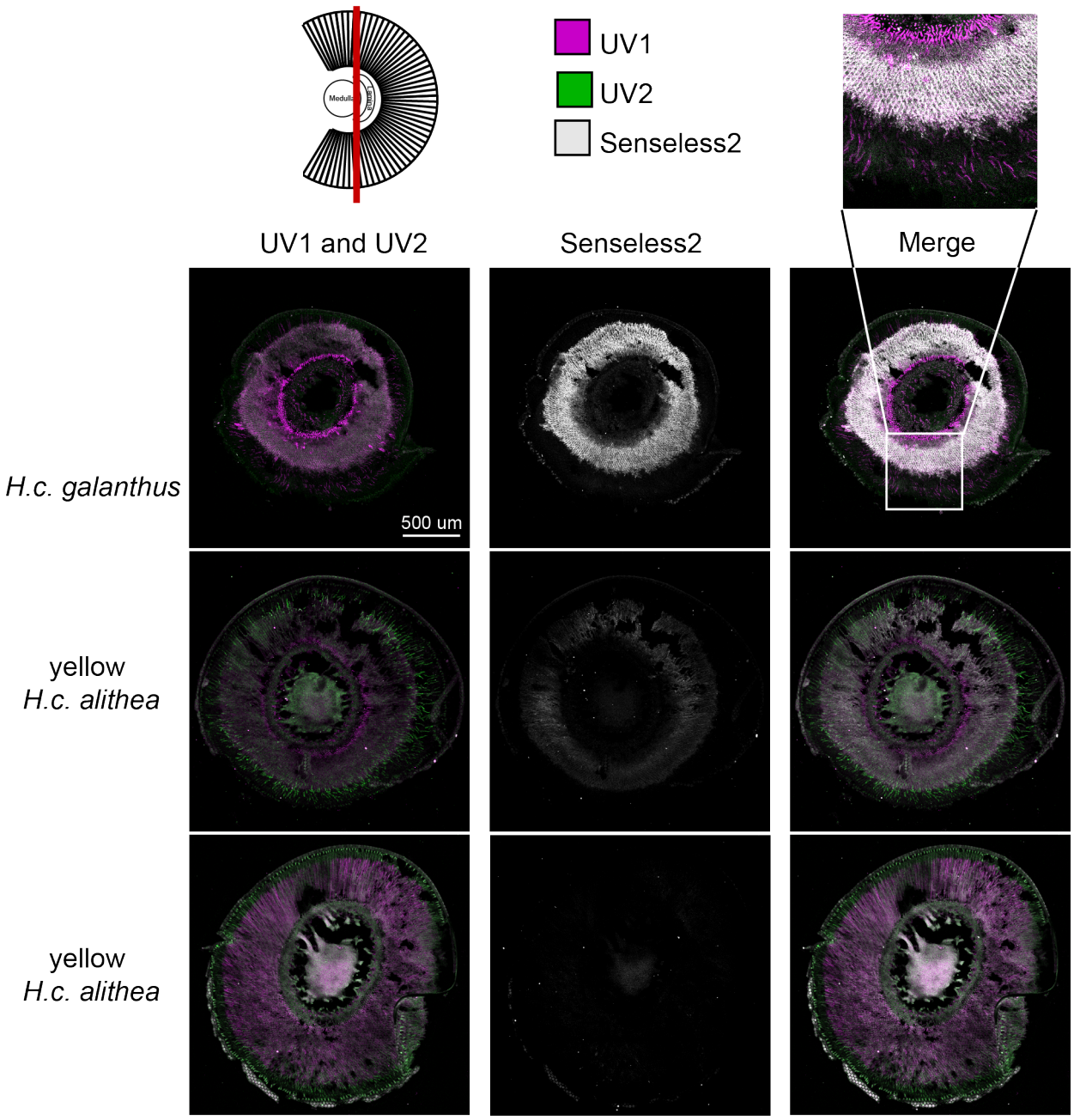

Figure 2.2: Antibody staining for senseless2
Thin sections of 3 hour old butterfly eyes were stained with antibodies specific to UV1, UV2, and senseless2. The eye diagram at the top left shows the approximate location of the slices shown, meaning the unstained center of the images are part of the optic lobes, and the radial staining pattern is a longitudinal view of photoreceptors. The top row is representative of all *H.c. galanthus* examined. Staining for sens2 in yellow *H.c. alithea* males could be either weak (middle) or absent (bottom). Sens2 staining only extends over the proximal 2/3 of the eye.

Drosophila suggests that expression might be found in the mushroom bodies [89].

Differential expression of the candidate mate choice gene, sens2, in the eyes of developing white and yellow *Heliconius* butterflies suggested the hypothesis that differences in the functional organization of the eye can explain differences in male mate preferences. Sens2 could affect eye physiology in numerous ways including changes in opsin expression, changes in the spatial distribution of photoreceptor types, or changes in the downstream synaptic connections. To test this hypothesis, I conducted a series of experiments examining both the spectral sensitivity of single photoreceptors and the distribution of these photoreceptor types across the eye. Considering that this group of species have generally similar ecological niches and behaviors outside of courtship preference, my experiments revealed a surprising amount of variability in eye organization. One feature of eye organization suggestive of changes in synaptic connectivity was correlated with mate preference and was also consistent with sens2 expression in long wavelength sensitive photoreceptors. Overall, these results are consistent with ideas about the periphery being an evolutionarily labile part of the nervous system that can rapidly evolve. Before describing these experiments, I begin with an overview of the general anatomy and physiology of the butterfly eye.

2.2.3 Butterfly eye anatomy

Butterflies have compound eyes that are broadly similar to the ancestral insect eye, but several evolutionary modifications have led to improved color vision in these diurnal, highly visual animals [90]. Compound eyes are comprised of optically isolated unit eyes called ommatidia that contain multiple photoreceptors and sample light from a restricted region of visual space (Fig. 2.3). Spatial resolution varies between species and between different regions of the eye but is typically $1 - 2^{\circ}$ for butterflies [91, 92]. With 12-15,000 ommatidia per eye, *Heliconius* have the largest eyes relative to body size of any butterfly studied and are also one of the few that do not vary between sexes [93].

In an ommatidium, incident light is focused into the light sensing rhabdom by a pair of

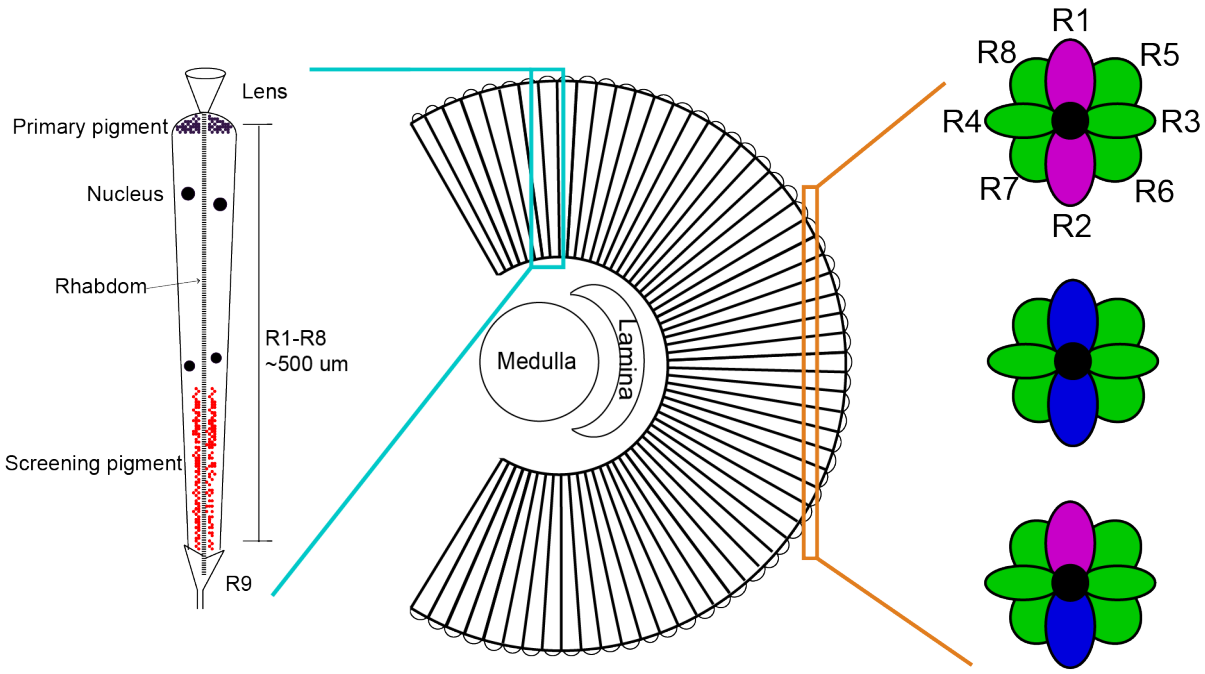

Figure 2.3: Anatomy of the eye
Butterfly eyes are composed of 1000s of unit eyes called ommatidia. The left shows a longitudinal view of an ommatidium and the right shows a cross section. There are 9 photoreceptors, with R9 being small and located at the most proximal part of the eye. In every ommatidium, the R3-R8 cells express the long wavelength sensitive opsin. The R1 and R2 cells express either a UV opsin or a blue opsin, which generates three distinct types of ommatidia.

lenses biologically analogous to a Keplerian telescope [94]. Photoreceptors express rhodopsin in microvilli called rhabdomeres, and for butterflies and other insects with apposition eyes, the rhabdom is formed through the fusion of rhabdomeres from every photoreceptor [95]. The rhabdom is approximately 500 μm long and 1-2 μm in diameter, and the behavior of light in it is well described using waveguide optics [96]. Light that is not absorbed in the rhabdom reaches the basement membrane where tracheae have been modified into a reflective tapetum that reflects light back through the eye [97]. The tapetum likely evolved to increase sensitivity in nocturnal moths and has been retained in most butterfly lineages.

Butterfly ommatidia have 9 photoreceptors that vary both in spectral sensitivity and their projections into the optic lobes [90]. In response to light, photoreceptors depolarize through a G protein coupled transduction cascade and release histamine as an inhibitory

neurotransmitter [98, 99]. The R3-R8 photoreceptors are homologous to the *Drosophila* R1-R6 photoreceptors and typically express a long wavelength sensitive opsin [100]. Although these photoreceptors extend the full length of the eye for *Heliconius*, the contribution to the distal part of the rhabdom can be minimal [101, 102]. This functional tiering is what suggests that sens2 is expressed is these photoreceptors. Axons extend into the lamina, which is the first optic neuropil and the start of motion processing. In most insects, lamina projections typically maintain a strict retinotopic organization, but in the butterfly *Papilio xuthus*, photoreceptors often extend axons into the projection areas of neighboring ommatidia [103, 104].

The R1 and R2 photoreceptors express short wavelength sensitive opsins that define three ommatidial types (Fig. 2.3)[90]. These two photoreceptors are a duplicated, homologous pair of the *Drosophila* R7 photoreceptor [100]. In the ancestral butterfly eye, expression of a UV or blue sensitive opsin is determined in a stochastic, cell-autonomous way [105]. This cell-fate process leads to three types of ommatidia (UV-UV, blue-blue, and UV-blue) that are heterogeneously distributed across the eye in a fixed proportion, although dorsal and ventral patterning can differ [106, 107]. In most insects, axons from this pair of photoreceptors bypass the lamina and project directly to the medulla, which is the second optic neuropil [108, 109]. However, electron microscopy in the butterfly *P. xuthus* has shown that synaptic connections with the R3-R8 photoreceptors are also found in the lamina [103, 104].

The R9 photoreceptor is small, occupies the most proximal part of the rhabdom, and is potentially non-functional [90]. It is homologous to the *Drosophila* R8 photoreceptor and also projects directly to the medulla. In *Drosophila*, opsin expression in this cell is dictated by the cell-autonomous decision of the R7 cell. Thus, the duplication of the R7 photoreceptor into the R1 and R2 photoreceptors is thought to be a developmental path to increasing the number of ommatidial types from 2 to 3 rather than a way to increase the number of functional photoreceptors [105].

The ancestral butterfly eye had only UV, blue, and green sensitive photoreceptors, but

a combination of screening pigments and gene duplications has led to a huge diversity in spectral tuning. Colored screening pigments that are expressed in photoreceptors near the rhabdom act as spectral filters (Fig. 2.3) [110, 111, 112, 113, 114]. By selectively absorbing some wavelengths of light, these screening pigments can shift and narrow the spectral sensitivity of a photoreceptor. Red screening pigments that absorb short wavelength light are commonly observed and typically function to convert a green sensitive photoreceptor into a red photoreceptor [106, 113, 115]. Despite expressing the same opsin, green and red photoreceptors are perceptually unique for most butterflies studied, including *Heliconius* [115, 116]. Several species have multiple screening pigments and between 8 and 15 unique photoreceptor types, but *Heliconius* appear to have only red and yellow pigments [117, 118, 119, 120, 121].

The second mechanism butterflies use to expand the number of photoreceptor types is duplication of the opsin coding genes [90, 122]. Duplication of the blue and green opsins have been observed in multiple butterfly lineages, and the derived opsin can shift in either the long or short wavelength direction. These duplications often have a relatively clear relationship to species specific behaviors such as courtship. For example, *Lycaenid* butterflies have a duplicated blue opsin sensitive to longer wavelengths than the ancestral blue, and this group often has wings with blue color patterns [123]. *Pierid* butterflies also have a duplicated blue gene, but the sensitivity of this novel opsin is shifted towards violet, and these butterflies typically have wings with UV color patterns [124].

The one known example of a UV gene duplication in butterflies occurred at the base of *Heliconius* [125]. UV1 is UV sensitive and its spectral sensitivity broadly matches the ancestral UV opsin, while the derived UV2 opsin has a sensitivity shifted towards violet [126]. Expression patterns of UV1 and UV2 vary across the genus and are often sexually dimorphic [127]. The evolution of UV2 has been hypothesized to function in discriminating two types of yellow [128]. Yellow wings in most butterflies have an unknown molecular composition, and the spectral reflectance has the appearance of a ramp function, with a slow and smooth increase in reflectance for longer wavelengths. *Heliconius*, in contrast,

have evolved 3-hydroxy-dl-kynurenine (3-OHK) as a genus specific yellow pigment. The reflectance spectrum of 3-OHK has the appearance of a step function, with a sharp transition from low to high reflectance around 450 nm. Although direct experimental evidence is lacking, a perceptual model has shown that UV2 is better at discriminating these two yellows than UV1 [128]. If true, in an environment where mimicry is common, improved ability to discriminate *Heliconius* yellow from non-*Heliconius* yellow would be advantageous.

2.3 Results

Experiments characterizing the functional organization of the *Heliconius* eye were conducted on 7 groups of butterflies separated on the basis of species, sex, and wing color. Six groups of males included: 1) white *H.c. alithea*, 2) yellow *H.c. alithea*, 3) white *H.c. galanthus*, 4) yellow *H. pachinus*, 5) F1 hybrids bred from crosses between *H.c. galanthus* and *H. pachinus*, and 6) red *H. melpomene* as a closely related outgroup. Corresponding groups of females were initially planned, but results showed that female eyes were similar regardless of species and were thus grouped together. Throughout the text, references to particular species are specific to males, and females are referred to as a distinct homogeneous group.

In order to interpret results in the context of male mate preference, it is first important to understand the differences between white and yellow wings beyond a binary classification based on human perception (Fig. 2.1A). White wing patterns are a structural color with a relatively flat reflectance spectrum between 300 and 700 nm. As described above, yellow is derived from 3-OHK and has a relatively sharp transition from low to high reflectance around 450 nm. For long wavelengths, yellow wings do have slightly stronger reflectance, but the shape of the reflectance differs little, suggesting this minor intensity difference may not be important for perception and preference. Thus, to a first approximation, white and yellow wings differ primarily in the presence and absence of short wavelength reflectance, respectively. Nothing is known about how the central brain processes visual information, but explaining mate preference needs to account for these differences in wing spectral reflectance.

	UV	Blue	Green	Red	Total
white *H.c. alithea*	43	21	27	2	87
yellow *H.c. alithea*	40	30	25	2	91
H.c. galanthus	12	22	22	5	61
F1 hybrids	19	21	7	0	47
H. pachinus	8	5	11	1	25
H. melpomene	25	15	29	14	83
females	22	12	28	9	71
Total	169	126	149	24	468

Table 2.1: Electrophysiology cell counts
Photoreceptors were recorded from 7 groups of butterflies. I identified four types of photoreceptors with distinct spectral sensitivities. Each line shows the number of each cell type recorded from each group.

2.3.1 Photoreceptor types

Butterflies have 4 spectrally distinct types of photoreceptors

To characterize the functional organization of the eye, I first measured the spectral sensitivity of single photoreceptors using intacellular electrophysiology. Voltage responses to monochromatic stimuli were transformed into a spectral tuning curve using the Naka-Rushton equation, which is standard for the field (see methods for details)[129]. These spectral tuning curves were then fit with a standard rhodopsin template that has the wavelength of peak sensitivity (λ_{Max}) as the single fit parameter [130, 131]. Across the seven groups of butterflies, I recorded from a total of 468 photoreceptors (Table 2.1) that could broadly be classified as UV sensitive (<400 nm), blue sensitive (400-500 nm), or long wavelength (LW) sensitive (>500 nm).

Although the *Heliconius* genome encodes only a single LW opsin gene [115], photoreceptor recordings revealed two distinct types of LW sensitive photoreceptor types defined as green and red, following previously published conventions (Fig. 2.4). For green photoreceptors, $\lambda_{Max} = 548.6 \pm 9.8$ nm, and this significantly different between species or sex (Fig. 2.4B,

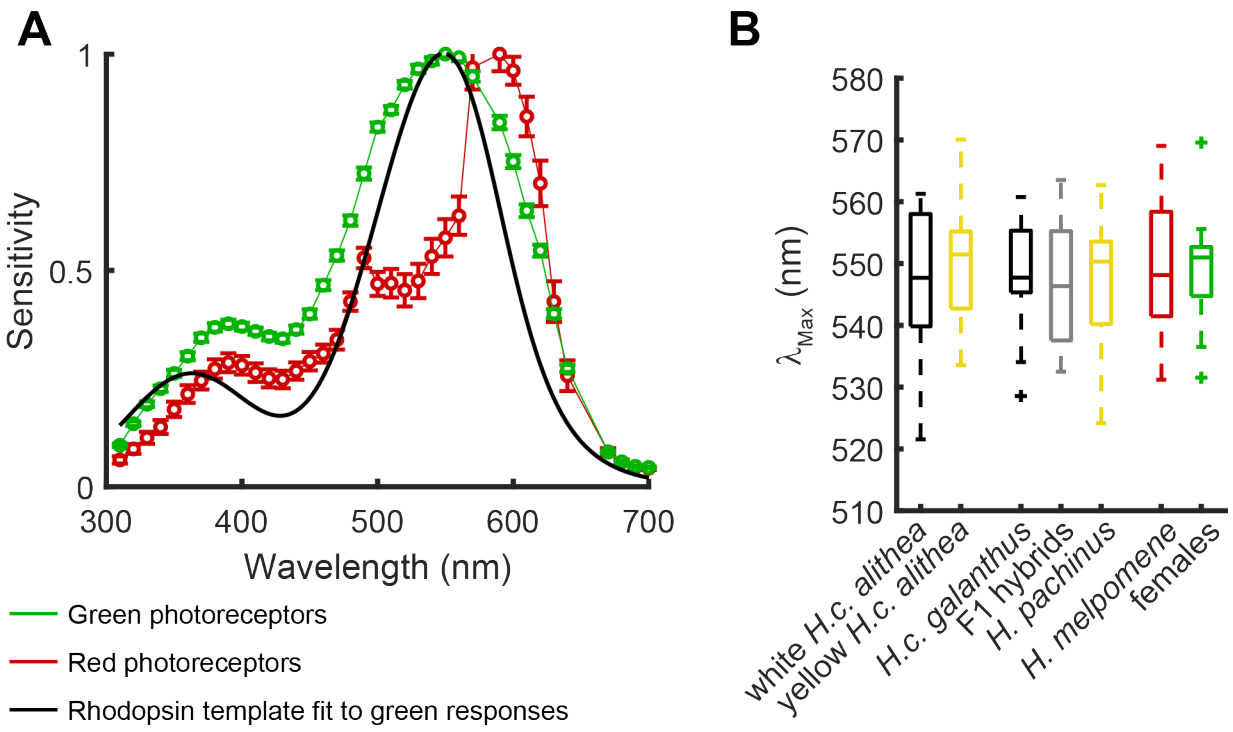

Figure 2.4: Long wavelength sensitive photoreceptors
A) Normalized spectral sensitivity is plotted for green and red sensitive photoreceptors. Data is shown as the mean ± SEM.
B) Box plots show λ_{Max} measured for each green photoreceptor using a standard rhodopsin template. Green photoreceptors did not vary with species or sex. Too few red photoreceptors were recorded for a similar analysis.

$F_{6,124} = 0.25$, p = 0.96). The overall shape of the spectral tuning curve matched the rhodopsin template, but the *Heliconius* photoreceptors had substantially broader tuning than expected. This broad tuning was consistent across cells and was not significantly affected by the magnitude of the voltage response (r = 0.11, p = 0.20).

Red photoreceptors were the second type of long wavelength sensitive cells (Fig. 2.4). These cells were narrowly tuned with λ_{Max} around 600 nm and presumably are tuned through a combination of the single LW opsin and red screening pigments [113, 126]. I recorded from only a small number of red photoreceptors, and these were primarily from *H. melpomene*. This is likely due to functional tiering of an ommatidium, with red photoreceptors proximal to the relatively distal electrode path I used to target UV and blue photoreceptors. The limited sample size prevented statistical analysis, but red photorecep-

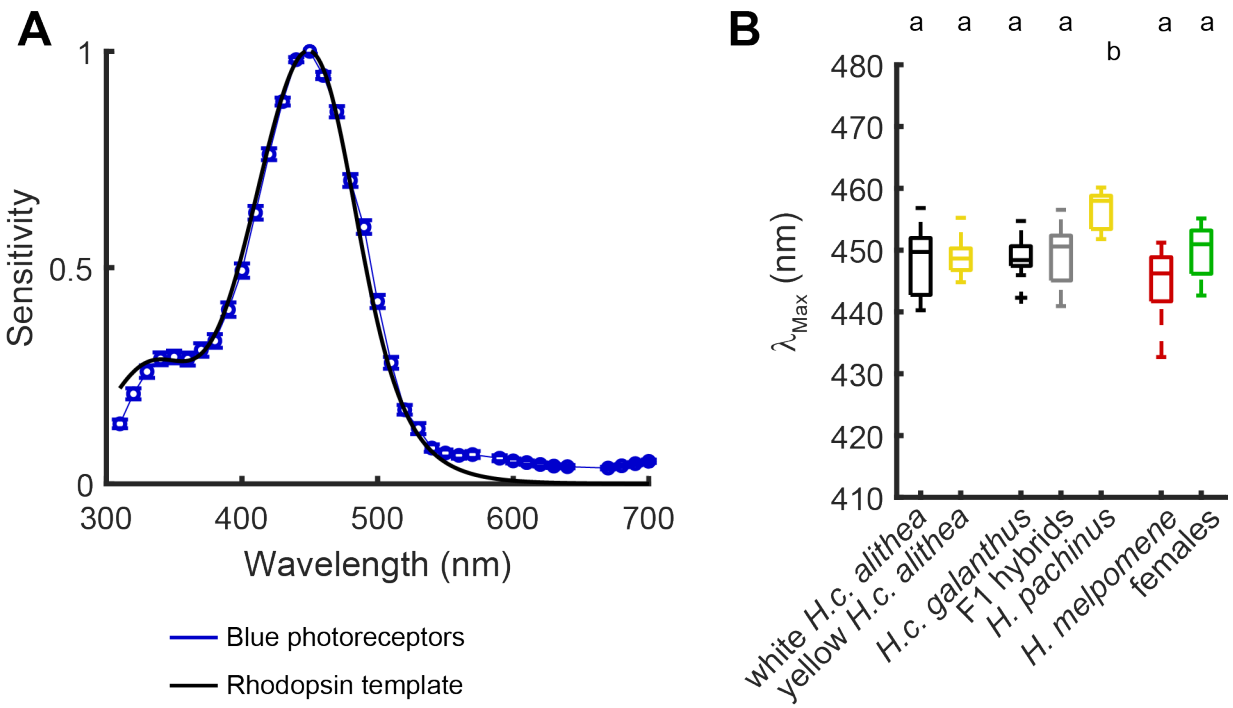

Figure 2.5: Blue photoreceptors
A) Normalized spectral sensitivity is plotted for blue photoreceptors. Data is averaged over all photoreceptors corresponding to group 'a' in panel B. Data is shown as the mean ± SEM. B) λ_{Max} was measured for each blue sensitive photoreceptor using a standard rhodopsin tuning template. Groups with different letters above the figure are significantly different with $p < 0.05$ using Tukey's HSD.

tors are unlikely to vary with species, sex, or wing color because every group has the same LW opsin gene (Fig. 2.4) and the same red screening pigment (Fig. 2.12).

Blue photoreceptors were maximally sensitive to wavelengths near 450 nm, and responses were generally well fit by the rhodopsin template (Fig. 2.5, $R^2 = 0.79 \pm 0.21$). Spectral sensitivity did not vary significantly across six of the seven butterfly groups ($\lambda_{Max} = 448.6 \pm 4.2$ nm), but peak sensitivity was shifted to a slightly longer wavelengths for *H. pachinus* males (Fig. 2.5, $\lambda_{Max} = 456.5 \pm 3.5$ nm, $F_{6,109} = 5.04, p < 0.001$, Tukey's HSD, $p < 0.05$ for all pairwise comparisons including *H. pachinus*). No blue photoreceptors were recorded from *H. pachinus* females, so I was unable to test if this was a sex dependent shift. Notably, my recordings from blue photoreceptors differ markedly from the blue photoreceptors recorded in *H. erato* ($\lambda_{Max} = 470$ nm) [126]. The protein coding sequence is nearly identical across

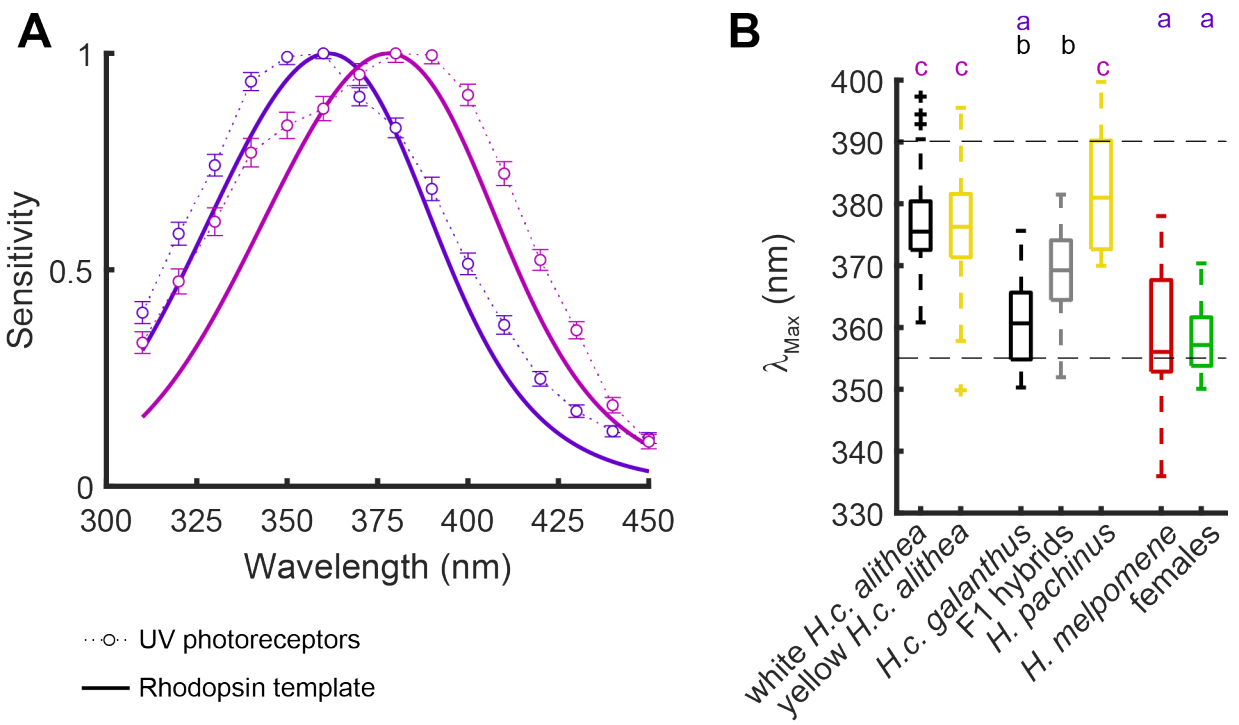

Figure 2.6: UV photoreceptors
A) Normalized spectral sensitivity is plotted for UV photoreceptors as mean ± SEM. The two tuning curves correspond to groups labeled 'a' and 'c' in panel B.
B) λ_{Max} measured for each UV photoreceptor using a standard rhodopsin tuning template. Dotted lines show the expected tuning of UV1 and UV2 based on results published in *H. erato*. Groups with different letters above the figure are significantly different with $p < 0.05$ using Tukey's HSD.

species, so the reason for the observed differences is unclear and possibly due to methodological differences.

In contrast to blue and green photoreceptors, the spectral sensitivity of UV photoreceptors showed substantial variability both within and between groups ($F_{6,148} = 21.70$, $p < 0.001$). Across all UV photoreceptors, λ_{Max} varied relatively continuously from 350 to 400 nm (Fig. 2.6), and standard deviations within a group were nearly 3 times larger than blue photoreceptors. Tuning width did not vary significantly and generally matched the rhodopsin template ($R^2 = 0.79 \pm 0.20$). For both females ($\lambda_{Max} = 357.8 \pm 5.2$ nm, $t_{21} = 1.6$ $p = 0.13$) and *H. melpomene* ($\lambda_{Max} = 359.1 \pm 10.4$ nm, $t_{29} = 1.6$ $p = 0.11$), spectral tuning was not significantly different from the expected tuning of UV1 ($\lambda_{Max} = 356$ nm).

Similarly, UV photoreceptors for *H. pachinus* ($\lambda_{Max} = 382.2 \pm 10.6$ nm, $t_7 = 2.1$, p = 0.076) were not significantly different from the expected tuning of UV2 ($\lambda_{Max} = 390$ nm).

For the remaining groups, however, UV photoreceptor tuning was intermediate to both UV1 and UV2 (Fig. 2.6). The shift away from UV1 tuning was small but significant for *H.c. galanthus* ($\lambda_{Max} = 361.0 \pm 7.3$ nm, $t_{11} = 2.4$, p = 0.036). Deviations from both UV1 and UV2 were clearer for both *H.c. alithea* ($\lambda_{Max} = 376.6 \pm 10.5$ nm, $p < 0.001$) and F1 hybrids ($\lambda_{Max} = 367.7 \pm 8.1$ nm, $p < 0.001$). Protein sequences for UV1 and UV2 are identical across all groups and most of the genus, so opsin variability cannot explain these differences. Previously published results [126], my results (see below), and the lack of tuning width variability all further suggested that screening pigments were unlikely to contribute to UV spectral sensitivity. Instead, these results suggested the hypothesis that UV photoreceptors can co-express both UV1 and UV2.

UV photoreceptors co-express UV1 and UV2

Electrophysiology alone was unable to test for co-expression, so I next turned to qPCR and antibody staining. qPCR was used to detect the relative expression levels of UV1 and UV2 mRNA in the eyes of adult butterflies and showed evidence supporting co-expression (Fig 2.7). *H.c. galanthus*, *H. melpomene*, and females predominantly expressed UV1 mRNA, but variable amounts of UV2 were also detected in all but one *H.c. galanthus* and one female. This generally matched the spectral tuning results, with these three groups having UV photoreceptor tuning close to but not perfectly matching the expected UV1 tuning. Similarly, *H. pachinus* predominately expressed UV2, but some UV1 mRNA was detected in every individual. Every *H.c. alithea* expressed more UV2 than UV1, but some individuals had expression levels showing nearly equal amounts of UV1 and UV2. This co-expression could potentially explain spectral sensitivity intermediate to both UV1 and UV2. F1 hybrids were not available for qPCR, but would presumably have relative expression levels similar to *H.c. alithea*.

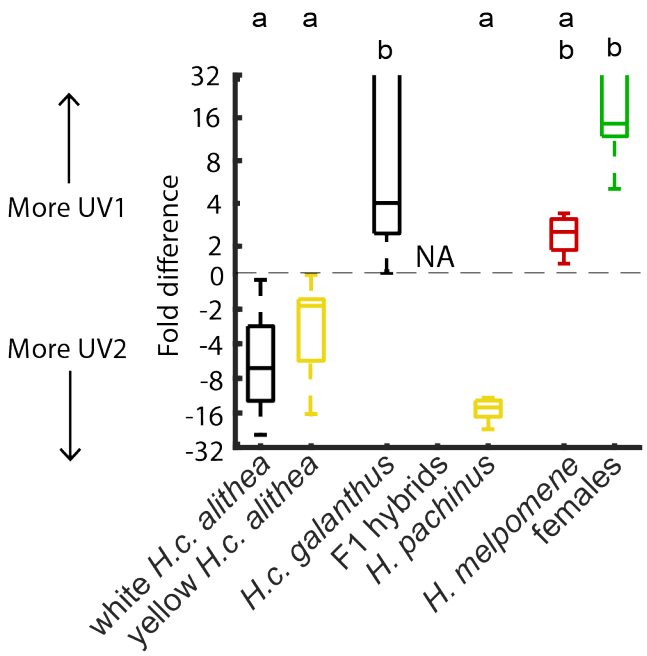

Figure 2.7: qPCR for UV1 and UV2
qPCR was used to detect the relative expression levels of UV1 and UV2 mRNA within a single butterfly. One *H.c. galanthus* and one female had no detectable UV2 expression. F1 hybrids were not available for qPCR. Groups with different letters above the figure are significantly different with $p < 0.05$ using Tukey's HSD. Note that data are shown on a log scale both above and below the zero line, with negative numbers indicating more UV2 expression.

Although qPCR was consistent with co-expression, detecting an mRNA does not ensure expression of the protein, as post-transcriptional regulation could potentially lead to selective translation of just one UV opsin [127, 132]. In order to ask if both UV opsins were expressed, I stained thin cross sections of the eye with antibodies specific to UV1, UV2, and blue rhodopsin (Fig. 2.8). Across all groups, butterflies always showed strong expression of the opsin matching the preferentially expressed mRNA, and co-expression of both UV1 and UV2 was also commonly observed. Because some butterflies had a clear lack of co-expression, the co-expression I did detect likely reflects a real signal rather than non-specific staining of opsins that have highly similar amino acid sequences.

Consistent with qPCR and electrophysiology, antibody staining also suggested that individuals differed in the relative levels of co-expression (Fig. 2.8). Strong and detailed claims

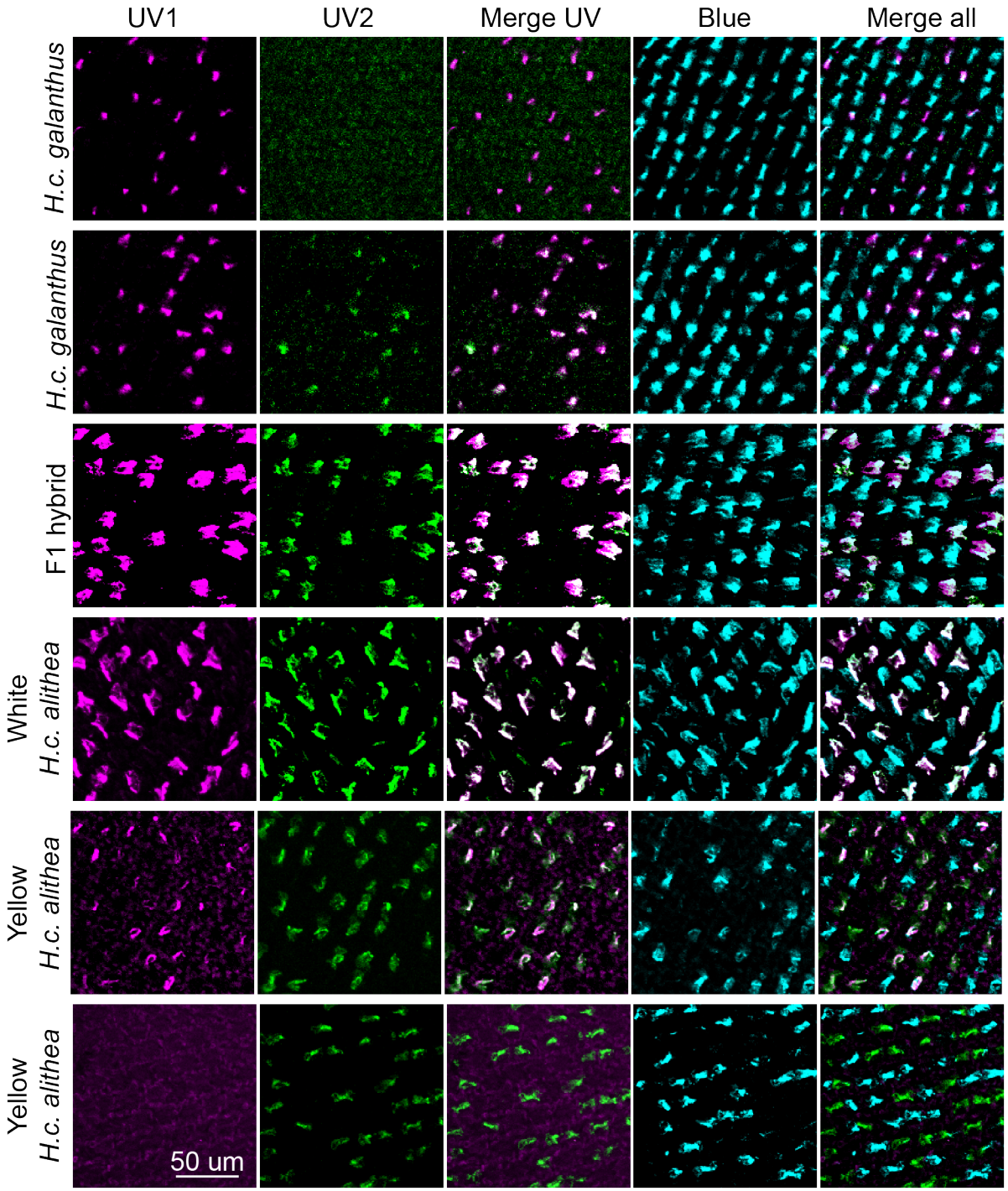

Figure 2.8: Antibody staining for UV1 and UV2
Cross sections of the eyes were stained for antibodies specific to UV1, UV2, and blue. Blue and one of the UV opsins were always strongly expressed. Fluorescent signals for the second UV opsin could be strong, weak, or absent. Expression patterns were consistent with qPCR results.

based on the intensity of a fluorescent signal is not feasible, but some basic conclusions were apparent. Only one UV opsin was detected in some butterflies, but it is unclear if the second UV opsin was not expressed or expressed at levels below the detection threshold. Other butterflies, including every F1 hybrid and many *H.c. alithea*, had strong fluorescent signals for both UV1 and UV2, suggesting relatively equal co-expression. Weak signals of the non-preferred opsin that were barely above background but matched the expression pattern of the preferred opsin were also observed in every group (Fig. 2.8). This variability in fluorescence intensity is consistent with qPCR and suggests that UV photoreceptors can vary continuously between expression of a single opsin and perfect co-expression. This variability both between and within groups could potentially explain the variable spectral sensitivities, with different proportions of UV1 and UV2 leading to shifts in λ_{Max}.

UV1 and UV2 co-expression shifts λ_{Max}

Antibody staining and qPCR provided strong evidence that UV photoreceptors have variable levels of UV1 and UV2 co-expression, but it remained unclear how this might affect spectral tuning. One possibility, which has been observed in *P. xuthus* photoreceptors that co-express opsins with peak sensitivities at 515 and 575 nm, is that UV1 and UV2 responses sum relatively independently, leading to an abnormally wide tuning curve [133]. Alternatively, matching my spectral sensitivity curves, co-expression could shift the tuning center with no effect on tuning width. To test these options, I created a linear model that combines UV1 and UV2 in variable proportions (Fig. 2.9).

For this model, I assumed that published recordings from *H. erato* with sensitivity peaks at 356 and 390 nm reflected purely UV1 and UV2 responses, respectively [126]. Using these values, I then generated UV1 and UV2 tuning curves using the standard rhodopsin tuning template. Combining these two tuning curves in variable proportions showed that co-expression can shift peak sensitivity to any wavelength between 356 and 390 nm (Fig. 2.9). Increases in tuning width were also observed, but this change was relatively small.

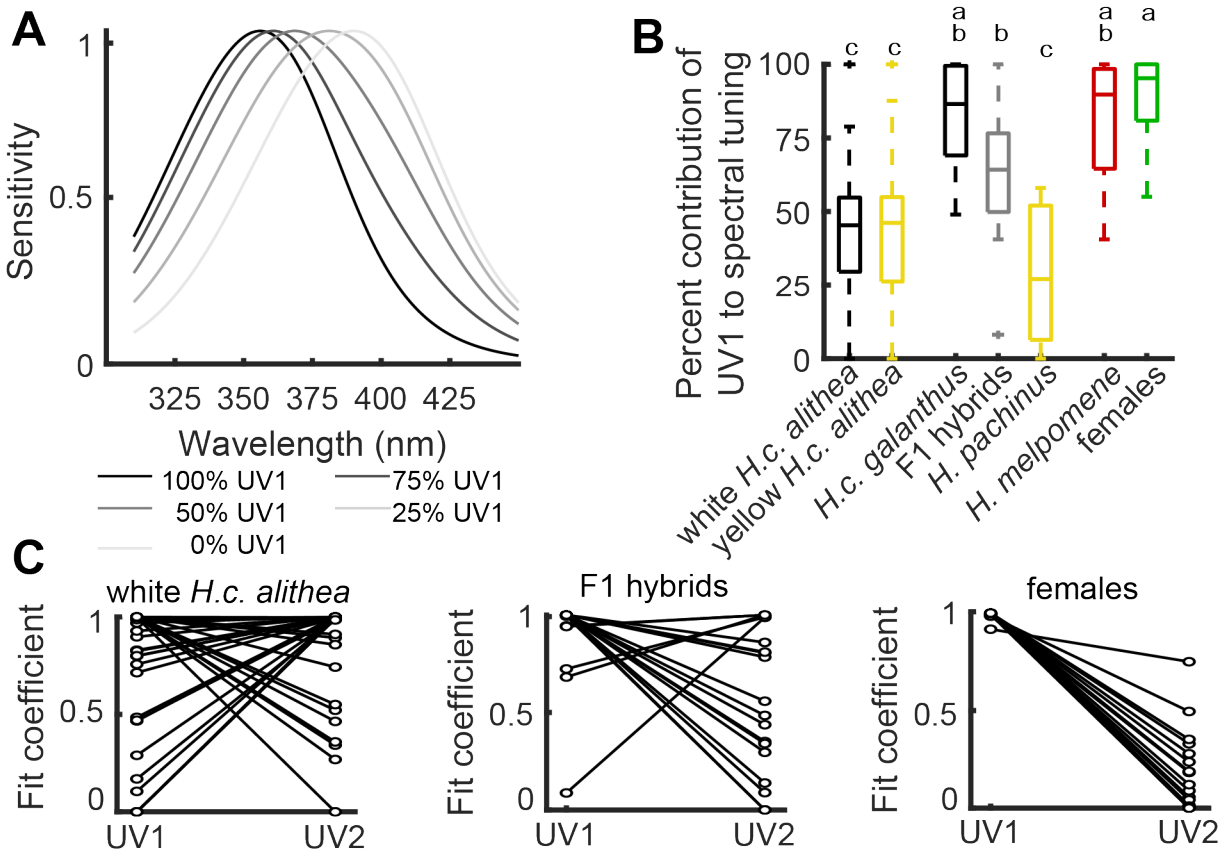

Figure 2.9: Effect of co-expression on UV spectral tuning
A) Spectral tuning curves for UV1 ($\lambda_{Max} = 356$ nm) and UV2 ($\lambda_{Max} = 390$ nm) were created and combined in variable proportions. This toy model shows that different proportions of UV1 and UV2 shift λ_{Max} substantially and lead to minor increases in tuning width.
B) The co-expression model was fit to each UV photoreceptor. Boxplot shows the percent contribution of UV1 to each tuning curve. Groups with different letters above the figure are significantly different with $p < 0.05$ using Tukey's HSD.
C) Fit coefficients of the mixed model are shown for every UV photoreceptor for three representative groups. Data in panel B was generated as UV1/(UV1+UV2).

To further verify the effect of UV1 and UV2 co-expression, I fit this model to the experimentally recorded UV photoreceptors. As expected, because co-expression has little effect on tuning width, the standard rhodopsin template ($R^2 = 0.79 \pm 0.20$) and this co-expression model ($R^2 = 0.81 \pm 0.17$) fit the data similarly well ($t_{312} = 0.94$, $p = 0.35$). Results broadly matched qPCR and antibody staining, as *H.c. galanthus*, *H. melpomene*, and female photoreceptors had a primary contribution from UV1, *H. pachinus* had a primary contribution from UV2, and *H.c. alithea* and F1 hybrids had relatively equal contributions from UV1 and

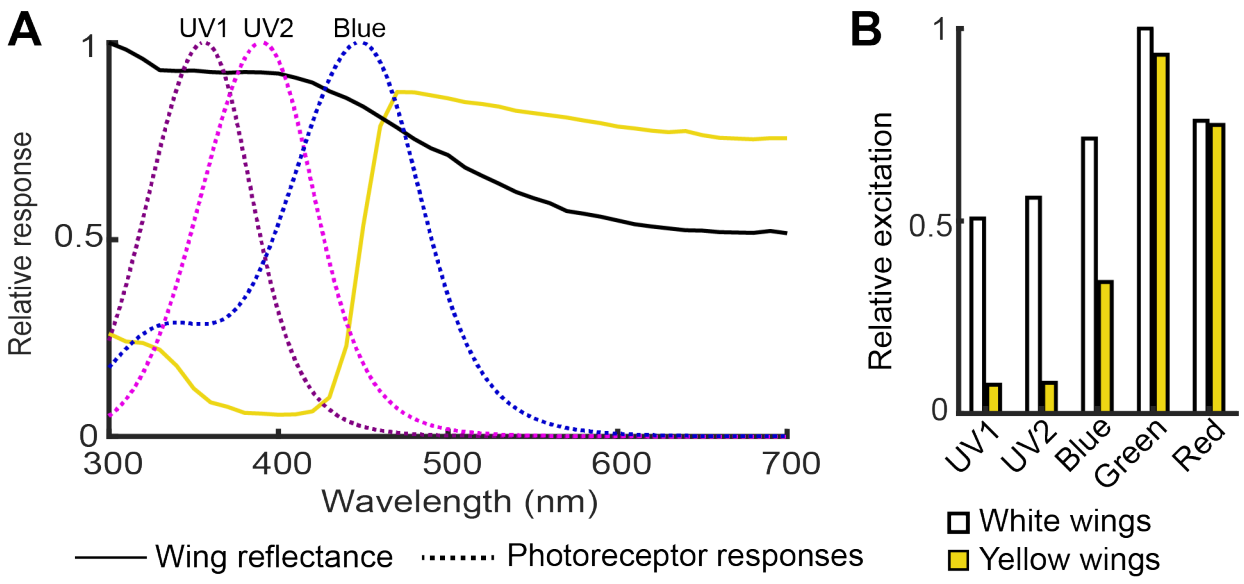

Figure 2.10: Predicted photoreceptor response to wings
A) Wing reflectance spectra are overlaid with spectral sensitivity curves for UV1, UV2, and blue photoreceptors generated with the rhodopsin template. Green and red photoreceptors are omitted for clarity.
B) Photoreceptor tuning curves were convolved with wing reflectance and normalized to 1.

UV2. For butterflies that I recorded multiple UV photoreceptors from, the percent contribution of UV1 and UV2 typically clustered closely together, suggesting that co-expression is similar within a butterfly and varies between individuals.

Together, these results show that the spectral sensitivity of photoreceptors in the cydno clade of *Heliconius* butterflies varies substantially for only for UV photoreceptors. This variability likely has biological significance for these closely related species [125, 128], and the degree to which the level of co-expression is precisely controlled remains an open question. However, UV photoreceptor spectral sensitivity is unlikely a contributing factor in male preference for white or yellow females. First, although there is a slight correlation between strength of UV2 expression and strength of preference for yellow females, the distribution of UV tuning was the same for white and yellow *H.c. alithea*. These butterflies do, however, have behavioral differences, so this interesting trend between preference and UV photoreceptors appears to be correlative rather than causal.

Second, from a computational perspective, the precise tuning of UV photoreceptors is

unlikely to have a large enough affect on color perception to flip preference between white and yellow (Fig. 2.10). White and yellow wings differ primarily in the presence or absence of UV reflectance, and it is unclear how small shifts in UV sensitivity could lead to a large change in perception and preference. A simple convolution between the spectral sensitivity of white or yellow wings and UV1 or UV2 rhodopsin confirms this intuition. White wings strongly excite and yellow wings weakly excite UV photoreceptors regardless of whether peak sensitivity is observed at 356 or 390 nm (Fig. 2.10B).

2.3.2 Distribution of photoreceptor types

A second aspect of eye organization that could potentially influence courtship preference is the spatial distribution of photoreceptor types across the eye. Different proportions of photoreceptor types have been shown to be behaviorally relevant for both *Drosophila* [134] and birds [135, 136]. In *Drosophila*, the number of blue and green sensitive photoreceptors are anti-correlated, and flies preferentially approach wavelengths exciting the photoreceptor that is predominately expressed [134]. This anti-correlated expression of photoreceptor types is also observed in *Heliconius*. The R1 and R2 photoreceptors always express either UV or blue, meaning an increase in one type necessarily results in a matching decrease in the other. Similarly, increases in the number of red photoreceptors leads to a matching decrease in the number of green photoreceptors.

Variability in the distribution of photoreceptor types could be important for *Heliconius* mate preference behavior, although the effect of photoreceptor distribution has never been behaviorally tested in any butterfly. Because white and yellow wing reflectance is similar for long wavelengths, the proportion of green and red photoreceptors is unlikely to influence this specific preference, but the proportion of UV and blue might. As shown above (Fig. 2.10), white and yellow wings strongly and weakly excite UV photoreceptors, respectively. Blue photoreceptors are also strongly excited by white wings, and perhaps importantly, have peak sensitivity closely matched to wavelengths where yellow wings transition from low to

high reflectance. Thus, although strength of excitation in single photoreceptors is unlikely to affect preference behavior, a population response that varies due to differing proportions of UV and blue photoreceptors could potentially affect perception and preference.

Eyeshine

My first approach to assess the distribution of photoreceptor types was to conduct eyeshine assays, which allow for quantification of the distribution of screening pigments across the entire eye [106, 114]. Using a modified epi-fluorescent microscope, this fast and non-invasive procedure generates images analogous to a cat's eyes reflecting light in the dark, with each ommatidium having a color indicating the type of screening pigment present (Fig. 2.11). Because red screening pigment is a necessary component of red photoreceptors [106, 126, 137], this method provides a relatively direct read out of the proportion of red and green photoreceptors. Additionally, each of the three ommatidial types (UV-UV, blue-blue, and UV-blue) have generally been shown to always be associated with the same screening pigment within a species [117, 120, 124, 138]. The mapping between screening pigment color and ommatidia type is unknown for any *Heliconius* butterfly, and whether this mapping is consistent across species is also unknown. With these caveats, a difference in eyeshine distribution would at least hint at a change in the relative distribution of UV and blue photoreceptors.

I imaged the eyeshine of each butterfly along the entire dorsal-ventral axis of the eye, passing through the approximate center (Fig. 2.11). An average of 12.1 ± 1.2 photos amounting to $3,714.8 \pm 784.0$ ommatidia were imaged for each butterfly, which is on the order of 1/4 of an eye [93]. Images from the ventral eye had nearly twice as many ommatidia per photo as the rest of the eye (476.8 ± 124.8 vs. 242.5 ± 37.7). This difference reflects an increase in ventral eye spatial resolution rather than a change in the experimental procedure [92, 114].

Consistent with eyeshine from other *Heliconius* butterflies [106, 115], every butterfly I examined had a heterogeneous combination of red and yellow ommatidia (Fig. 2.11). Measuring the spectral transmittance of these two pigment types confirmed that these were

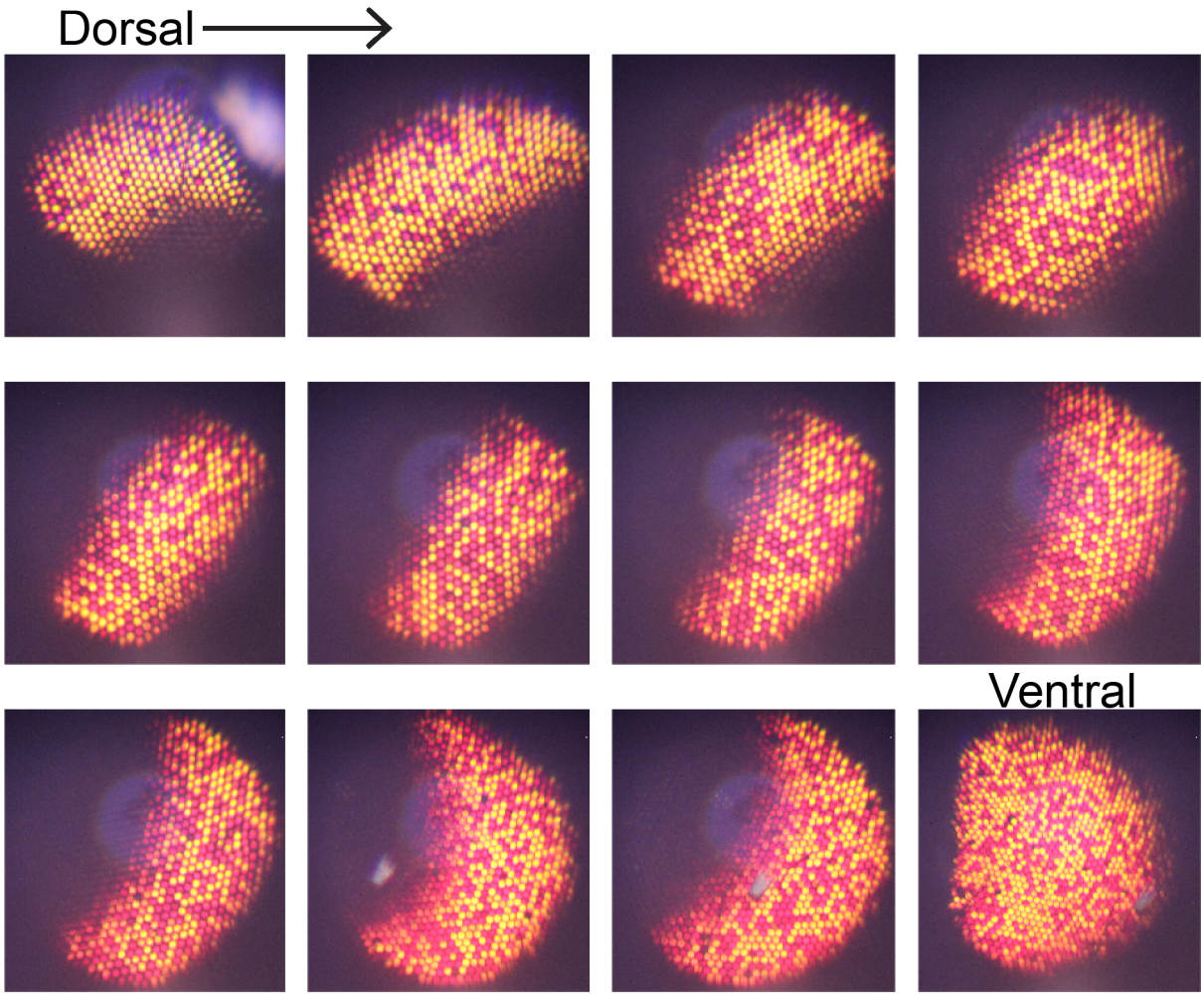

Figure 2.11: Example eyeshine images
Shown are all 12 eyeshine images from an *H. pachinus* male. Non-overlapping images progress from the dorsal eye to the ventral eye, with the first and last image adjacent to the head capsule. Note that the increased number of ommatidia in ventral images reflects increased spatial resolution and not a difference in methodology.

the same across butterflies (Fig. 2.12). PCA on the transmittance spectra of the 4,751 ommatidia examined clearly separated red and yellow ommatidia, but the data did not cluster by species or sex (data not shown). Transmittance spectra for red and yellow ommatidia were quite similar, which is consistent with Nymphalid butterflies having only a single type screening pigment [101, 106, 114]. Color differences are instead thought to arise either from changes in the concentration of pigment or distance from rhabdom [118].

The two pigments were the same across butterflies, but the distribution of red and yellow

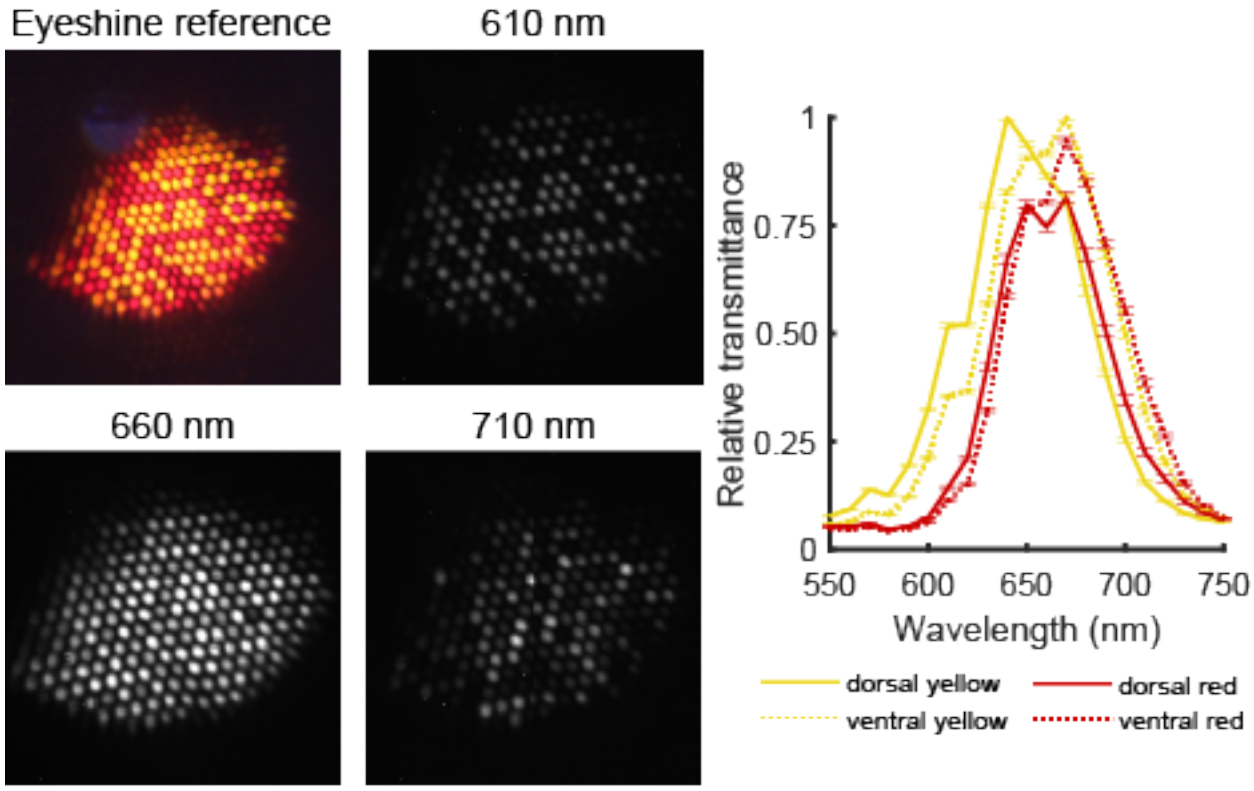

Figure 2.12: Screening pigment spectral transmittance
A) Transmittance spectra of screening pigments were measured using a monochromatic camera and intensity matched monochromatic light. Red or yellow pigment color was determined visually, and transmittance was measured as pixel intensity at each wavelength.
B). Screening pigment transmittance is shown for red and yellow ommatidia measured in both the dorsal and ventral eye. Transmittance did not vary with species or sex, so data was grouped together and plotted as the mean ± SEM.

pigments varied across the eye (Fig. 2.13). In the dorsal eye, ommatidia were primarily yellow, and this was generally similar across all individuals, although F1 hybrids had significantly more yellow than *H. melpomene* (Tukey's HSD, p = 0.018) and females (Tukey's HSD, p = 0.012)(Fig. 2.15A). The ventral eye, in contrast, had a more even mix of red and yellow ommatidia. To examine the transition from the dorsal yellow eye to the mixed ventral eye, I modified the experimental set-up to image the anterior portion of the eye in several butterflies (Fig. 2.14). The proportion of yellow ommatidia switched from the dorsal distribution to the ventral distribution over a span of approximately 50 rows of ommatidia, showing a relatively sharp boundary matching observations in other butterfly species [117].

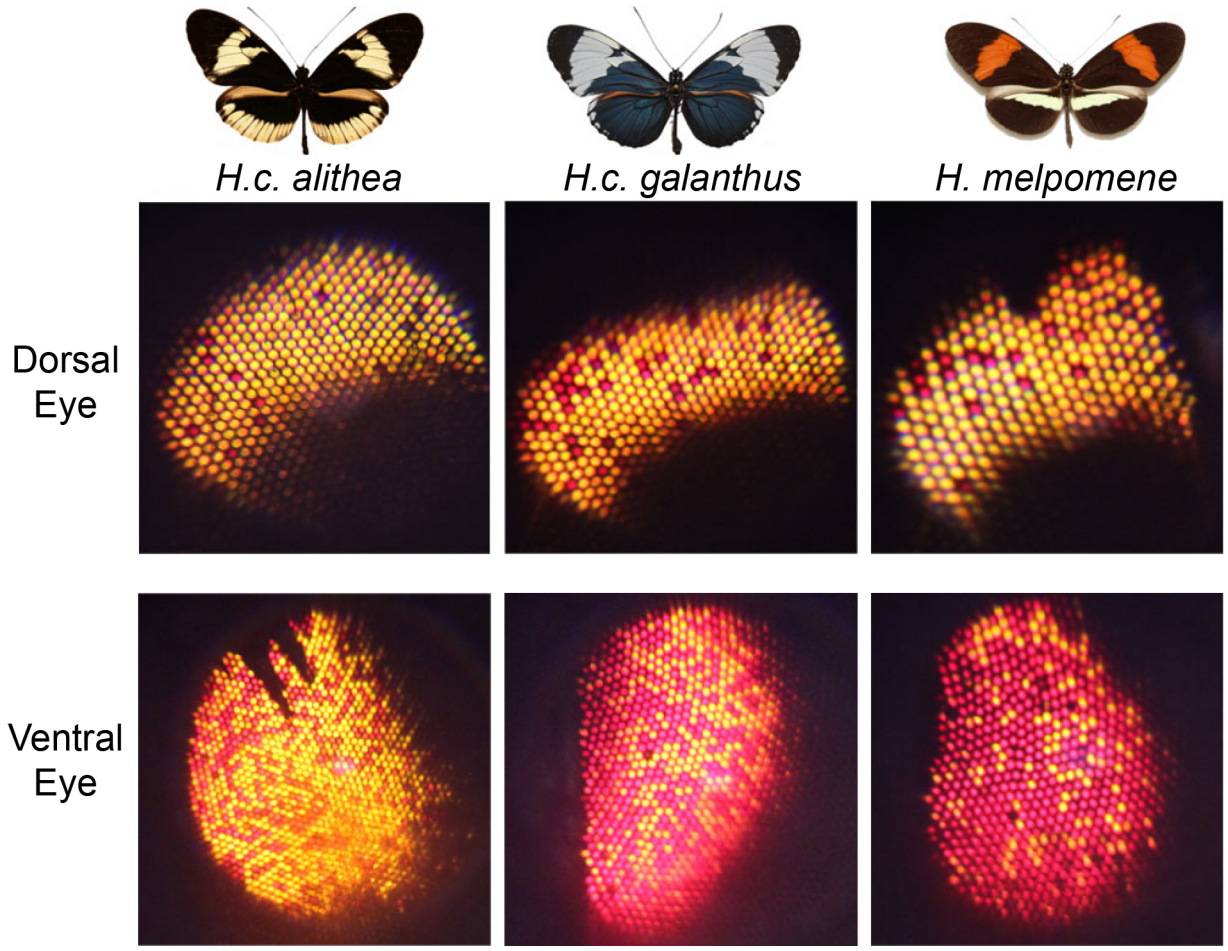

Figure 2.13: Dorsal-ventral differences in eyeshine distribution
Example eyeshine images show differences in the proportion of red and yellow ommatidia in the dorsal and ventral eye for three males.

In the ventral eye, the proportion of red and yellow screening pigment varied significantly with both species and sex ($F_{6,79} = 182.3$, $p < 0.001$, Fig. 2.15B). Female distributions clustered together regardless of species and had more red ommatidia than yellow. *H. melpomene* eyes had even more red ommatidia, perhaps reflecting a need for red photoreceptors in this red-winged species. *H.c. galanthus* eyes had an approximately equal mix of red and yellow ommatidia, and *H. pachinus* males had significantly more yellow (Tukey's HSD, $p < 0.05$). F1 hybrids had eyeshine distributions intermediate to but not significantly different from these two parent species. Finally, the ventral eyes of *H.c. alithea* had the most yellow ommatidia, but the lack of significant differences between white and yellow individuals (Tukey's

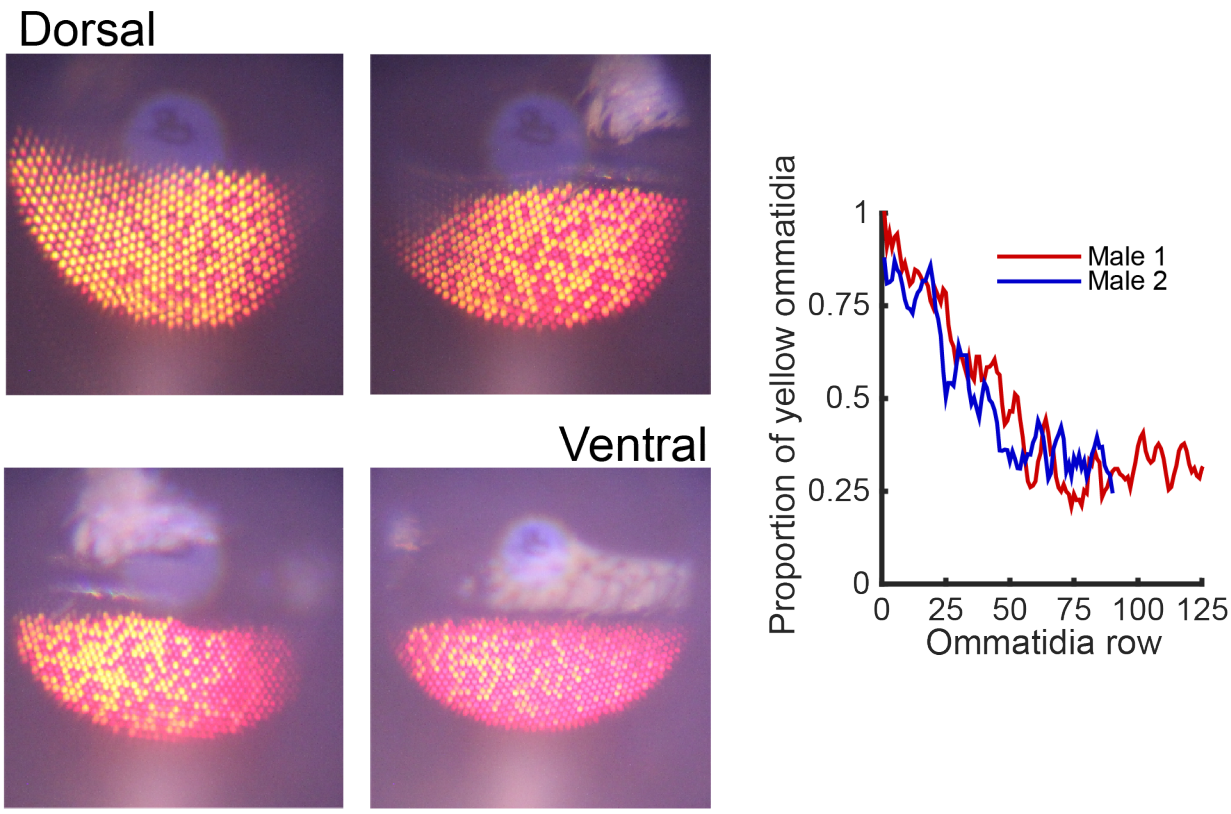

Figure 2.14: Transition from dorsal to ventral eyeshine distribution.
A) Example eyeshine images along the anterior portion of an *H. melpomene* eye. The top of each image is adjacent to cuticle.
B) The proportion of yellow ommatidia was quantified for each row of ommatidia. Shown is data for two *H. melpomene*. Results are similar but less clear for other species that substantially more yellow in the ventral eye.

HSD, $p = 0.90$) suggests screening pigment distributions are not related to male mate preferences. Regardless, variability between species with similar ecological niches and a strong sexual dimorphism suggests that these distributions are involved in a sexually dimorphic behavior such as courtship.

Ommatidia types

Variation in the proportion of red and yellow ommatidia in the ventral eye suggested that variation also existed in the proportion of UV and blue photoreceptors. If screening pigments are predictive of ommatidial type, there should be a linear correlation between the percent

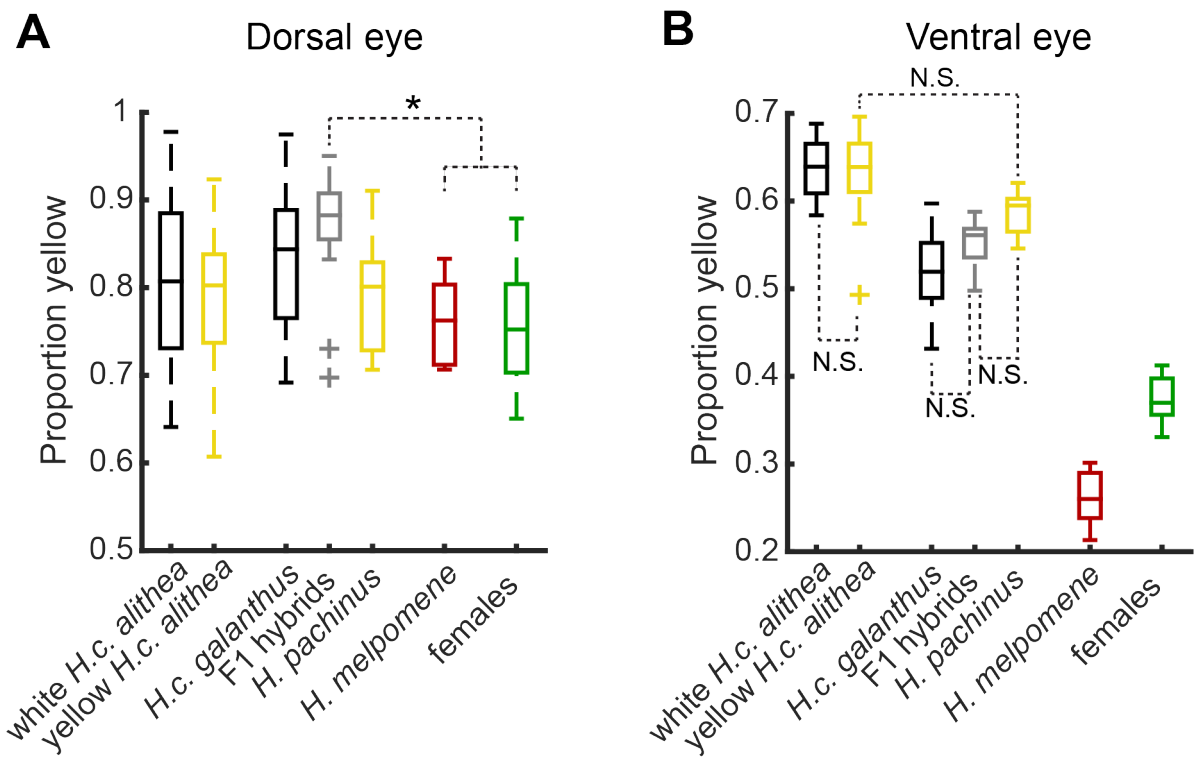

Figure 2.15: Quantification of eyeshine distributions
A) The proportion of red and yellow ommatidia were calculated for the most dorsal regions of the eye. Asterisks indicate significant differences with $p < 0.05$.
B) Same as A, but for the ventral half of the eye. All pairwise comparisons are significant with Tukey's HSD and $p < 0.05$ except where noted.

of yellow ommatidia and the percent of UV photoreceptors. However, qPCR comparing the relative mRNA expression for UV and blue opsins suggested the relationship between ommatidia screening pigment and ommatidia type was not consistent between groups (Fig. 2.18B). *H.c. alithea* males had the largest proportion of yellow ommatidia, while *H. melpomene* and females had the least amount of yellow ommatidia, yet qPCR showed similar proportions of mRNA for UV and blue. Further, even though *H.c. galanthus* and *H. pachinus* had intermediate proportions of yellow ommatidia, *H.c. galanthus* appeared to have less UV and *H. pachinus* more UV than the other groups. Overall, these results suggested screening pigment and ommatidia type were uncoupled between groups, but qPCR is a relatively imprecise method to draw clear conclusions.

To more directly test how the proportion of UV and blue photoreceptors varied across

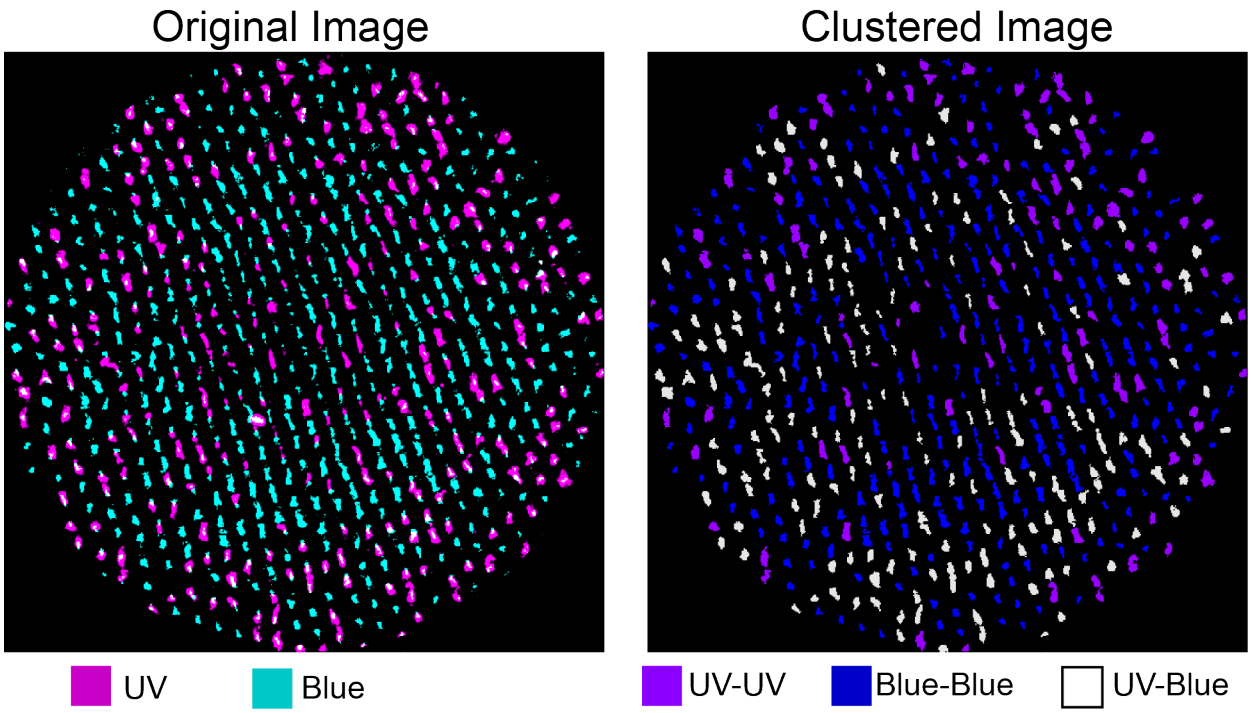

Figure 2.16: Detecting ommatidial types
In eye sections stained with UV1, UV2, and blue opsin antibodies, the proportion of UV-UV, blue-blue, and UV-blue ommatidia was measured with an automated program. The left shows the original antibody staining for a white *H.c. alithea* female. UV1 and UV2 are combined into a single UV channel. Fluorescence is binarized. The right shows the results of the automated program.

groups, I quantified the proportion of ommatidia types using antibody staining. Photoreceptors in cross sections of the eye were labeled with antibodies specific to UV1, UV2, and blue rhodopsin. UV1 and UV2 were combined into a single color channel because butterflies did not have distinct UV1 and UV2 photoreceptors but were instead co-expressed. Each ommatidia was then classified as UV-UV, blue-blue, or UV-blue using an automated program (Fig. 2.16). Each cross section of eye contained an average of 559.8 $\pm$ 236.3 ommatidia (range 159-1296).

Results for the quantification of ommatidial types are shown in Fig. 2.17. Each of 7 groups have 3 values that add up to 100%, which makes any sort of quantitative analysis difficult (but see below and Fig. 2.18). Inspection of the plots, however, do show that the distribution of ommatidial types varies with species and sex, but not wing color. The

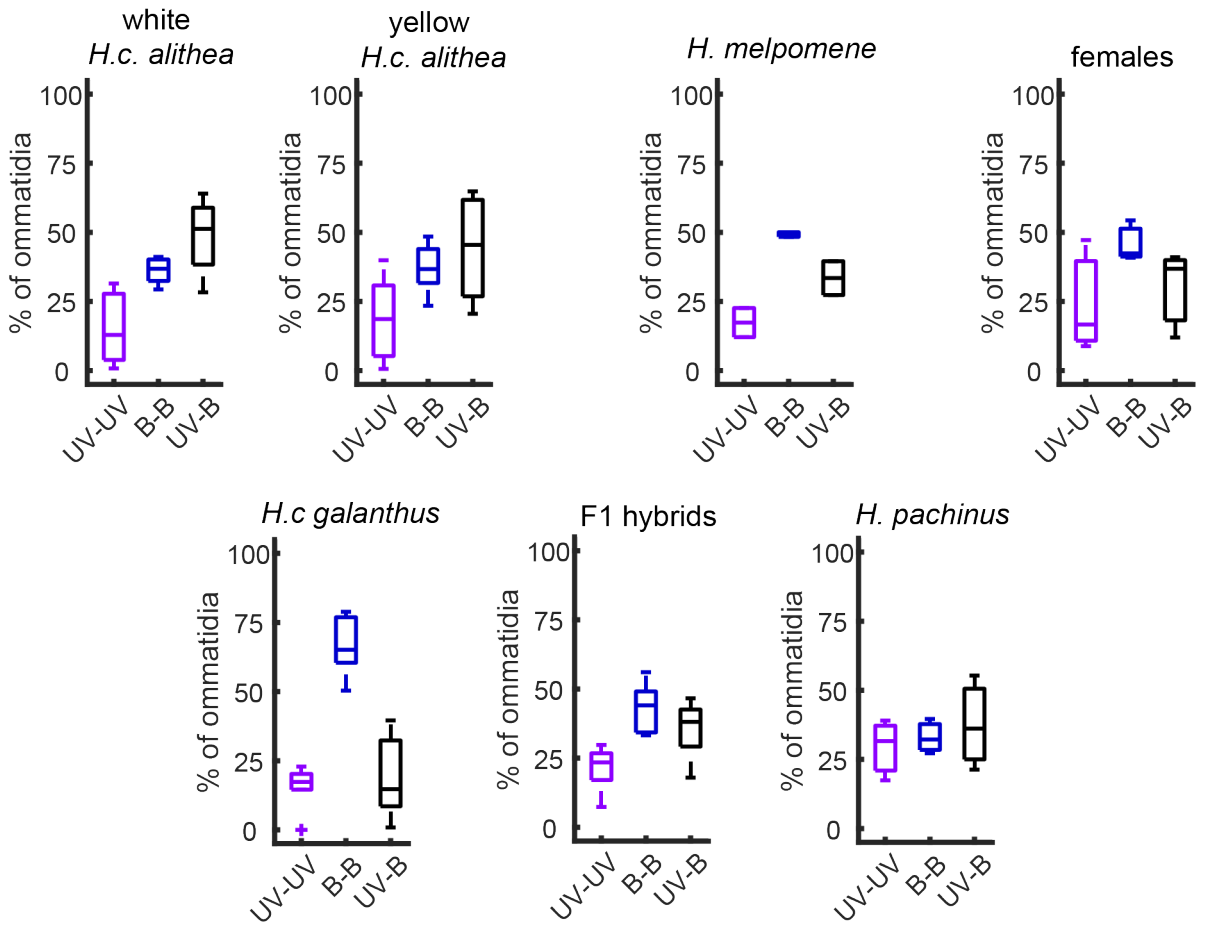

Figure 2.17: Distribution of 3 ommatidial types
Each panel shows the percent of ommatidia that had 2 UV, 2 blue, or 1 UV and 1 blue photoreceptor.

distributions for *H.c. alithea* were similar for individuals with white and yellow wings, but they did appear different from the other species. In particular, the plurality of ommatidia was UV-blue for *H.c. alithea*, but was blue-blue for every other group. Relating this distribution to the eyeshine distribution, the percent of yellow ommatidia matched the sum of the UV-UV and UV-blue types. Thus, for *H.c. alithea*, it seems that red ommatidia are blue-blue, and yellow ommatidia are either UV-UV or UV-blue.

A similarly clear relationship between eyeshine and ommatidia types could not be established for the remaining groups. However, a relationship matching *H.c. alithea* was unlikely. In particular, *H. melpomene* and females have a small number of yellow ommatidia that

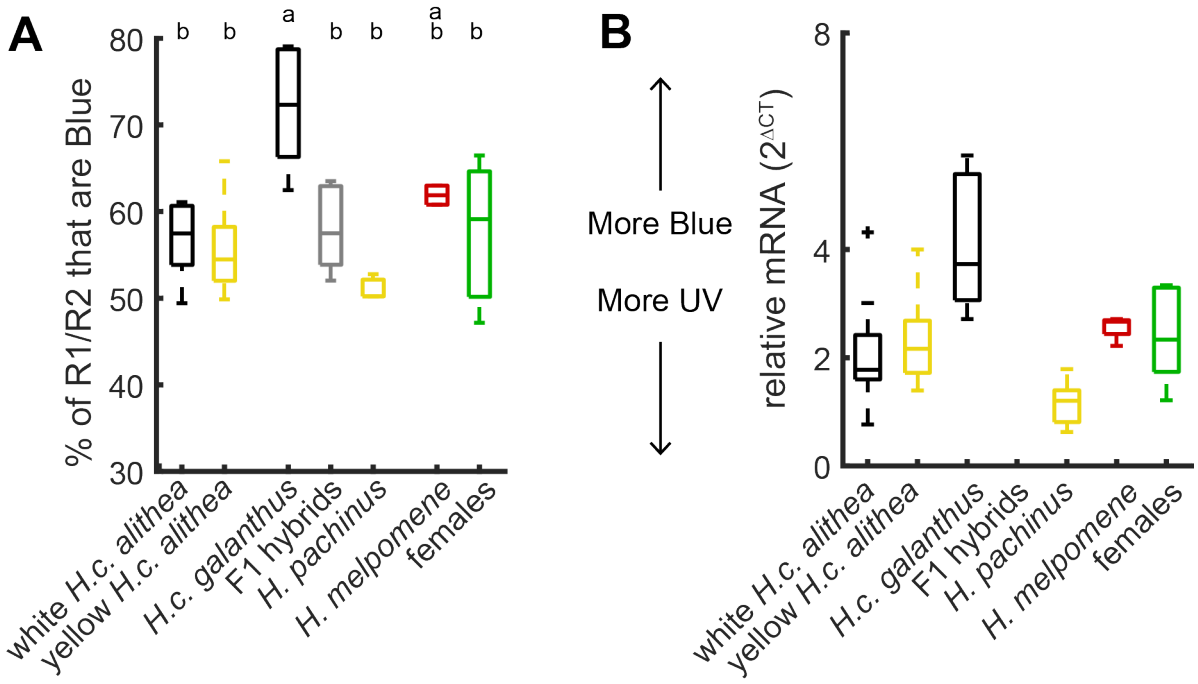

Figure 2.18: Proportion of photoreceptors expressing blue rhodopsin
A) Every ommatidia has two photoreceptors expressing either UV or blue rhodopsin. The plot shows the percent of these 2 photoreceptors that expressed UV rhodopsin.
B) qPCR was used to detect the relative expression levels of mRNA for UV and blue opsins

cannot match the sum of UV-UV and UV-blue ommatidia (Fig. 2.17). Instead, yellow ommatidia most likely correspond to either UV-UV or UV-blue ommatidia, but not both.

Hypothesizing a relationship for F1 hybrids and their *H.c. galanthus* and *H. pachinus* parents was not feasible as multiple combinations were possible (Fig. 2.17). Consistent with qPCR, *H.c. galanthus* had predominantly blue-blue ommatidia. These proportions for *H.c galanthus* also match the distribution from previously published results [127]. The best prediction for the relationship between screening pigment and ommatidia type in *H.c. galanthus* is the opposite of *H.c. alithea*, with yellow corresponding to blue-blue. *H. pachinus* had a relatively even mix of the three ommatidial types, and F1 hybrids were intermediate to the two parent species. For these two groups, a relationship between eyeshine and ommatidia types matching *H.c. alithea* was the best fit. Overall, however, no confidence can be given to predictions of the relationship between screening pigment and ommatidia type for these three groups since other associations were nearly equivalent.

Reducing each group from three types of ommatidia to the percent of photoreceptors expressing blue rhodopsin allowed for a more quantitative comparison (Fig. 2.18A). These data largely agreed with results from qPCR, although limited sample sizes for some groups limited the statistical power. *H.c. galanthus* had significantly more blue photoreceptors ($71.9\% \pm 6.6\%$) than every group except for *H. melpomene* ($p = 0.30$). *H. pachinus* similarly had the most UV, although this was not significantly different from the other groups except *H.c. galanthus* ($p < 0.001$).

Overall, the distribution of photoreceptor types and screening pigments vary substantially with species and sex, but no clear relationship emerged that relates these differences to mate choice. The lack of differences between white and yellow *H.c. alithea* further reject a possible mate choice relationship. The data do suggest that, within a species or sex, screening pigments and ommatidia type are correlated. However, the relationship is almost certainly not maintained across groups. The strong sexual dimorphism does suggest a role in a sexually dimorphic behavior. One possibility is that males eyes vary to match differences in seemingly similar habitats that have not yet been fully characterized. Female eyes may instead be optimized for a behavior such as egg laying.

2.3.3 Photoreceptor synaptic connections

Photoreceptor spectral tuning and the distribution of ommatidial types varied with species and sex, and these differences likely have important biological consequences. However, without differences between white and yellow *H.c. alithea*, these differences are unlikely to contribute to male preference for white or yellow females. Additionally, from a computational perspective, there is no obvious mechanism for these relatively simple and linear changes in eye organization to lead to changes in preference. Every photoreceptor responds more strongly to white wings than yellow wings, so no changes to λ_{Max} or the proportion of photoreceptor types can make the eye respond more strongly to yellow (Fig. 2.10). Instead, flipping preference between colors that primarily differ in the presence or absence of

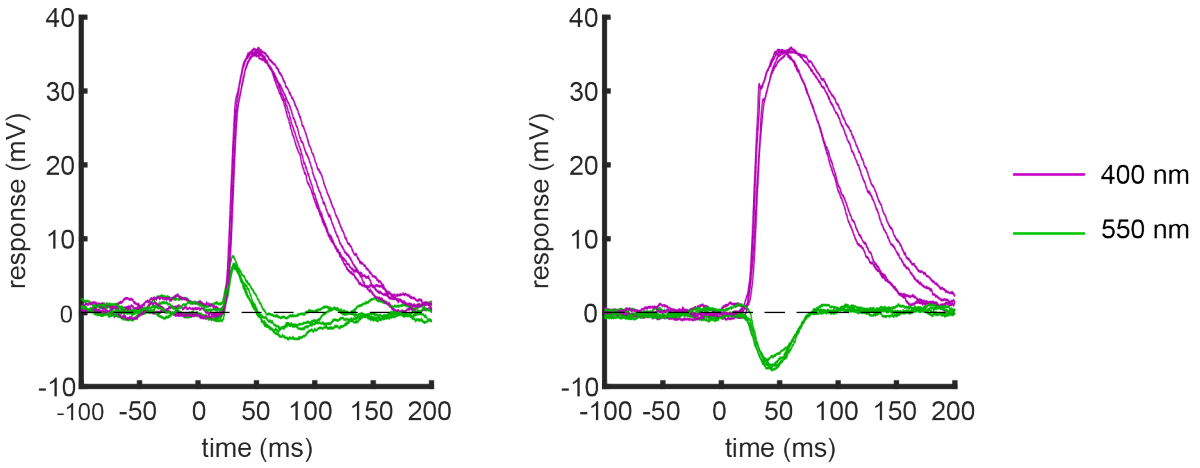

Figure 2.19: Example data
Shown are the responses of a UV photoreceptor from two different white *H.c. alithea* males. Both cells had similar responses at λ_{Max} = 400 nm. Responses to 550 nm, in contrast, varied in response polarity. Each line shows a single trial. On the x-axis, 0 marks the onset of a 25 ms light flash. For photoreceptors with negative responses to long wavelength light, differences in the temporal response to UV light were common across trials.

short wavelength reflectance likely requires a substantial nonlinear transformation of sensory information.

The voltage response of UV and blue photoreceptors to off-peak, long wavelength light showed a signature of such a non-linear computation that has the potential to influence courtship preferences. Photoreceptor responses to wavelengths surrounding λ_{Max} were generally well described by a rhodopsin tuning template, but UV and blue photoreceptors also had residual responses to long wavelength light that varied in polarity (Fig. 2.19). When rhodopsin absorbs a photon, it begins a transduction cascade leading to photoreceptor depolarization [139]. Residual responses to long wavelength light matched this expected depolarizing response for some photoreceptors, but others surprisingly showed hyperpolarizing responses that cannot be explained by photoreceptor transduction cascades (Fig. 2.20, 2.21). Instead, negative responses must originate from an external source, which is presumed to be long wavelength sensitive photoreceptors. Notably, voltage responses for cells with negative tail tuning return to positive for wavelengths $>$ 650 nm, suggesting the positive tail represents the default tuning state of a photoreceptor.

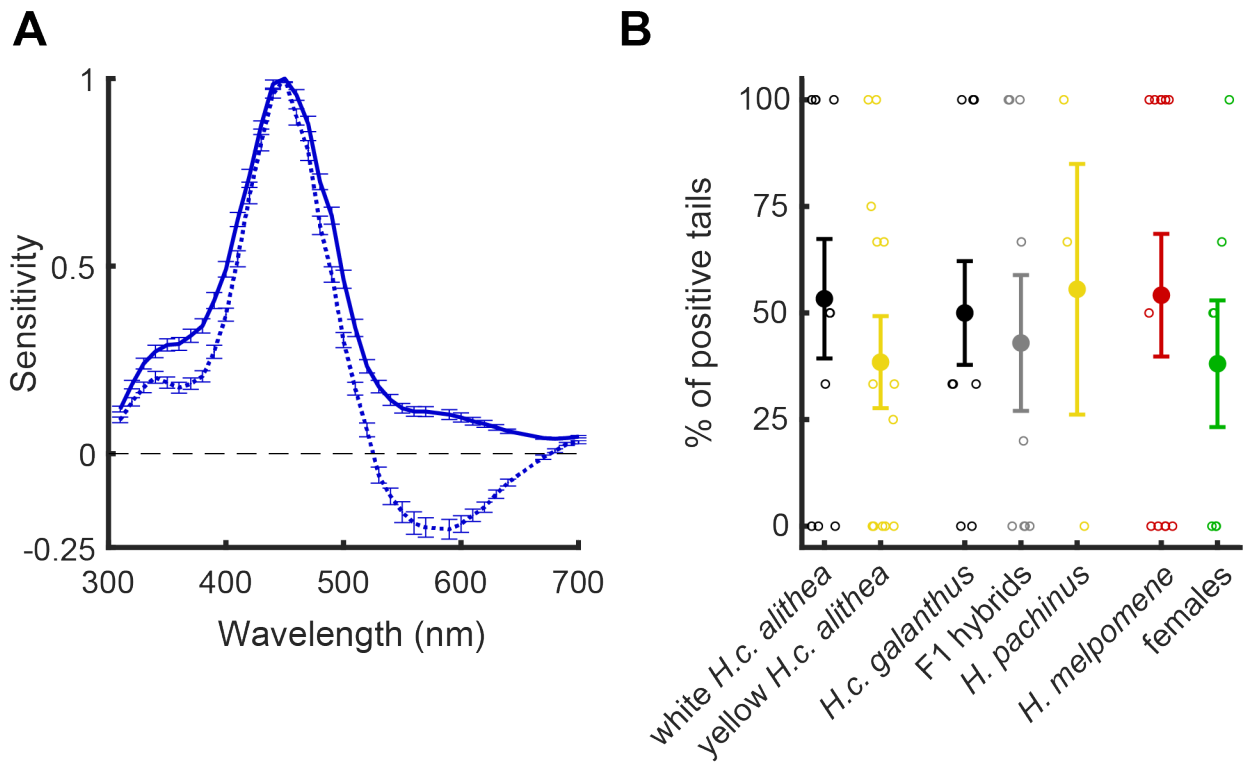

Figure 2.20: Tail tuning in blue photoreceptors
A) Spectral tuning curves are shown for blue cells that have either depolarizing responses to all stimuli or hyperpolarizing responses to a subset of stimuli.
B) The proportion of cells with positive tails was measured for each group. The percent of positive cells was measured for each individual, shown as small open circles. Filled circles with errorbars show the mean ± SEM.

The two most likely origins of the negative tails were either experimental noise or synaptic connections. When photoreceptors depolarize, the extracellular media hyperpolarizes and can be detected as the electroretinogram (ERG) with an extracellular electrode. If a photoreceptor is poorly isolated, the negative tails could reflect ERG signal leaking into the electrode rather than a real biological signal. Alternatively, negative tails could be a signature of inhibitory synaptic connections from LW sensitive photoreceptors. Insect photoreceptors use histamine as an inhibitory neurotransmitter [99], so inhibitory connections between long wavelength photoreceptors and UV or blue photoreceptors could be detected as a hyperpolarizing response. Based on anatomical data from the well-studied butterfly *P. xuthus*, these connections would most likely occur in the lamina, although it is unclear how

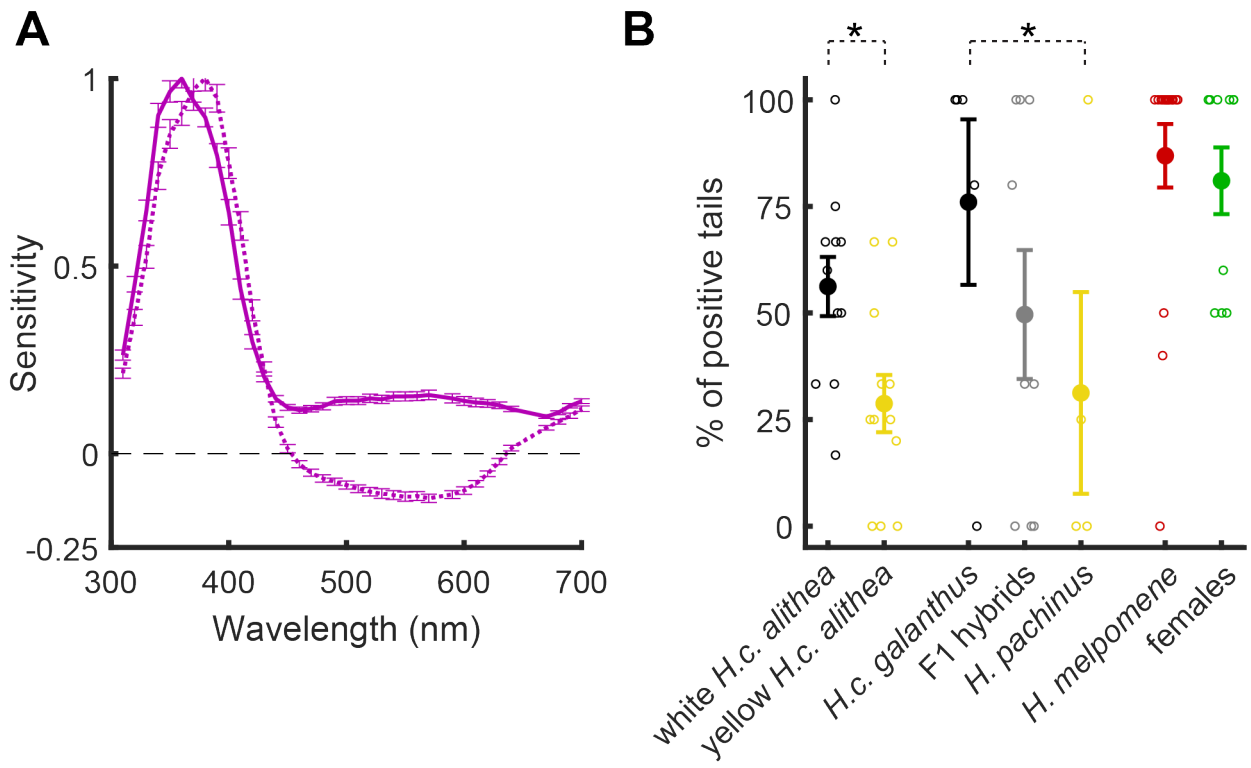

Figure 2.21: Tail tuning in UV photoreceptors
A) Spectral tuning curves are shown for blue cells that have either depolarizing or hyperpolarizing responses to long wavelength stimuli.
B) The proportion of cells with positive tails was measured for each group. Small open circles show the percent of positive tails for cells measured in a single butterfly. Filled circles show the average percentage ± SEM. Asterisks denote significance with $p < 0.05$.

these hyperpolarizing currents would propagate and be detected by the electrode located in the distal eye.

One way to distinguish between these potential sources of the negative tails was to measure response latency. The ERG represents the collective response of potentially hundreds of photoreceptors. Because 6 of 8 photoreceptors per ommatidium express the LW opsin that respond strongly to long wavelength light, an ERG response should occur more quickly than the depolarizing response of a single photoreceptor. Synaptic connections, in contrast, should have delayed response times, with monosynaptic connections typically having delays on the order of 5-10 ms. Thus, the relative response latencies should suggest the origin of the hyperpolarizing response.

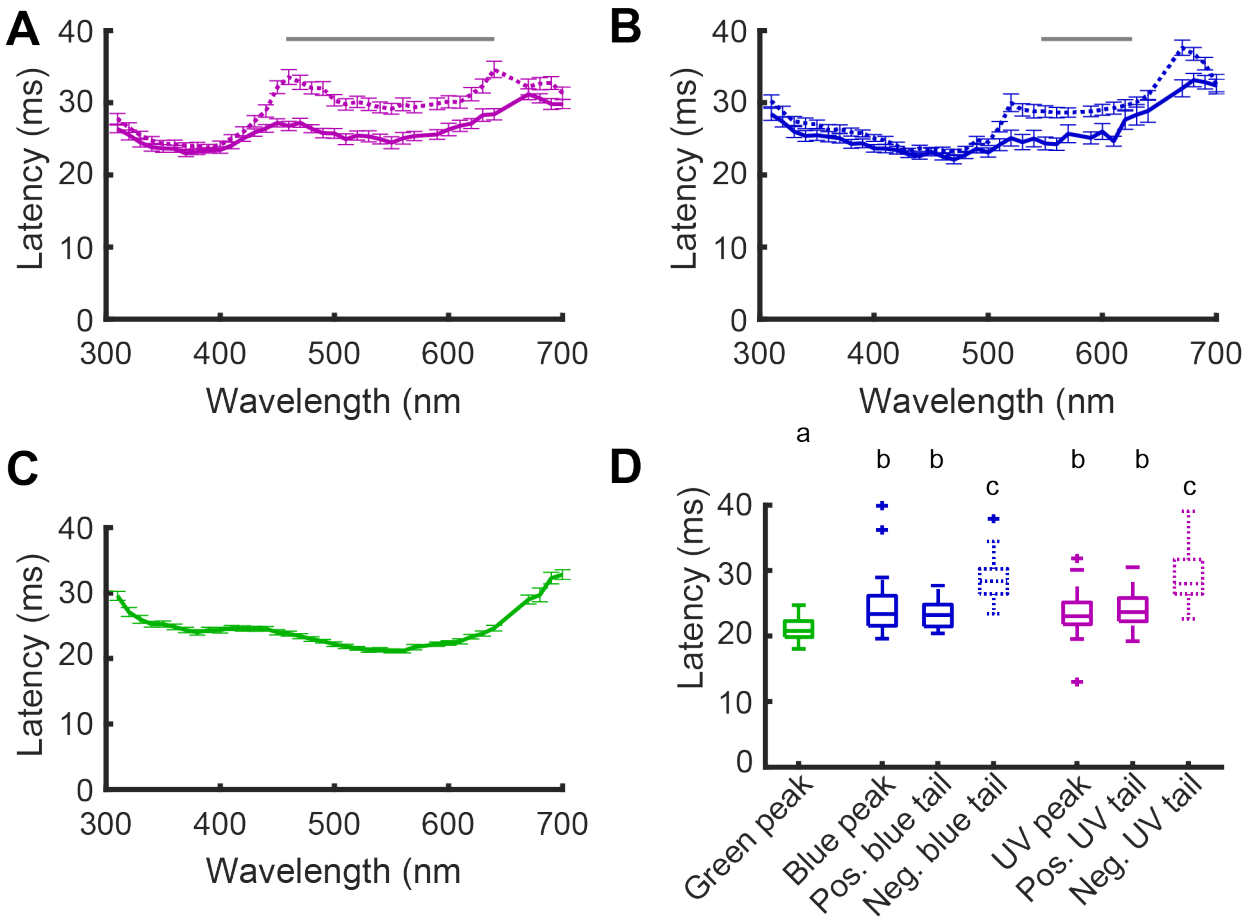

Figure 2.22: Photoreceptor response latencies for intensity matched stimuli
A, B, C) Latencies to the onset of a photoreceptor response were measured for UV (A), blue (B), and green (C) photoreceptors. Solid lines show latencies for cells with positive tails and dotted lines show latencies for cells with negative tails. Error bars show SEM.
D) Boxplots show latency distributions for λ_{Max}, and tail latencies for 550 nm. Groups sharing the same letter above are statistically the same. Green photoreceptors respond the fastest, but post-hoc analysis of the tuning curves showed that I used slightly higher intensity light for green tuning curves, on average. See Fig. 2.23 for details.

Response latencies for both UV and blue photoreceptors were consistent with negative tails originating from monosynaptic inhibition (Fig. 2.22, 2.23). Latencies were first measured for spectral tuning curves using intensity matched stimuli spanning the full visual range (Fig. 2.22). For the wavelengths surrounding λ_{Max}, latencies for cells with positive and negative tails were not significantly different for UV ($t_{62} = 1.2$, p = 0.23) or blue ($t_{43} = 0.33$, p = 0.74) cells and were on the order of 20-25 ms (see below for precise quantification).

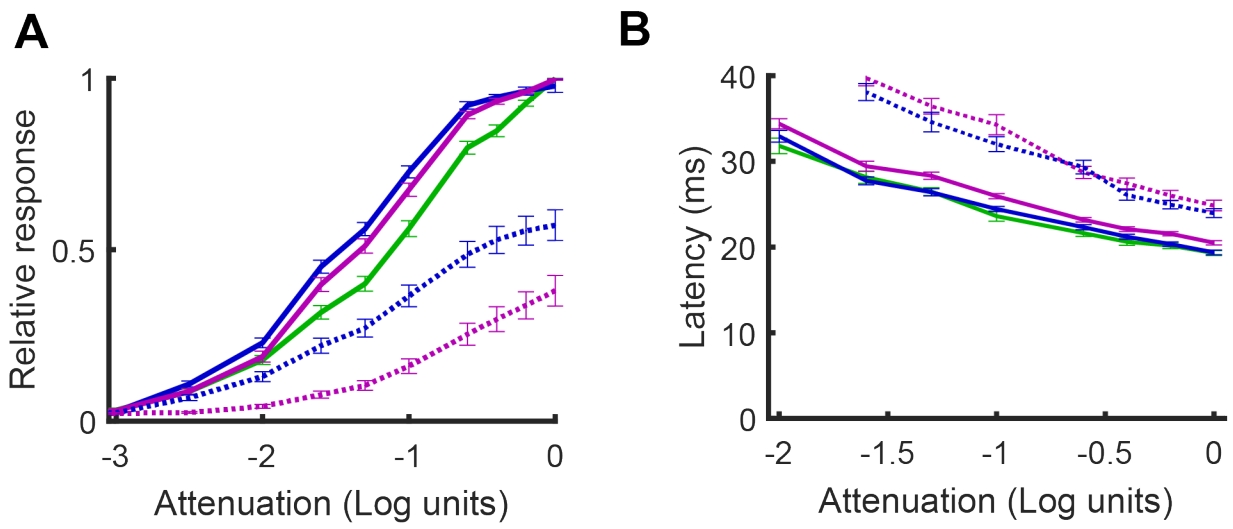

Figure 2.23: Photoreceptor response latencies for different light intensities
A) Normalized voltage response at λ_{Max} in solid lines and negative tails in dotted lines over 3 log units of light attenuation.
B) Response latencies for the curves shown in panel A. Error bars in both panels are SEM.

Positive tail responses were slightly delayed compared to λ_{Max} for both UV (mean delay = 1.8 ± 3.5 ms, median delay = 0.9 ms, $t_{187} = 57.3$, $p < 0.001$) and blue (mean delay = 2.1 ± 3.5 ms, median delay = 0.8 ms, $t_{85} = 5.5$, $p < 0.001$) photoreceptors. For UV cells, negative tails were delayed significantly more compared to both λ_{Max} (mean delay = 5.5 ± 3.6 ms, median delay = 4.8 ms, $t_{183} = 62.2$, $p < 0.001$) and the positive tail ($t_{308} = 9.3$, $p < 0.001$). Negative tails for blue cells were also delayed significantly more compared to both λ_{Max} (mean delay = 5.2 ± 3.4 ms, median delay = 4.6 ms, $t_{125} = 17.2$, $p < 0.001$) and the positive tail ($t_{210} = 6.5$, $p < 0.001$). Together, these results are consistent with monosynaptic inhibition from LW photoreceptors being the source of negative tails.

Response latencies can depend on light intensity, response magnitude, or both. To assess the effect of these variables on response latency, I next measured responses and latencies for λ_{Max} and negative tails (λ =550 nm) over 4 log units of light intensity (Fig. 2.23). At λ_{Max} for the highest light intensity, blue and green photoreceptors responded with a latency of 19.3 ± 1.7 ms ($t_{73} = 0.2$, $p = 0.85$). Latencies of 20.5 ± 1.7 ms for UV photoreceptors at λ_{Max} were slightly but significantly slower than both green ($t_{78} = 3.1$, $p < 0.01$) and

blue (t_{93} = 3.1, p < 0.01) photoreceptors. Light intensity had a similar effect on latency for all photoreceptors, with latencies increasing by an average of 5.6 ms per log unit of light attenuation.

Similar to the spectral tuning curves, negative tails for these intensity-response curves were delayed relative to λ_{Max} for both UV and blue photoreceptors (Fig. 2.23). At the highest light intensity, negative tails for UV and blue photoreceptors had similar delays of 5.3 ± 2.6 ms (t_{41} = 0.13, p = 0.89) that was significantly longer than λ_{Max} latencies (t_{42} = 93.6, p < 0.001). This delay was maintained over 2 log units of attenuation, increasing at a slightly higher rate of 7.9 ms per log unit of light intensity.

Overall, these results indicate that negative tails in UV and blue photoreceptors originate from monosynaptic connections with LW sensitive photoreceptors. For UV cells, negative tails spanned from 460 nm to 630 nm, suggesting that inhibition came from broadly sensitive green photoreceptors (Fig. 2.21, 2.24). Negative tails were shifted for blue cells, with hyperpolarizing responses between 530 nm and 670 nm (Fig. 2.20). This could possibly mean that blue cells receive inhibition from red photoreceptors rather than green. However, the tuning of blue photoreceptors overlaps substantially with green photoreceptors, so it is possible that this overlap obscures inhibition from green photoreceptors at shorter wavelengths.

The presumed anatomical correlate of these positive and negative tails are the absence and presence, respectively, of synapses connecting LW photoreceptors to UV and blue photoreceptors. Antibody staining for sens2 (Fig. 2.2) similarly pointed towards expression in LW photoreceptors, suggesting a possible role of this candidate mate choice gene in the formation of these synapses. If this is true, I would expect butterflies with different mate preferences to have different proportions of positive and negative tails since sens2 is differentially expressed in the eyes of white and yellow males. To test this hypothesis, I next compared the proportion of UV and blue cells with positive and negative tails across the seven groups.

The proportion of blue photoreceptors with positive tails was not significantly affected

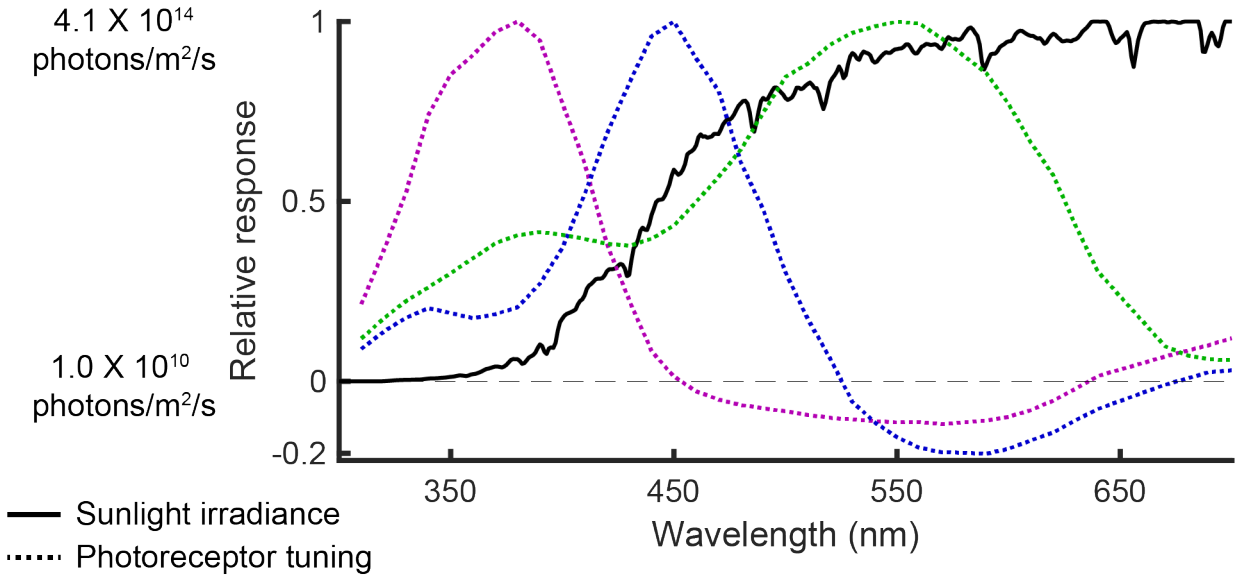

Figure 2.24: Sunlight irradiance
Figure shows the irradiance of sunlight overlaid with the tuning curves of UV and blue photoreceptors with negative tails as well as green photoreceptors. Green photoreceptor tuning overlaps substantially with negative tails. Sunlight irradiance data was provided to me by Susan Finkbeiner.

by species, sex, or wing color (Fig. 2.20B, $F_{6,57} = 0.26$, p = 0.95). I recorded from a total of 126 blue photoreceptors across all groups, and 46.9% had positive tails. Similar proportions across all groups suggest that tails in blue photoreceptors serve a more general biological purpose rather than courtship. Blue photoreceptors, but no other photoreceptor types, also appear to be inhibited by LW photoreceptors in the butterflies *Troides aeacus formosanus* [120] and *P. xuthus* [140], suggesting that this result may be widespread across butterflies.

The proportion of positive and negative tails for UV photoreceptors, in contrast, did vary across groups, including differences based on wing color and mate preference (Fig. 2.21B, $F_{6,63} = 6.37$, $p < 0.001$). For females and *H. melpomene*, 80.8% of UV photoreceptors had positive tails, suggesting positive tails are the ancestral tuning state. Similarly, 83.3% of UV photoreceptor tails (10 of 12) in *H.c. galanthus* were positive. This ratio was reversed in *H. pachinus*, with only 25% (2 of 8) UV photoreceptors having positive tails ($\chi^2 = 6.8$, $p < 0.01$). F1 hybrids had an intermediate proportion of 52.6% of UV photoreceptors with positive tails (10 of 19), which was not significantly different from either parent species.

Differences between *H.c. galanthus*, *H. pachinus*, and their F1 hybrid offspring were consistently found for every aspect of eye organization I examined. However, unlike the other features, the proportion of UV cells with positive tails also varied between white and yellow *H.c. alithea* (Fig. 2.21B). For white males, 53.5% of UV photoreceptors had positive tails (23 of 43), which matches F1 hybrids both in tail proportion and lack of courtship color preference. Yellow males, in contrast, had only 30% of UV photoreceptors with positive tails (12 of 40), which matches *H. pachinus* both in tail proportion and preference for yellow females. These proportions were significantly different between white and yellow males both when analyzing total counts ($\chi^2 = 4.7$, p = 0.030) and when proportions were calculated for each individual and then compared ($t_{24} = 3.5$, p = 0.002).

Together, tail tuning of UV photoreceptors correlates well with male mate preferences. Males that prefer white females as well as females and the outgroup *H. melpomene* predominantly have UV photoreceptors with positive tails. Males preferring yellow females, in contrast, primarily have UV photoreceptors with negative tails suggesting inhibition from LW sensitive photoreceptors. Males with no preference are intermediate, with a relatively even mix of positive and negative tail photoreceptors. The difference between white and yellow *H.c. alithea* is particularly important, as these butterflies are genetically similar across the population, with the only consistent genetic difference being at the wing color locus. This result also fits with the differential expression of sens2 in LW photoreceptors, suggesting that expression of this candidate mate choice gene might inhibit the formation of synaptic connections between LW and UV photoreceptors.

Tail tuning affects the adaptation state of UV photoreceptors

Positive and negative tails reflecting differences in synaptic connectivity between photoreceptors could have numerous different effects on neural computation, perception, and behavior. Inhibition of UV and blue photoreceptors could lead to both shortened temporal responses of the photoreceptor or a decrease in total neurotransmitter release to downstream synaptic

partners. Understanding how these differences in synaptic connectivity in the peripheral visual system influence behavior and perception would necessitate identifying and recording from neurons in the central brain.

These positive and negative tails could also have an effect on the responses and excitability of the photoreceptors themselves. In a natural environment, short wavelength light is relatively limited, with UV irradiance approximately 4 log units less than wavelengths > 400 nm (Fig. 2.24). Photoreceptors adapt to ambient light levels in a mostly cell-autonomous way to maintain sensitivity. Thus, the null hypothesis in a natural environment is that UV photoreceptors would be relatively dark-adapted compared to LW photoreceptors. However, tails make UV photoreceptors responsive to long wavelength light that might affect the adaptation state of a cell. Positive tails respond to the relatively intense long wavelength light in an environment, and this could potentially make the UV photoreceptors less sensitive by making them relatively light adapted. In contrast, UV cells with negative tails might not be affected by long wavelength light or even be sensitized.

To test this hypothesis, I recorded from UV photoreceptors under conditions simulating natural light. Bright green LEDs ($\lambda = 534$ nm) were added to the electrophysiology set-up to selectively stimulate photoreceptors responsive to long wavelength light. Spectral tuning curves were then measured both in the presence and absence of the green LEDs. Turning on the LEDs suppressed the responses of green photoreceptors to $20.9 \pm 10.6\%$ of the original response (Fig. 2.25A), showing that the LEDs had the intended effect. I then recorded from UV photoreceptors with positive and negative tails to examine if or how long wavelength stimulation affected responses to UV light.

Using the green LEDs, I measured UV photoreceptor spectral response curves (Fig. 2.25B) and the response to λ_{Max} over 4 log units of light intensity (Fig. 2.26). Results for the two types of recording agreed with each other. With the green LEDs turned on, the resting potential of UV photoreceptors decreased by 5.6 ± 4.8 mV ($t_{18} = 5.1, p < 0.001$), which is consistent with the addition of inhibitory currents from LW photoreceptors (Fig.

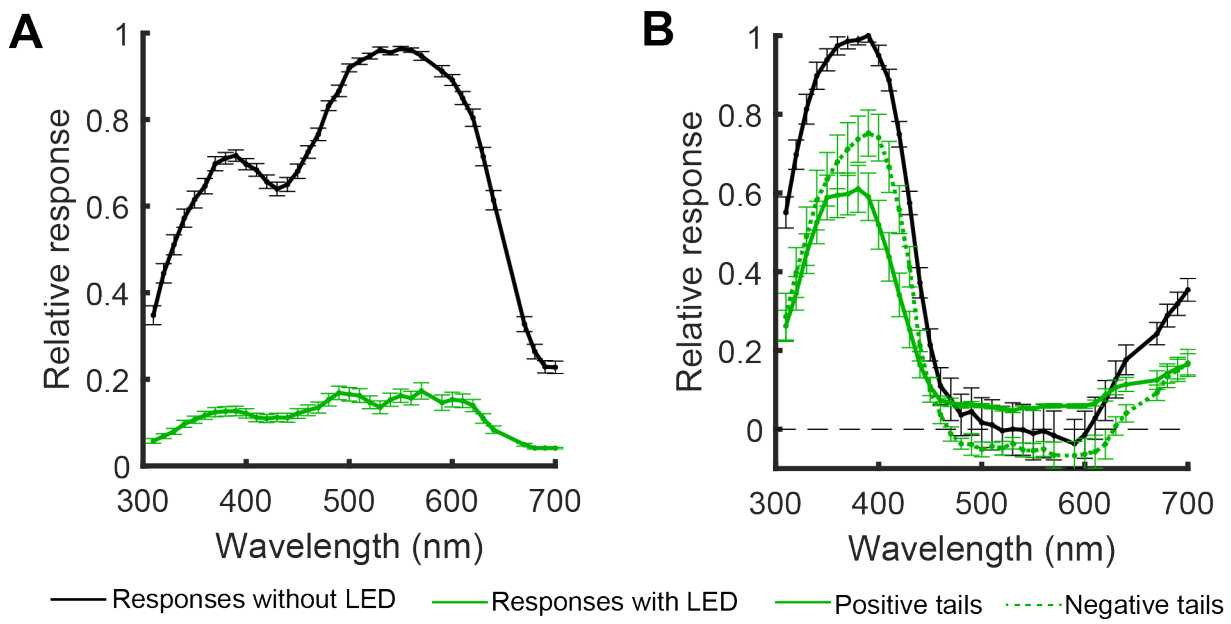

Figure 2.25: Photoreceptor tuning curves in the presence of green LEDs
A, B) Voltage responses were measured in A) green cells and B) UV cells in the absence and presence of LEDs simulating natural light conditions.

2.26C). The resting potential of UV photoreceptors with positive tails were not significantly affected by the LEDs ($t_{17} = 1.7, p = 0.10$). Response magnitudes were decreased for nearly every UV photoreceptor when the LEDs were turned on. For photoreceptors with negative tails and maximum light intensity, the LEDs reduced the λ_{Max} response to 78.8 $\pm$ 18.0% of the response without LEDs (Fig. 2.26B). LEDs attenuated the response of photoreceptors with positive tails significantly more ($t_{29} = 2.4, p = 0.01$, Cohen's d = 0.77) to 65.1 $\pm$ 17.6% of the maximum response.

Responses at λ_{Max} to different light intensities showed that the true effect of the LEDs on UV photoreceptor responses was unclear (Fig. 2.26A). In the absence of the LEDs, UV photoreceptor responses began to saturate at the highest light intensities. In contrast, responses in the presence of the LEDs were still in the linear part of the response curve at the highest light intensity. Thus, it is unclear if the LEDs lowered the maximum response of a photoreceptor, shifted the intensity needed to elicit a half maximum response, or both.

Together, these results showed that long wavelength light influences the responses of UV

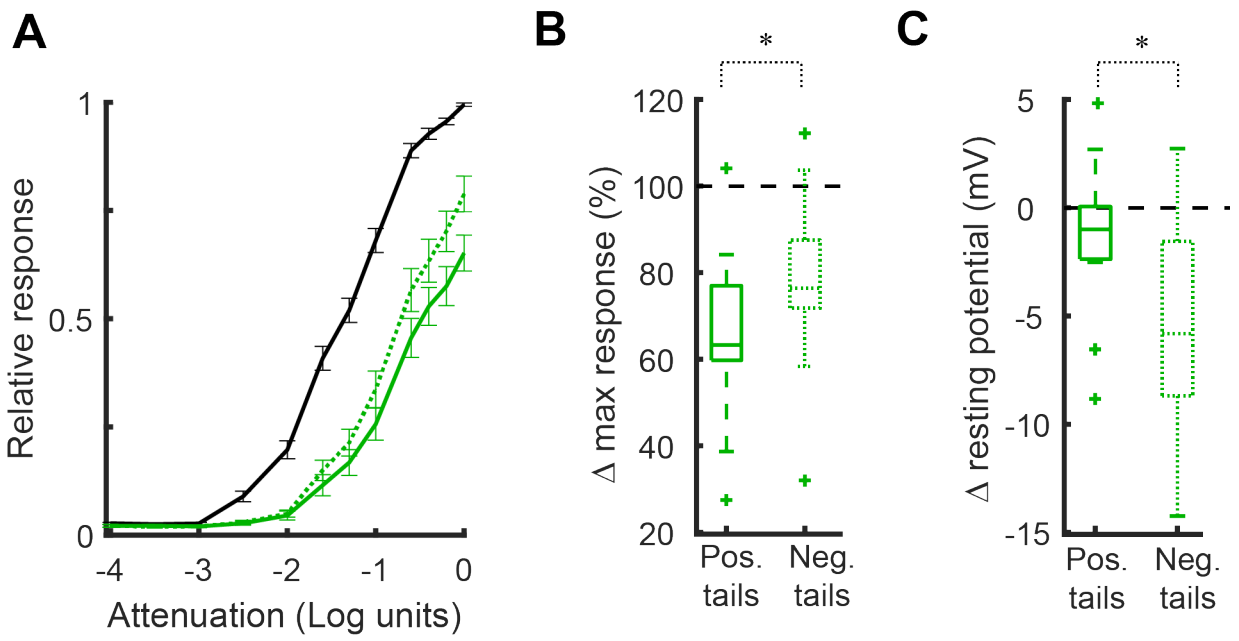

Figure 2.26: Effect of green LEDs on photoreceptor responses
A) Voltage responses to λ_{Max} was measured over 4 log units of light intensity in the presence and absence of LEDs simulating natural light conditions.
B) The change in voltage response at 0 log units of attenuation was quantified.
C) The change in resting potential after turning on the LED was measured and different for UV cells with positive and negative tails.

photoreceptors. A 13% difference in response magnitude for positive and negative tailed cells seems modest, and how it might influence downstream circuits is unclear. This small difference might also be underestimated due to the lack of response saturation in the presence of the LEDs. This effect could also be amplified and have a compound effect with any potential effects on synaptic transmission that inhibition from LW photoreceptors might have.

2.3.4 Photoreceptor temporal dynamics

Finally, I noticed throughout my recordings that photoreceptors appeared to have different temporal responses depending on spectral sensitivity. I explored this observed difference by measuring the temporal response of photoreceptors to 25 ms flashes of light at λ_{Max} and the highest light intensity (Fig. 2.27). The slope of the onset response did not differ between

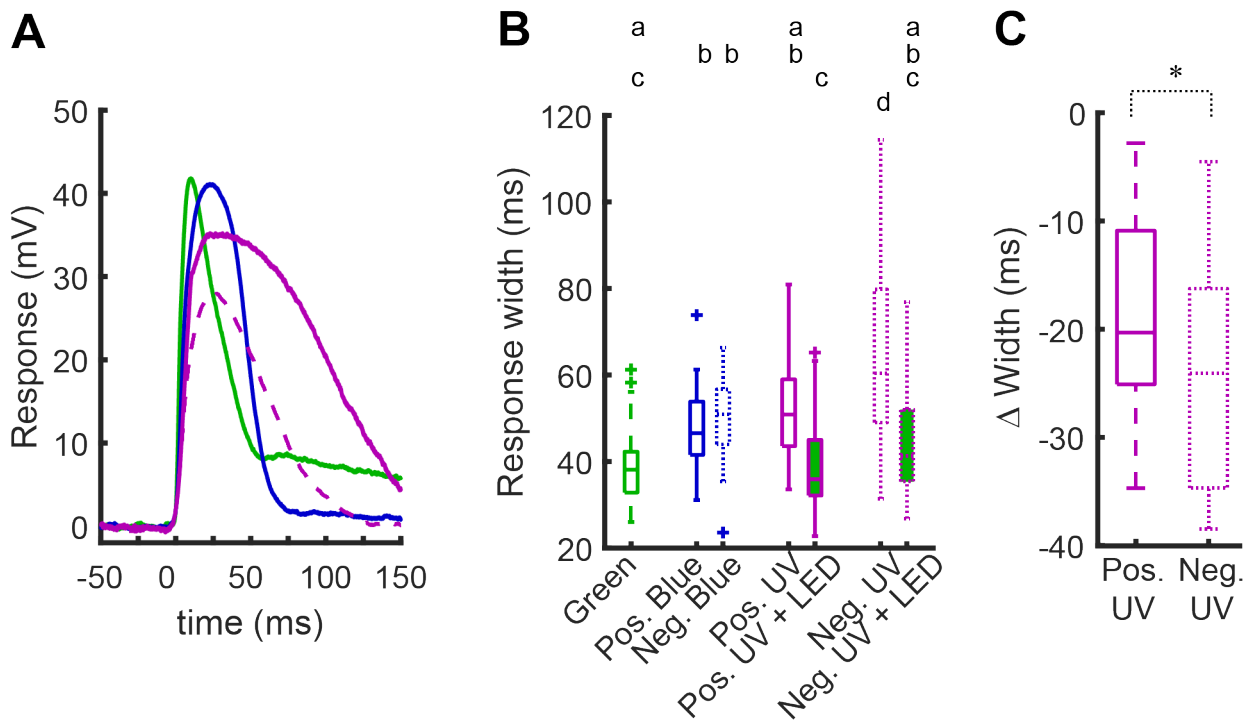

Figure 2.27: Temporal dynamics of photoreceptor responses
A) Example traces show the response of green, blue, and UV photoreceptors to the λ_{Max} stimulus.
B) The temporal width of photoreceptor responses at λ_{Max} was measured as the time spent voltage was above 50% of the maximum.
C) The presence of an LED decreased response widths in UV photoreceptors to match the temporal response of green photoreceptors.

cell types, but the decay time did. I quantified this by measuring the length of time the voltage response of a had a response voltage greater than 50% of the maximum.

The temporal width of a photoreceptor response varied with the type of opsin it expressed (Fig. 2.27B, $F_{6,328} = 29.92$, $p < 0.001$). Green photoreceptors had the narrowest response profile, with a temporal width of 38.2 ± 7.3 ms. All blue cells and UV cells with positive tails had significantly longer response widths of 50.5 ± 10.3 ms (Tukey's HSD, $p < 0.01$). UV photoreceptors with negative tails had the widest temporal responses, with an average of 64.9 ± 19.4 ms (Tukey's HSD, $p < 0.001$). Response widths for these UV photoreceptors could be over 100 ms, with a relatively continuous distribution across the range of observed temporal profiles. The presence of the green LEDs decreased the response widths of UV

photoreceptors, and widths were not significantly different from green (Tukey's HSD, $p > 0.05$). Blue photoreceptor tuning curves overlapped with the 534 nm LEDs too much to conduct a similar analysis, but I would expect a similar result for these cells.

2.4 Discussion

Vision is the primary sensory modality mediating courtship behavior in *Heliconius* butterflies. With limited understanding of *Heliconius* visual perception and its neural basis, characterizing the functional organization of the eye and determining the visual information broadly available to the central brain was an important first step in studying the neural basis for male courtship preferences. Additionally, differential expression of the candidate mate choice gene, sens2, in the eyes of white and yellow males indicated that the peripheral visual system might be a source of circuit differences contributing to male choice. Here, I used a combination of electrophysiology, eyeshine, and antibody staining to provide a relatively complete picture of eye organization in the cydno clade of *Heliconius*. Considering that these closely related butterflies appear to have similar ecological niches and habitats, my experiments identified a surprising amount of diversity in eye organization.

2.4.1 Photoreceptor spectral sensitivity

The *Heliconius* genome encodes four different opsin proteins sensitive to wavelengths between 300 and 700 nm [125]. Across the genus different species consistently express the blue and LW opsins, with the LW opsin combining with red screening pigment to generate a distinct and behaviorally relevant red photoreceptor [115, 127]. Expression of either the ancestral UV1 or derived, genus-specific UV2 opsin, in contrast, varies substantially across the genus [127].

Within the group of butterflies I examined, UV spectral sensitivity varied substantially and relatively continuously between 350 and 400 nm. The combination of electrophysiol-

ogy, qPCR, and antibody staining pointed towards variable levels of UV1 and UV2 co-expression leading to tuning differences between cells. Co-expression of multiple opsins has been observed in several butterfly species [119, 123, 124, 133, 141]. Expression of UV1 and UV2 in different photoreceptors of an individual is relatively common in *Heliconius*, but co-expression in the same photoreceptor has only been detected in the eye of female *H. doris* [127]. The biological relevance and the degree to which co-expression levels are precisely controlled within an individual are interesting questions worthy of future investigation.

There was an intriguing trend relating UV opsin expression to mate preference in my data. In general, groups with stronger preferences for yellow females typically had stronger expression of UV2. However, the lack of differences between white and yellow *H.c. alithea*, the simple convolution between wing reflectance and photoreceptor sensitivity, and sens2 expression most likely in LW photoreceptors all point towards this relationship being correlative rather than causal. Regardless, this trend cannot be entirely discounted without a more thorough investigation.

This relationship between UV opsin expression and color preference is consistent with an alternative hypothesis about the genus-wide function of UV2. The 3-OHK based yellow pigment is unique to *Heliconius* and the spectral reflectance differs substantially from yellow pigments in non-*Heliconius* species [125]. Although direct behavioral evidence is lacking, substantial circumstantial evidence including a modeling study indicates that UV2 is better than UV1 for discriminating the two types of yellow pigment [128, 142]. Males that prefer yellow females would then benefit from expressing UV2, while UV1 may be optimal for non-courtship behaviors and preferentially expressed in other males. If true, it is unclear why some butterflies such as *H. erato* express UV1 and UV2 in different photoreceptors, while the cydno butterflies here co-express the two in the same photoreceptors.

Blue photoreceptors also showed a degree of spectral tuning differences. In particular, *H. pachinus* males had blue photoreceptors with a λ_{Max} that was shifted to longer wavelengths by 8 nm. Protein sequences are the same across groups, so opsin differences cannot

explain this variability. One possibility is that, since photoreceptors share a rhabdom, UV photoreceptors act analogously to a screening pigment by absorbing short wavelength light before it reaches a blue photoreceptor [143]. Since UV photoreceptors for *H. pachinus* males had the longest λ_{Max} that was not significantly different from the expected tuning of UV2, absorbance of slightly longer wavelength light could lead to this apparent shift in tuning. The cause of the large, 20 nm difference in blue tuning between my recordings and recordings from *H. erato* [126] is unclear, but a similar phenomenon of optical coupling in the rhabdom could play a role.

2.4.2 Origin of tail tuning

UV and blue photoreceptors had residual tail tuning that cannot be explained by standard rhodopsin tuning templates. Positive tails were somewhat understandable, as the depolarizing response matches the expected response of a photoreceptor responding to a visual stimulus. For stimuli $>$ 650 nm, cells with negative tails returned to positive, suggesting that the residual depolarizing responses are the default tuning state of the photoreceptors. However, the tuning of this positive tail was abnormally long and flat, particularly for UV photoreceptors. It is unclear where this tail originates, and a previous report of positive tails in photoreceptors was similarly unable to identify a possible source [120]. Sensitizing pigments have been identified in the R1-6 photoreceptors of *Drosophila* that contribute to UV sensitivity in LW sensitive cells [144, 145]. A similar mechanism may play a role here, although there is no prior data to support this claim.

Latency measurements indicated that negative tails most likely originate from monosynaptic inhibition. The wavelengths evoking hyperpolarizing responses overlapped substantially with green photoreceptor tuning, suggesting LW photoreceptors as the specific source. Green photoreceptors most likely form synaptic connections with the UV photoreceptors, and a contribution from red photoreceptors is unclear but possible. Synapses from green or red is unclear for the blue cells with negative tails. These connections may serve a similar

function to horizontal cells found in the vertebrate retina.

Similar reports of negative tails indicative of synaptic inhibition have also been reported for the butterflies *T.a. formosanus* [120], *P. aegeus* [146], and *P. xuthus* [140]. All of these studies found inhibition of blue photoreceptors specifically, while my experiments are the first to detect inhibition of UV photoreceptors. Electron microscopy in the lamina of *P. xuthus* has provided a potential anatomical correlate of these responses, finding synapse like structures between photoreceptors [103]. A more recent investigation specifically interested in the possibility of inhibition between photoreceptors used antibody staining for the two known histamine channels in the optic lobes of *P. xuthus*. Photoreceptor axons were found to express the *Drosophila* homolog of the HisCl1 channel, which was previously known to be expressed only in glia [140].

2.4.3 Tail tuning and courtship

White and yellow wings differ primarily in the presence and absence of short wavelength reflectance. Discriminating the two colors is most likely a simple task for the butterflies just like it is for humans. Courtship preference, however, is complex decision and behavior rather than a simple discrimination. To shift the preference from one color to the other would likely require a more substantial transformation of sensory information than simple, small shifts in spectral sensitivity or photoreceptor type distributions.

Differences in UV photoreceptor tail tuning that likely correspond to differences in synaptic connectivity provide the potential for a large change in sensory processing. The differential expression of sens2 presumably in LW photoreceptors of white and yellow males lends further support to the role of peripheral synaptic connectivity in mate preference. Males preferring white females generally lacked inhibition of UV photoreceptors, while UV photoreceptors for yellow preferring males usually showed signatures of inhibition. Males without preference showed an even mix of positive and negative tails. The molecular mechanism of sens2 action is unknown, but it is predicted to be a transcription factor that may cause the expression of

synapse forming proteins. How butterflies have different proportions of positive and negative tails rather than all or none is also unclear. There could be stochastic expression with biased probabilities of sens2 expression due to the SNPs identified in the GWAS. Such a mechanism would be similar to the stochastic, cell-autonomous decision of the R1 and R2 photoreceptors to express either a UV or blue opsin [105].

Synaptic inhibition in the periphery could have a multitude of large and small effects on sensory processing. The central brain processing associated with mate choice or visual behavior in *Heliconius* is effectively completely unknown except for a couple studies of gross anatomy [147, 148]. Speculating on the possible downstream effectors of mate choice and generating a model would likely be relatively easy but so unconstrained that it would be biologically uninformative.

2.4.4 Vision in a natural environment

Butterflies are highly visual, diurnal animals that live in complex natural environments. The butterflies examined here generally live in heavily forested regions of the neotropics. Of particular interest to behavior and perception related to eye organization is that short wavelength light is limited in a natural environment. The forested habitats of these butterflies further decreases the relative amount of short wavelength light. The eyes of *Heliconius* may be adapted to these differences in ambient light levels in natural environments.

Differences in the ambient light conditions could be related to the slight differences I observed in the distribution of UV and blue photoreceptors. Most groups I examined had between 50 and 60% of the R1 and R2 photoreceptors expressing blue rhodopsin, but *H.c. galanthus* increased significantly to more than 70% blue. Behavioral experiments have shown that one subspecies of *H. cydno* preferentially choose habitats that are shaded rather than in open sunlight (Brett Seymoure, unpublished data). This might decrease the need and usefulness of UV photoreceptors for these butterflies, leading to less UV opsin expression. However, these comparisons were between distantly related species and careful comparisons

within the cydno clade or butterflies with known opsin distributions have not been conducted.

The temporal dynamics of photoreceptor responses may also be tuned to natural conditions. In my experiments that were primarily conducted in a dark adapted state, different photoreceptor types had different temporal response profiles. Green photoreceptors were the narrowest and followed the stimulus with relatively good fidelity. Blue and UV photoreceptors, in contrast, had responses that were temporally extended, especially for UV photoreceptors with negative tails. However, simulating natural conditions with the LEDs narrowed the temporal response of UV photoreceptors to match green photoreceptors.

One possible explanation for this is that the molecular biology of individual photoreceptors changes to account for these differences in temporal response. Green LEDs simulated natural conditions and led to significant decreases in the temporal response of UV photoreceptors. If the cellular biology of every photoreceptor was the same, UV photoreceptors might then have severely truncated temporal responses in a natural environment. However, different photoreceptor types may have different cellular compositions that account for this effect. For natural conditions to evoke similar temporal responses across cell types, UV photoreceptors would need to have temporally extended responses as the default, which is what I observed in my experiments using unnatural, dark adapted conditions.

2.4.5 Sexual dimorphism

Every aspect of eye organization that I examined was sexually dimorphic. In each case, male eyes varied substantially with species, but female eyes were similar regardless of species or wing color. These dimorphic features of the eye suggest a role in a dimorphic behavior such as courtship. Both the UV photoreceptor sensitivity and UV tail tuning appeared related to different aspects of courtship behavior. Large differences in eyeshine, however, had no clear relationship to courtship. Eyeshine could instead be related to a different sexually dimorphic behavior.

An alternative dimorphic behavior that might be responsible for the similarities across

females is egg laying. Females lay eggs exclusively on *Passiflora* plants, and choosing good plants plays an important role in lifetime fitness. Anecdotal experience from rearing butterflies in a green house suggests that *Heliconius* females are very picky about what plants they use. In some cases, it seemed that females might prefer not to lay eggs over laying eggs on poor quality host plants. Vision is probably an important sensory modality for this behavioral decision, and female eyes may be optimized for this task. Male eyes would then be more free to vary with respect to natural light conditions.

2.4.6 Future directions

An important next step in understanding the neural mechanism of courtship preference is to confirm the role of tail tuning in courtship behavior. One approach to achieve this would be to knock out sens2 expression in males that typically prefer white females and ask if both courtship behavior and UV photoreceptor tail tuning change. If sens2 is important for courtship preferences, the lack of this gene should increase the attractiveness of yellow females to *H.c. galanthus* and also increase the proportion of UV cells with negative tails. Antibody staining for sens2 in the central brains of white and yellow butterflies is also needed to assess if sens2 might affect courtship in multiple brain regions.

Second, direct experimental evidence is needed to confirm that negative tails are in fact created through monosynaptic inhibition from LW photoreceptors. Response latencies, different proportions among groups, and sens2 expression all suggest that it is, but each of these results is subject to noise or error. Anatomical studies could first be used and compared to the results from *P. xuthus* [103, 140]. Physiological evidence could also be gained through the use of histamine antagonists or agonists. Antagonists should eliminate the negative tail and have no effect on positive tail cells. Agonists, in contrast, should give results similar to the LED experiments. Effects on positive tail cells would be less clear, as all UV photoreceptors may express histamine channels, but only some may have synaptic connections.

A final step would be to investigate the overall neural basis for courtship behavior and how these peripheral changes might influence downstream circuitry. This would require gaining experimental access to a potential mate choice circuit. In *Drosophila*, the transcription factor Fruitless is expressed in approximately 2,000 neurons that are both necessary and sufficient for courtship behavior [83]. This expression is also sexually dimorphic, limited to only males. Extensive work in *Drosophila* has shown that this transcription factor specifies and marks almost the entire courtship circuit [149].

Work on Fruitless outside of *Drosophila* is limited, but siRNA knockdowns of this gene in developing locusts also impairs courtship [82]. Locusts are hemimetabolous insects that diverged from holometabolous insects more than 350 million years ago, suggesting deep homology of this gene and its role in courtship. A first step to gaining access to the *Heliconius* courtship circuit would be to confirm the role of Fruitless using a CRISPR knockdown. Assuming that is successful, integrations of of either GFP or gCaMP would facilitate study of a circuit potentially dedicated to mating behavior.

2.5 Methods

Animals

The animals used in this study were reared in a greenhouse at the University of Chicago, and the population was regularly supplemented with shipments from breeders located in South America. The *H.c. galanthus*, *H. pachinus*, and *H. melpomene* were from Costa Rica, while *H.c. alithea* were from Ecuador. Exact age of each experimental animal was unknown, but butterflies were at least 3 days old, and the best data typically came from individuals without naturally occurring wing damage suggesting they were relatively young.

For all experiments, butterflies were prepared in the same way under a dissecting microscope using beeswax containing a small amount of Canada balsam that increased wax viscosity. For each step, a metal spatula was heated with an alcohol lamp and a small amount of wax was melted onto it. I first removed the legs, waxed the abdomen to the thorax, and waxed the wings together and to the thorax. The butterfly was then placed in a collar made from electron microscope film with the tip folded at 90 degrees. In the folded edge was a small rounded triangular cut that snugly held the butterfly neck in place. The butterfly was then waxed to the collar by its belly and its 'shoulders'. The head was then stabilized by waxing the mouth parts to the collar and finally a small amount of wax behind each eye. A light push with a forceps on the head capsule that resulted in no head movement meant that the butterfly was well restrained.

2.5.1 qPCR

Eyes were dissected from a butterfly with a razor blade, immediately placed in RNAlater and stored at $-80°C$. Prior to mRNA extraction, eyes were repeatedly washed and spun in a centrifuge to remove residual RNAlater. mRNA was then extracted and converted to cDNA using a standard kit (Qiagen). Expression levels for UV1, UV2, blue, and green rhodopsin mRNA were measured using qPCR with SYBR green. Primers for each opsin

Primer	
UV1 Forward	5'-CGCTCACTGTGTGCTTCCTCTT-3'
UV1 Reverse	5'-AGTCTTGCAAGCTACCGCGG-3'
UV2 Forward	5'-TACCGTGTGCTTCCTTTATGTTG-3'
UV2 Reverse	5'-ACCCTTGCAAGCGATCGCAG-3'
Blue Forward	5'-TGCGACATATTTGCCGTGCT-3'
Blue Reverse	5'-GAGACGCCTGCACTCTGTTC-3'
Green Forward	5'-GATGTTCATGATGGCACCGC-3'
Green Reverse	5'-CATTGTAGCGGTCGAAAGCG-3'

Table 2.2: qPCR primers

are shown in table 2.2. Each primer was tested for specificity using Sanger sequencing and efficient amplification using qPCR with serial 10 fold dilutions of genomic DNA. For each individual, all primers were tested on the same qPCR plate in triplicate. Results with standard deviations greater than 1 across the replicates were discarded and tested again. Relative expression level differences were then measured as the difference in PCR cycles to reach threshold for two different genes.

2.5.2 Antibody staining

The eyes of restrained butterflies were dissected into 0.01 M phosphate buffered saline (PBS) using a razor blade. Excess cuticle, fat, and tracheae were removed from the eye. A small amount of cuticle was left attached and served as landmarks for identifying the dorsal-ventral axis of the eye. Dissected eyes were then transferred to 4% paraformaldehyde in PBS for 15 minutes. Fixed eyes were then cryoprotected in a solution of 25% sucrose in PBS overnight at 4° C. *Heliconius* eyes float in both the fixative and sucrose, so eyes were submerged using a plastic mesh grid.

Thin eye sections for antibody staining were cut using a cryostat. An eye was coated in a small droplet of TissueTek OCT and frozen at −20° C. The eye was oriented to slice the middle and slightly ventral part of the eye. The first 5-10 sections that stained well as cross sections were sliced at 14 μm and placed on adhesive slides (SuperFrost Plus, Fisher Scientific). Longitudinal sections from deeper in the eye were difficult to slice due to the

presence of lens, retina, and neural tissue with different degrees of density and hardness, so slices were increased to 20-25 μm.

Eyes were stained with antibodies specific to UV1, UV2, and blue or sens2. Animal injections, serum collection, and affinity purification were performed by GenScript for each antibody. UV1 and UV2 antibodies targeted the same but divergent N-terminal portion of the protein. UV1 antibodies were made in guinea pig against the peptide DGLDSVDLAVIPEH, and UV2 antibodies were made in mouse against the peptide AISHPKYRQELQRRMP. Blue antibodies were a gift from Michael Perry and were made in rabbit against the peptide INHPRYRAELQKRLPC. The blue antibody was used on butterflies that were at least 3 days old, while sens2 was used on butterflies that were less than 12 hours old.

Eyes were stained on slides in a humid chamber using a 2 day procedure. Slides were first washed for 5 minutes in cold acetone, 3 X 10 minutes in PBS, and 3 X 10 minutes in 0.3% Triton X-100 in PBS (PBST). These washing steps removed excess melanin from the eyes. Slides were then washed for 5 minutes in 1% sodium dodecyl sulfate in PBS as an antigen retrieval step and 3 X 10 minutes in PBST. Slides were then blocked for 1 hour in 1% bovine serum albumin (BSA) in PBS. Primary antibodies, all at a 1:300 dilution in blocking solution, were then applied overnight at 4° C. Prior to staining with secondary antibodies, eyes were first washed 5 X 10 minutes in PBST. Goat anti-rabbit Alexafluor 488 (Abcam), donkey anti-guinea pig Alexafluor 555 (Abcam), and donkey anti-mouse Alexafluor 647 (Abcam) were all diluted 1:2000 in blocking solution and slides were stained for 2 hours at room temperature. After staining, slides were washed 6 X 10 minutes in PBST and stored for imaging using a coverslip and Polymount (Fisher Scientific). Stained eyes were imaged using a Zeiss LSM 510 confocal microscope using a 20X objective. Minor adjustments in contrast and brightness were made using ImageJ [150].

The distribution of UV-UV, blue-blue, and UV-blue ommatidia were counted using an automated MatLab program and checked visually. First, binary images of the UV stain, blue stain, and merged stain were generated in imageJ. In MatLab, ommatidia were detected from

the merged binary image using the program bwareafilt. Minimum and maximum sizes were used to exclude noise, typically only analyzing clusters that were between 20 and 200 pixels in size. The binary UV and blue images were then analyzed to determine if each ommatidia contained that opsin. Blue typically had lots of background staining, so at least 10% of the pixels defining an ommatidium needed fluorescence of an opsin to be considered expressed.

2.5.3 Electrophysiology

Recording apparatus

After butterflies were restrained in the collar, a small triangular hole was cut in the dorsal eye using a razor blade, with the hole positioned such that the electrode would pass through a relatively distal part of the eye. A small drop of silicon grease was applied immediately to prevent desiccation. A silver chloride reference electrode was inserted in a small hole cut in the anterior portion of the head capsule that avoided the central brain. The butterfly was then placed in a Faraday cage with the eye positioned at the center of a Cardan arm perimeter device. This device is a pair of rotational platforms with a 3-D printed arm that created an imaginary sphere holding the light source a fixed distance from the eye.

Photoreceptor responses were evoked using monochromatic light. The light source was a combination of a 26 W deuterium lamp and 20 W halogen lamp that primarily provide UV and human visible light, respectively (DH-2000S, Ocean Optics). This white light was connected to a scanning monochromator with 1 nm resolution and a full width half maximum of 4 nm using a 1 mm fiber optic cable. The output of the monochromator was connected to the Cardan arm perimeter device using two more 1 mm fiber optic cables and an optical shutter (OZ optics). The Cardan arm was equipped with a collimator and lens that had a 4 cm focal length (Edmund Optics).

Stimuli ranged from 310-700 nm in 10 nm steps. The deuterium lamp created high and unstable intensities at 590, 650, and 660 nm, so these were excluded from experiments. The

intensity of each stimulus was calibrated to 1.5 X 10^{15} photons/cm^2/s using a variable neutral density filter in a rotational motor (Newport) mounted on the Cardan arm perimeter device between the lens and the butterfly. Stimulus intensity was calibrated before each experiment using a photodiode (Newport) placed at the location of the butterfly eye. The light source also had a filter holder that allowed for light attenuation between 0 and 4 log units.

Experimental procedure

Photoreceptor responses were recorded using intracellular sharp electrodes. Electrodes were pulled from borosilicate glass with a 1.0 mm outer diameter and 0.5 mm inner diameter using a P-97 electrode puller and 2.5 mm box filament (Sutter instruments). Electrodes were pulled to a resistance between 90 and 120 MΩ and filled with 3 M KCl. Exact parameters for electrode creation varied over time and new filaments, but were generally around ramp + 10, pull 65, velocity 70, delay 100, and pressure 350. Electrode recordings were amplified by a 0.1X headstage and high impedance amplifier (AxoClamp 900A, Molecular Devices) and digitized at 10 kHz (DigiData1550, Molecular Devices). Responses were collected and saved as 600 ms trials using Clampex.

The electrode moved along the dorsal-ventral axis of the eye using a micromanipulator (Sutter Instruments), passing through the approximate center of the eye. Recordings were made primarily from the ventral half of the eye. When a photoreceptor was penetrated by the electrode, the baseline voltage dropped to between -40 and -60 mV and hyperpolarizing ERG responses changed to a depolarizing response. Typically only cells with at least a 25 mV response to light were recorded. This threshold was relaxed to 15 mV for UV photoreceptors in order to better estimate the percent of positive and negative tails in an individual. The maximum voltage response did not affect the probability of observing a positive or negative tail.

Photoreceptor responses to monochromatic stimuli were presented in a pseudo-random order using an automated program written in MatLab. Light flashes of 25 ms were presented

with 3 s between each trial, which was sufficient to prevent adaptation. Each stimulus was presented four times, and the standard deviation of the response was typically less than 1 mV. When possible, photoreceptor responses were recorded for multiple levels of overall log attenuation.

In addition to recording photoreceptor tuning curves, I also measured the relationship between the voltage response and light intensity (V-Log(I) curves). After recording the tuning curve, I identified the wavelength that evoked the largest response. I then recorded the response to this stimulus for 12 different intensities ranging from full intensity to 4 log units of attenuation. Similar to the tuning curves, each V-Log(I) curve had 4 trials separated by 3 s.

For some green and UV photoreceptors that maintained stable recordings over long periods, I also measured the responses to monochromatic stimuli in the presence of green LEDs meant to simulate natural daylight. Surrounding the stimulating lens were 6 LEDs with peak tuning at 534 nm and a full width half maximum of 12 nm, with an intensity of 3.2 X 10^{15} photons/cm^2/s. Prior to presenting monochromatic stimuli, LEDs were turned on for 15 s. Tuning curves and V-Log(I) curves were measured in the same way described above. Responses were measured again after turning off the LEDs, and data for photoreceptors that failed to recover at least 80% of the original response were discarded.

Data analysis of tuning curves

One issue with recording the response to isoquantal stimuli is that photoreceptors have a saturating non-linearity. This non-linearity causes the observed width of photoreceptor tuning to be affected by stimulus intensity. To control for this, photoreceptor response curves were transformed into sensitivity curves by fitting the data with the Naka-Rushton equation (equation 2.1), which is essentially a modified Hill equation. This transformation normalizes the width of photoreceptor tuning (Fig. 2.28) and is standard for the field.

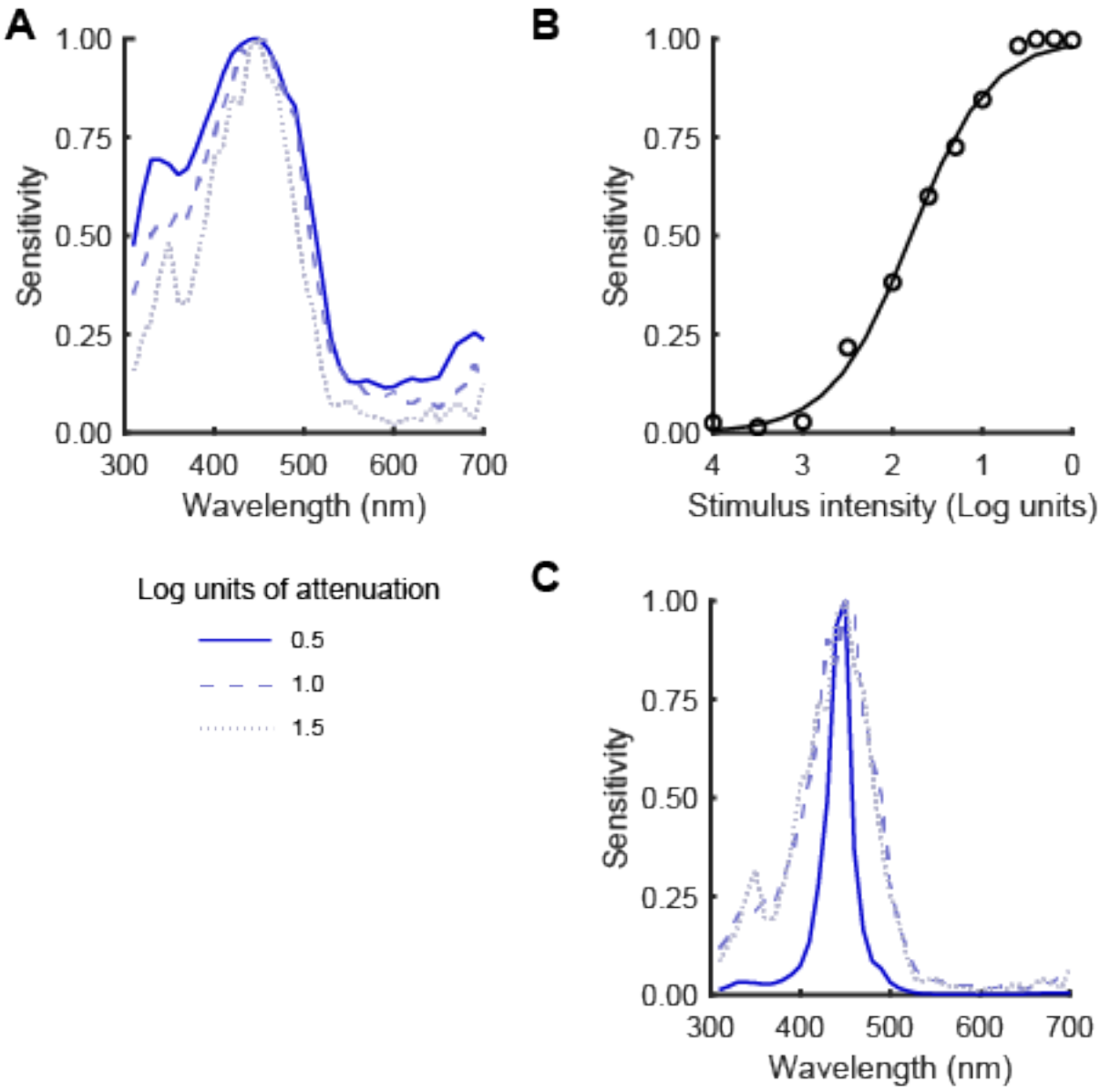

Figure 2.28: Naka-Rushton transformation
A) Responses to monochromatic light were measured at 3 intensities for this blue photoreceptor. Response amplitudes are normalized to 1 to show the effect of intensity on tuning width.
B) A V-Log(I) curve was generated in response to 450 nm for this photoreceptor and fit with the Naka-Rushton equation.
C) Tuning curves in A were adjusted using the fit parameters from the V-Log(I) curve. Intensities that are too high lead to abnormally narrow tuning curves. Intensities in the linear part of the V-Log(I) curve get adjusted to similar widths.

$$\frac{V}{V_{Max}} = \frac{I^n}{(I^n + K^n)} \tag{2.1}$$

I fit these spectral sensitivity curves with an established rhodopsin template [130, 131]. This model has 11 parameters that describe the shape of the tuning curve for a photoreceptor (Equations 2.2 to 2.6, but λ_{Max} was the only free parameter that varies between cells.

$$S = \frac{1}{[e^{A(a-x)} + e^{(B(b-x)} + exp^{C(c-x)} + D]} + A_\beta exp\frac{-(\lambda - \lambda_\beta)^2}{d} \tag{2.2}$$

$$x = \frac{\lambda_{Max}}{\lambda} \tag{2.3}$$

$$a = 0.8795 + 0.0459e\frac{-(\lambda_{Max} - 300)^2}{11940} \tag{2.4}$$

$$\lambda_\beta = 189 + 0.315\lambda_{Max} \tag{2.5}$$

$$d = -40.5 + 0.195\lambda_{max} \tag{2.6}$$

and constants A = 69.7, B = 28, b = 0.922, C = -14.9, c=1.104, D = 0.674, and A_β = 0.26. For UV photoreceptors, I set A_β = 0, and thus only fit the alpha peak of the photoreceptor.

I also used this template to ask if UV photoreceptor responses had both UV1 and UV2 components. For this analysis, I assumed that photoreceptor responses in *H. erato* represented exclusively UV1 or UV2 rhodopsin tuning, which would be consistent with RNA-Seq results. I used this data to generate a UV1 template and a UV2 template with tuning centers of 356 nm and 390 nm, respectively and fit equation 2.7 to each individual cell, with a and b representing the relative contribution of each gene to the response of a photoreceptor and

c is a normalizing factor that adjusts response amplitude.

$$S = \frac{a * UV1 + b * UV2}{c} \tag{2.7}$$

Tail tuning analysis

Response latencies were measured as the time from light onset to response onset. TTL pulses controlling the light shutter were split and sent to the computer in addition to the shutter. Using the photodiode, light onset consistently occurred 11.9 ± 0.1 ms after sending the TTL pulse. To measure response latency, the standard deviation of the resting potential was measured over the 100 ms preceding the TTL pulse. Response onset was then defined as the time for voltage response to first exceed five times this baseline variability.

2.5.4 Eyeshine

Apparatus

Eyeshine images were collected using a custom built epi-fluorescent microscope based on a previously published design (Fig. 2.29) [106]. This procedure makes use of a reflective tapetum in the back of the eye, as incident light that is not absorbed by rhodopsin or screening pigments exits the eye as a colored eye shine. This eye shine was then imaged using a 20X objective with a 0.4 numerical aperture (Zeiss LD-Plan-Neofluar). Two arms of the microscope that create the light beam and magnify the image are connected by a half silvered mirror.

In the vertical arm of the microscope, a collimated white light source was expanded and re-collimated. Light entered the microscope through a fiber optic cable and collimator connected to the same halogen-deuterium lamp described above. Because the light source was effectively a point source, this arm served to expand this light beam by two lenses with focal lengths 4.0 and 8.0 mm placed confocal to each other. An adjustable diaphragm was

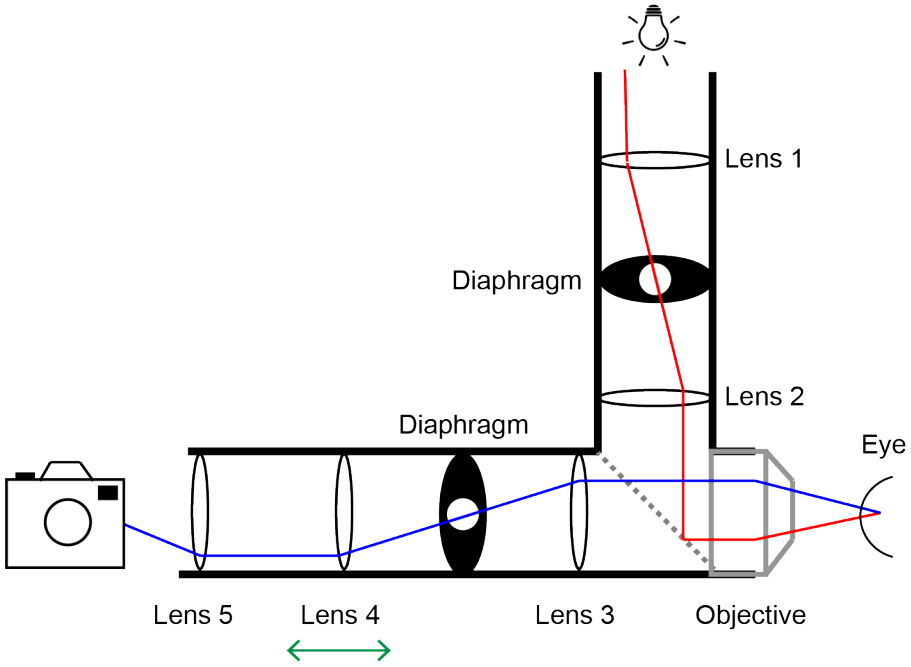

Figure 2.29: Diagram of eyeshine microscope
The eye was imaged by a 20X microscope objective with a high numerical aperture and long working distance. In the vertical arm of the microscope, a point source of white light is expanded and collimated by lenses 1 and 2, which are placed confocal to each other. Light reflects off a tapetum in the butterfly eye, and light that is not absorbed by rhodopsin or screening pigments re-enters the microscope. Lenses 3 and 4 in the horizontal arm, which are confocal to each other, magnify the image, which is then photographed. Diaphragms are placed in the focal plane of all lenses to limit background illumination. The arrow under lens 4 indicates that the exact position varies from image to image to focus the image. Red and blue lines show the light path before and after entering the eye, respectively.

placed at the focal point of both lenses to control the amount of background light.

In the second arm of the microscope, the eyeshine was imaged by a digital camera (Canon EOS Rebel T5). Two lenses with focal lengths of 8.0 and 2.0 mm were used to magnify the eyeshine image. These lenses were approximately confocal with each other. However, the best focused images typically required small adjustments in the location of the second lens for unknown reasons. A diaphragm between these two lenses was adjusted in order to eliminate background illumination. This magnified image was then photographed by a a lens with a 12.0 mm focal length immediately adjacent to an infinity focused digital camera.

Experimental procedure

Butterflies were restrained in the collar and placed on a rotating platform in front of the microscope. The eye was positioned near the axis of rotation, but precision was not necessary. The rotation platform was attached to a a series of linear stages that allowed for adjustments in all three dimensions. To prevent light adaptation that eliminates an observable eyeshine, light was applied as 1 s flashes with 5 s between flashes.

Eyeshine images were collected along the entire dorsal-ventral axis of the eye. Eyeshine was first located in the dorsal eye adjacent to the head capsule. The butterfly and lens 4 positions were then adjusted until the maximum number of ommatidia were observed and in focus. The eyeshine was then imaged with a shutter time of 300 ms. Image quality was assessed on line and new images were taken until an image with sufficiently high quality was generated. After each area of the eye was imaged, the butterfly was then rotated and positioned. The new location where eyeshine was imaged was close but non-overlapping with the previous image.

Data analysis

To analyze group differences, the number of yellow and red ommatidia were quantified manually. Images for all butterflies were randomized, and the number of red and yellow ommatidia in each image were counted blind to the species, sex, and wing color of the butterfly in each image. Statistical comparisons required deciding how to reduce the set of images for each butterfly to a single percentage of yellow ommatidia. I conducted four analyses by grouping images into the dorsal two images, middle two images, ventral two images, and ventral half of the images. The groups were then compared using a one factor ANOVA and post-hoc t-tests with p-values corrected using Tukey's HSD.

Screening pigment spectral transmittance

The spectral reflectance of screening pigments was measured using images of the eyeshine generated from monochromatic light stimuli and captured by a monochromatic camera. I first located and focused the eyeshine on a region of the eye and took a reference image using the standard eyeshine set up described above. I then switched the DSLR with a monochromatic camera fitted with an infinity focused lens that had millisecond control over the shutter time (Allied Vision Technologies, Model GX1050). Additionally, rather than directly connecting the white light source to the microscope, light was first passed through a monochromator (Monoscan 2000).

The main challenge for this experiment was controlling for light intensity across different wavelengths. The white light source and monochromator resulted in variable intensities that could not be adjusted on the eyeshine microscope. However, preliminary tests using a mirror rather than a butterfly showed that shutter times could be adjusted to account for these differences. Neutral density filters were used to normalize the intensity of each wavelength as much as possible. Remaining differences were accounted for by adjusting the shutter time. Pixel intensities on the camera using a mirror in front of the objective were similar across wavelengths using these dynamic shutter times.

To conduct an experiment, I first positioned the butterfly and generated an eyeshine image using white light and the DSLR as described above. The camera was then switched to the monochromatic camera and the light source was switched to monochromatic. Because the microscope objective was UV-resistant, images were only collected from 400-800 nm in 10 nm steps. Each stimulus was applied for a time that amounted to 1 X 10^{15} photons, which was an average of 6.6 seconds across all stimuli. After all stimuli were presented, the DSLR and white light were again placed on the microscope and a second reference eyeshine was taken to ensure the same location was imaged across the entire experiment.

Eyeshine reflectance spectra were measured using ImageJ. Using the reference eyeshine image, ommatidia were manually selected as either yellow or red. These regions of interest

were then analyzed for pixel intensity for each wavelength of stimulation. Ommatidia with maximum pixel intensities below 50 or above 250 were removed from the analysis. PCA was then used on the reflectance spectra to test for differences. Each wavelength was a variable and each ommatidium was an observation. The first 3 principle components were compared between screening pigment color, species, and sex.

CHAPTER 3

ANCESTRAL COMPUTATIONS CONSTRAIN THE EVOLUTION OF NOVEL COMPUTATIONS

3.1 Abstract

Phylogenetic history has the capacity to constrain and bias future evolutionary trajectories by varying how accessible novel phenotypes are. These constraints may be especially important for the evolution of complex neural circuits mediating diverse animal behaviors. Here, I simulated the evolution of color vision circuits using standard machine learning algorithms to ask how ancestral trichromatic networks influence the performance and computations of tetrachromatic networks. I trained multiple trichromatic networks to simulate different trichromatic ancestors, biologically analogous to butterflies, birds, spiders, etc. The input layer of these trichromatic networks was then mutated to tetrachromatic, simulating the evolution of a novel photoreceptor. Each network was re-trained multiple independent times to simulate multiple independent origins of independent origins of a novel color vision phenotype. Performance metrics showed that trichromatic ancestry did not prohibit the evolution of tetrachromatic vision, but the rate of learning was affected by the specific trichromatic network. Examining the computations implemented by the hidden layer showed that trichromatic ancestry severely constrains tetrachromatic computations to a limited region of the theoretically available computational state space. Together, our network results suggest that phylogenetic history is an important aspect of the functional organization of neural circuits. Considering the role of evolution on neural circuit function could be valuable for improving our understanding of basic principles that dictate brain organization, neural computation, and behavior.

3.2 Introduction

Biological systems such as the nervous system are not constructed as a *de novo* search for optimality [2, 151]. Instead, existing phenotypes are the product of evolutionary processes that are constrained and biased by phylogenetic history [14]. Complex, high dimensional adaptive landscapes may prevent some evolutionary trajectories even if they would be beneficial, while also making other paths more accessible [4, 5]. Examining the interaction between phylogenetic constraints and a purely adaptive view of evolution is is an important aspect of understanding larger patterns of evolution and the observable biodiversity.

Due to the complex organization of neural circuits, phylogenetic history may impose especially strong constraints on the evolution of the brain and behavior [14]. Systems neuroscientists often view neural computation through a perspective that either implicitly or explicitly assumes optimal neural coding. However, constraints may prevent a system from reaching a globally optimal solution. Instead, computations may be implemented in ways that are only locally optimal and not intuitive. For example, the jamming avoidance response in weakly electric *Gymnotiform* fish is elegant in its implementation, but substantially simpler algorithms are theoretically possible [152]. Constraints on the system may be an important factor for the observed computations in this well-studied system. An appreciation and consideration of phylogenetic history and its role in shaping neural circuit structure and function could lead to greater insights into principles defining how nervous systems process information and generate behavior.

Motivated by insect visual systems, color vision represents an attractive system for studying the evolution of neural computation. The ancestral insect eye most likely comprised ultraviolet (UV), blue, and green photoreceptors potentially capable of trichromatic color vision [153]. A common adaptation, most notably in butterflies, is the addition of a fourth, red sensitive photoreceptor used to expand the range of color vision to tetrachromatic [102, 115, 154]. No clear ecological or selective pressures have been identified to explain which insects do and do not have tetrachromatic vision, raising the possibility that evolutionary constraint in-

fluences and possibly impedes color vision evolution [153]. Evolving a new photoreceptor is genetically simple, and the periphery is generally thought to be evolutionarily flexible [22, 122, 155]. A novel photoreceptor alone, however, might be unable to confer expanded and improved color vision. Instead, making use of the novel color dimension may require changes to processing circuits, which is where constraints may be important.

The relatively simple and well-described opponent coding mechanism underlying color vision makes it especially amenable to evolutionary questions. Opponent neurons compare different photoreceptor responses with spectrally antagonistic excitation and inhibition and arise early in visual circuits [156, 157]. In theory, tri- and tetrachromatic vision require only 2 and 3 unique channels, respectively [158, 159, 160], and this simplicity can facilitate comparisons across species and color vision circuits (Fig. 3.1A). Moreover, despite this low dimensional computation, the available computational state space is large, as numerous unique combinations of opponent channel can lead to perceptually equivalent color discrimination [158, 159]. Assuming discrete inputs to an opponent neuron, this leads to an upper bound of 15 and 560 unique ways to implement tri- and tetrachromatic vision, Relaxing this assumption of discrete inputs to continuous can lead to an effectively infinite computational state space. This lack of constraint on how to implement opponent coding means that similarities between independent origins of tetrachromatic vision can more confidently be ascribed to evolutionary rather than computational constraints.

Experimental data on the computations underlying color vision are relatively sparse outside of primates and bees. A long history of color vision research in bees has identified opponent cell types that have every combination of spectral inputs from UV, blue, and green photoreceptors [161], and a recent modeling study suggests the population of color neurons are developed using a random wiring scheme [162]. These cells, however, are a randomly selected subset of the population, and the functional role of these neurons is unclear. While these recordings are valuable, a clear test of evolution would require identifying and comparing homologous neurons [3, 163]. Butterflies have both species diversity in color perception

and the potential to record from a specific subset of neurons, although these experiments are difficult.

For this study, I adopted a theoretical approach using machine learning algorithms to simulate the evolution of color vision. This approach allowed us to simulate numerous trichromatic ancestors and numerous independent origins of tetrachromatic vision for each one. Comparisons of network performance, network computation, and homologous hidden units allowed us to formulate predictions about how phylogenetic history may impact the evolution of novel computations in a neural circuit implementing color vision computations. Overall, the results of my simulations suggest that the evolution of neural computation is heavily constrained by circuit history, with the ancestral trichromatic computation biasing evolved tetrachromatic computations into a severely restricted portion of the theoretically infinite computational state space.

3.3 Model

Feed-forward, 3-layer neural networks were trained to learn color vision computations using a standard backpropagation learning algorithm (Fig. 3.1, see methods for details). The input layer represented an eye with UV, blue, green, and red photoreceptors and responded to monochromatic light stimuli (Fig. 3.1B). Photoreceptor responses were scaled by a random luminance factor to remove brightness as a learnable cue (Fig. 3.S1). The output layer was a filter bank of narrowly tuned Gaussians (Fig. 3.1D) that mimicked wavelength selective neurons found in both insects [164, 165] and primates [166, 167]. Networks had a single hidden layer, and my analyses focused on networks with 30 hidden units, but results were qualitatively similar regardless of hidden layer size (Fig. 3.S1).

Using this simple network design, I simulated color vision evolution using a two stage training procedure (Fig. 3.1C). First, a network was initialized with random starting weights and pre-trained for trichromatic vision with an input layer that had UV, blue, and green photoreceptors. This trained network, mimicking a trichromatic ancestor, was then 'mutated

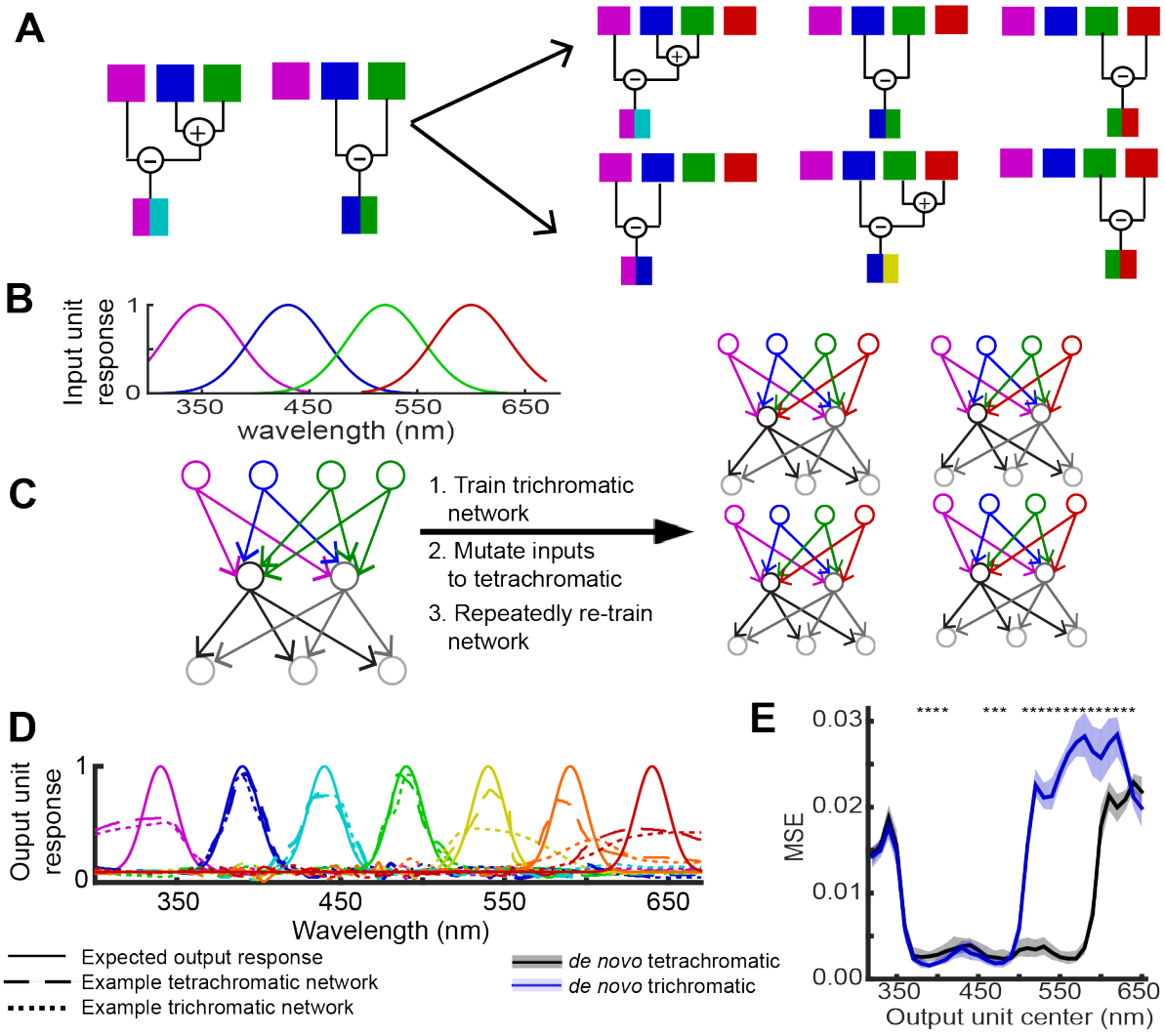

Figure 3.1: Network Design
A) Trichromatic circuits have two color opponent channels. Evolving tetrachromacy, which requires a third opponent channel, could occur through inheriting the original two channels and adding a third (top) or a novel three channels could be generated (bottom).
B) Tuning curves for input layer simulating UV, blue, green, and red photoreceptors.
C) A network was first trained with a trichromatic input layer. Trained networks then had a green photoreceptor mutated to red and the network was repeatedly and independently retrained, simulating an ancestral trichromatic network and numerous independent origins of tetrachromatic vision.
D) The output layer was a filter bank of narrowly tuned Gaussians tiling the visual range. Shown are 7 of the 34 output units with the RFs for a representative trichromatic and tetrachromatic network shown.
E) Network performance was measured as the MSE between the expected and observed RF for each individual output unit. By design, long wavelength output units perform significantly worse than tetrachromatic networks. Shading shows the 25th and 75th percentile. Asterisks indicate significance with Cohen's d > 0.50.

by converting a subset of green photoreceptors to red, matching the known evolutionary history of butterfly photoreceptors [90]. This mutated network was then retrained for tetrachromatic vision 100 unique times, which I viewed as biologically analogous to 100 species that independently evolved tetrachromatic vision from the same trichromatic ancestor. I generated and evolved 100 trichromatic networks to simulate distinct phylogenetic lineages (e.g. butterflies, spiders, birds, etc.), for a total of 10,000 networks.

If ancestry constrained evolutionary trajectories, I expected networks sharing the same trichromatic starting weights to be more similar than networks with different trichromatic starting weights. These potential constraints could be unique to a trichromatic ancestor, but they could also be more broadly applicable to any set of starting weights. To control for this possibility, I trained and analyzed an additional set of *de novo* networks. These networks lacked a pre-training step and were instead trained for tetrachromatic vision directly from random starting weights. Mirroring the evolved networks, I generated 100 sets of random starting weights and trained each starting point 100 unique times, again for a total of 10,000 *de novo* networks.

3.4 Results

3.4.1 Network performance

Tetrachromatic networks have an expanded range of good color vision

I first validated my network design and training protocol by comparing the performance of tri- and tetrachromatic networks trained from random starting weights. Because trichromatic networks lacked a red photoreceptor, I expected performance differences primarily for long wavelength stimuli. Thus, rather than measuring overall network performance, I instead opted to analyze each output unit individually. For each output unit, I constructed a tuning curve by measuring its response to the full range of wavelengths and luminance factors (Fig. 3.1D). Performance was then defined as the mean squared error (MSE) between the observed

tuning curve and the training target.

Performance generally followed the Fisher Information of the input layer, with output units centered on wavelengths where photoreceptors intersect having the lowest MSE. Tetrachromatic networks performed generally well across the entire visual range, while long wavelength output units for trichromatic networks performed poorly (Fig. 3.1E). This impaired performance was because only green photoreceptors responded to long wavelength stimuli, which made luminance a confounding variable. In the absence of luminance variation, tri- and tetrachromatic networks performed similarly well for all output units (Fig. 3.S1). Notably, for short and middle wavelength output units, trichromatic networks performed slightly but significantly better than tetrachromatic networks, which likely reflected a smaller range of learnable stimuli but an equal number of hidden units.

Mutating the input layer impairs network performance

De novo networks demonstrated that tetrachromatic networks have an expanded range of color vision but did not address questions about color vision evolution. To simulate evolution, the input layer of fully trained trichromatic networks was mutated by converting a subset of green photoreceptors to red (Fig. 3.1C). This mutation, prior to any retraining, resulted in a mismatched tetrachromatic input layer and trichromatic hidden layer. This situation likely mirrors biology, where a novel photoreceptor necessarily precedes changes to central brain circuitry. Output units tuned to short wavelengths were unaffected by the mutation, while performance was significantly impaired for middle and long wavelength output units (Fig. 3.2A). Interestingly, the effect of mutation was similar across all networks (Fig. 3.2A, note error bar size), suggesting that changes to peripheral sensing caused similar disruptions to sensory perception regardless of the specific computations implemented by each network.

The impaired MSE performance of mutant networks could arise through numerous changes to the tuning of output units. To examine the specific tuning changes, I fit Gaussians to output unit tuning curves and compared the fit parameters (Fig. 3.S2). For tri- and tetra-

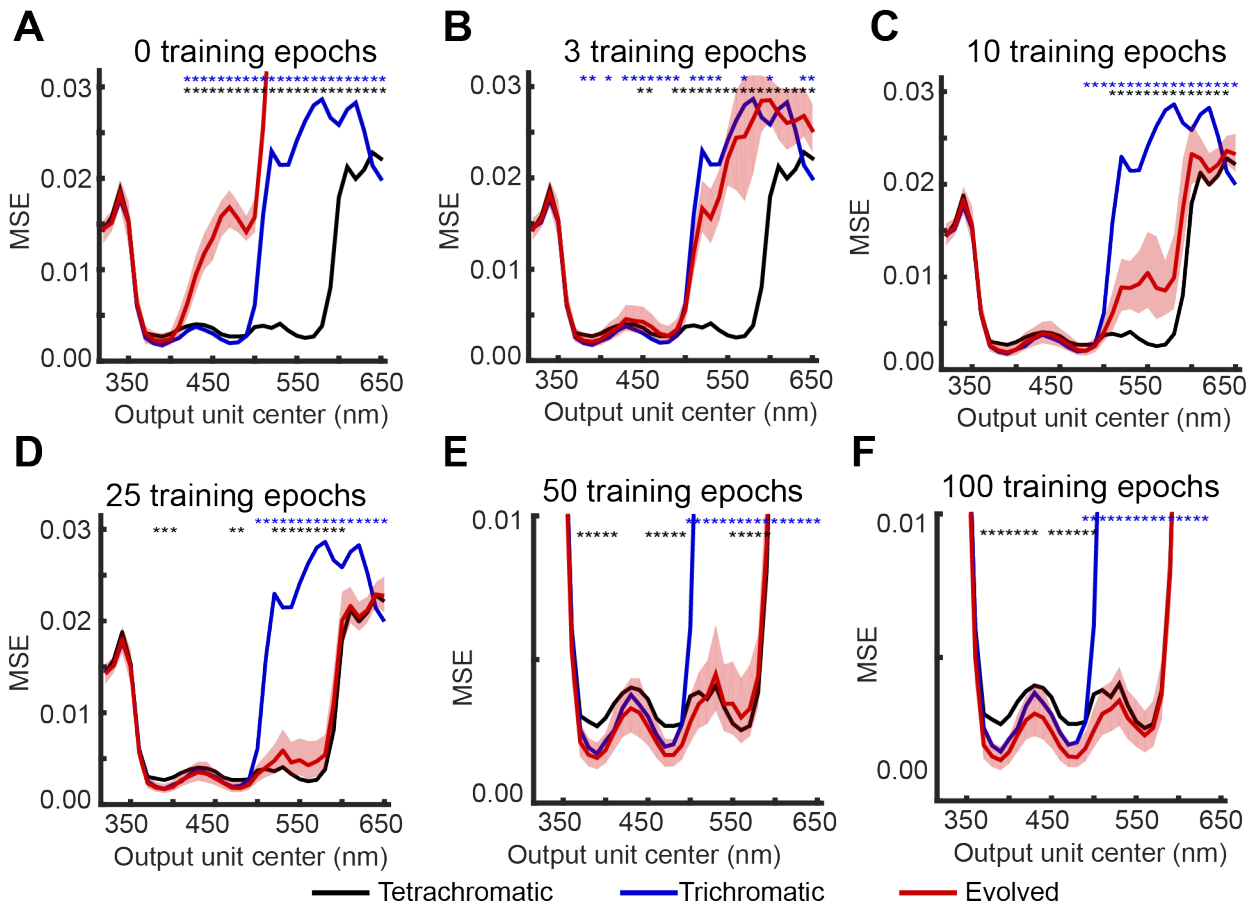

Figure 3.2: Evolved network performance over training time
The performance of evolved networks was tracked over training time and compared to tri- and tetrachromatic networks trained from random starting weight after A) 0, B) 3, C) 10, D) 25, E) 50, and F) 100 training epochs. 50 training epochs matches the total training time of the tri- and tetrachromatic networks. Shading shows the 25th and 75th percentile and was omitted for tri- and tetrachromatic networks for clarity. Blue and black asterisks show performance that is significantly different between the evolved networks and tri- and tetrachromatic networks, respectively, with Cohen's d > 0.50.

chromatic networks, the tuning centers, widths, and amplitudes generally matched the target tuning. Mutant networks typically maintained a narrow, single peaked tuning curve, with tuning widths and amplitudes largely matching the original network. The primary difference accounting for impaired MSE performance was a 5-10 nm shift in the tuning center. This result suggests that the effect of a novel photoreceptor on color vision may be smaller than the MSE performance metric initially showed, with mutant networks likely retaining trichromatic color vision. However, even small perceptual deficits could lead to selection against

the expression of a novel photoreceptor in a natural population.

Every network successfully gained tetrachromatic performance

Peripheral sensory structures have been proposed as an important and especially flexible target for evolutionary change that can lead to adaptive behavior without large-scale changes to central processing. The seemingly minor fitness cost associated with a novel photoreceptor in mutant networks was consistent with peripheral structures being evolutionarily labile. However, a novel red photoreceptor alone was insufficient to expand the range of color vision, indicating that modifications to color computation were necessary. To ask whether ancestral trichromatic circuits were capable of adapting to a mutated input layer, I next re-trained mutant networks and tracked performance over training time (Fig. 3.2).

Networks compensated for the impaired performance of mutant networks quickly, but improvement to tetrachromatic vision proceeded slowly. Within 3 re-training epochs, evolved network performance broadly matched the performance of the original trichromatic networks (Fig. 3.2B). Long wavelength output units continued to improve over training, becoming effectively tetrachromatic within 25-50 training epochs, which matched the total training time of *de novo* networks (Fig. 3.2C). Interestingly, short and middle wavelength output unit performance matched trichromatic networks, which was significantly better than tetrachromatic networks. However, this improvement came at the expense of long wavelength output unit performance, which remained slightly but significantly worse than *de novo* networks. Extending training to 100 epochs improved this performance to match the long wavelength output unit performance of *de novo* networks (Fig. 3.2D).

Different starting networks learn at different rates

With enough re-training epochs, every evolved network performed similarly to *de novo* tetrachromatic networks, indicating that trichromatic ancestry did not prohibit the eventual evolution of tetrachromacy. However, rather than strictly prohibiting an adaptive phenotype,

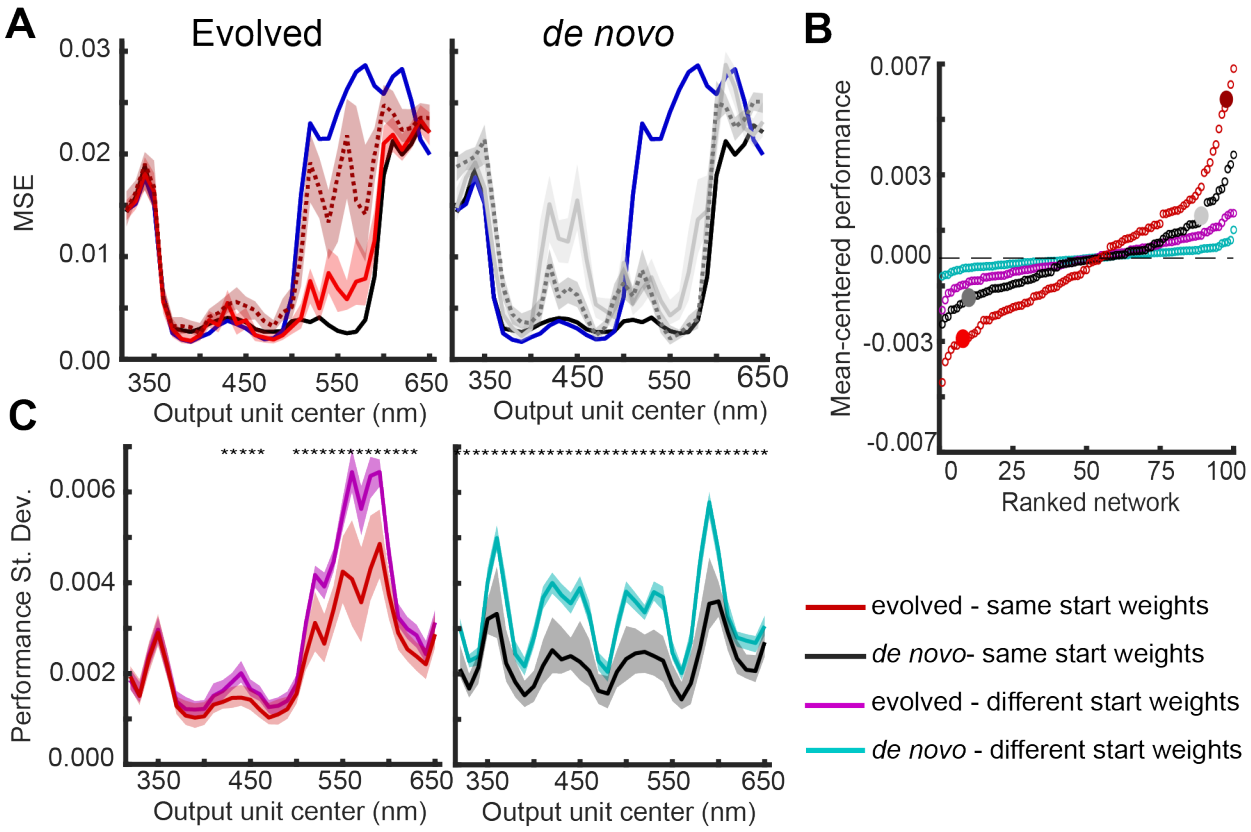

Figure 3.3: Starting weights constrain learning rates
A) Performance after 10 training epochs is shown for networks that share the same starting weights. Examples for networks derived from two sets of starting weights are shown for evolved (left) and *de novo* (right) networks.
B) For each group of 100 networks, performance after 10 training epochs was reduced to a single performance metric by averaging across all 100 networks and 34 output units. Each distribution was mean-centered and plotted in order of decreased performance. Large solid circles correspond to the examples shown in panel A.
C) For each group of 100 networks, the performance variability was measured for each output unit after 10 training epochs. Asterisks indicated significance with Cohen's d > 0.50.

evolutionary constraints are primarily thought to affect how accessible an adaptive phenotype is [4]. For my networks, this could mean that some trichromatic network configurations were amenable to tetrachromacy while others resisted adapting to the novel red photoreceptor. To investigate this possibility, I compared the performance of networks derived from the same trichromatic starting point after 10 re-training epochs.

Visual inspection of network performance after 10 training epochs suggested that starting weights influenced learning rate (Fig. 3.3A). Some trichromatic networks facilitated evolu-

tion, with the average performance approaching tetrachromatic performance after 10 epochs (Fig. 3.3A). Other trichromatic networks impeded evolution, with descendant networks showing minimal performance improvements beyond the original trichromatic network (Fig. 3.3A). Starting weights appeared to similarly affect learning for *de novo* networks trained from random starting weights. Regardless of starting weights, *de novo* networks tended to perform well in regions that became MSE minima, while performance between these regions of good performance were more variable (Fig. 3.3A). This result was reminiscent of experimental behavior, where discrimination thresholds near Fisher Information maximums are often similar across species, while thresholds between these regions of best discrimination vary more substantially [154, 168].

I quantified these visually observed effects by separating networks into groups of 100 networks that either shared or did not share the same starting weights, resulting in four classes: 1) evolved networks with the same trichromatic starting weights, 2) evolved networks with different trichromatic starting weights, 3) *de novo* networks with the same random starting weights, and 4) *de novo* networks with different random starting weights. Since I started with 100 sets of starting weights, each class comprised 100 unique groups. Groups were first reduced to a single value representing mean performance by averaging performance across all networks and long wavelength output units within a group. The distribution of this performance metric for each class was then mean-centered and compared to the other classes (Fig. 3.3B). The distribution of this performance metric was significantly different for every pairwise comparison between classes (Kolmogorov-Smirnov test with Bonferroni correction, $p < 0.001$). The performance distribution for groups of evolved networks sharing the same starting weights was the most variable, suggesting that trichromatic ancestry imposed stronger constraints than random starting weights would have predicted.

Group differences in mean performance could emerge in two different ways. First, every network derived from the same set of starting weights could follow a similar learning trajectory that differs from other sets of starting weights. Alternatively, networks sharing

the same starting weights could have a broad range of performance, with the specific starting weights skewing the proportion of networks that learn quickly or slowly. To distinguish between these options, I calculated performance variability for each output unit within a group of 100 networks. For both evolved and *de novo* networks, groups of networks sharing the same starting weights showed significantly less performance variability than groups with different starting weights (Fig. 3.3C). Interestingly, the total variability across all networks and output units was the same for every class of networks, but the distribution of variability varied substantially between evolved and *de novo* networks. Because evolved networks were pre-trained to perform well for short and middle wavelength output units, variability was mostly confined to long wavelength output units. *De novo* network variability was more evenly distributed across all output units, but MSE minima were less variable.

Together, network performance results showed that starting weights affect the early evolutionary response to a novel photoreceptor but do not strictly prohibit evolution. Mutant networks compensated for the modified input layer quickly, but learning new computations was comparatively slow. Given the gradient descent learning algorithm, this result was expected with enough training epochs. Interestingly, pre-training networks with a trichromatic input layer facilitated evolved network performance that exceeded expectations set by networks trained from random starting weights. This result matches ideas both in biology and machine learning about curriculum learning, where learning through the iterative addition of complexity facilitates improved learning outcomes [169]. In this way, constraints imposed by an ancestral circuit might actually be beneficial in some evolutionary contexts.

3.4.2 Hidden layer computations: Opponent channels

Starting weights constrain the overarching computational structure of the hidden layer

Every network successfully evolved tetrachromacy, which I viewed as biologically analogous to convergent evolution both within and across distinct phylogenetic lineages. A convergent phenotype alone, however, is not sufficient to conclude that starting weights constrained the network and could instead reflect similar selective pressures (i.e. the same training cost function). Differences in learning rate hinted at constraint, but a rigorous test required assessing the degree of similarity in the underlying computational mechanism of color vision. Thus, I next turned to analyzing the hidden layer, focusing on the weights connecting the input layer to the hidden layer. The high dimensionality of the hidden layer posed an analytical challenge, which I first approached by using principle component analysis (PCA) to examine the overarching structure of hidden layer computations.

Consistent with color vision theory [158, 159, 170], PCA reduced the dimensionality of the hidden layer from 30 hidden units to 3 color opponent channels (i.e. eigenvectors) that described 48.5 $\pm$ 12.2, 27.6 $\pm$ 5.5, and 16.0 $\pm$ 5.7 percent of the variance in hidden unit computations. Each channel had a UV, blue, green, and red component that consistently showed opponent interactions indicated by a combination of positive and negative input weights (Fig. 3.4A). To assess computational similarities, networks were again separated into classes and groups that either shared or did not share the same starting weights. The three opponent channels for each network were concatenated into a single 12 dimensional vector (3 channels X 4 input weights) and compared within a group of 100 networks using hierarchical clustering (Fig. 3.4).

I first analyzed groups of *de novo* networks where each network had different random starting weights. Networks in these groups used diverse sets of opponent channel, spanning the full range of color opponent combinations (Fig. 3.4B). Networks rarely clustered together,

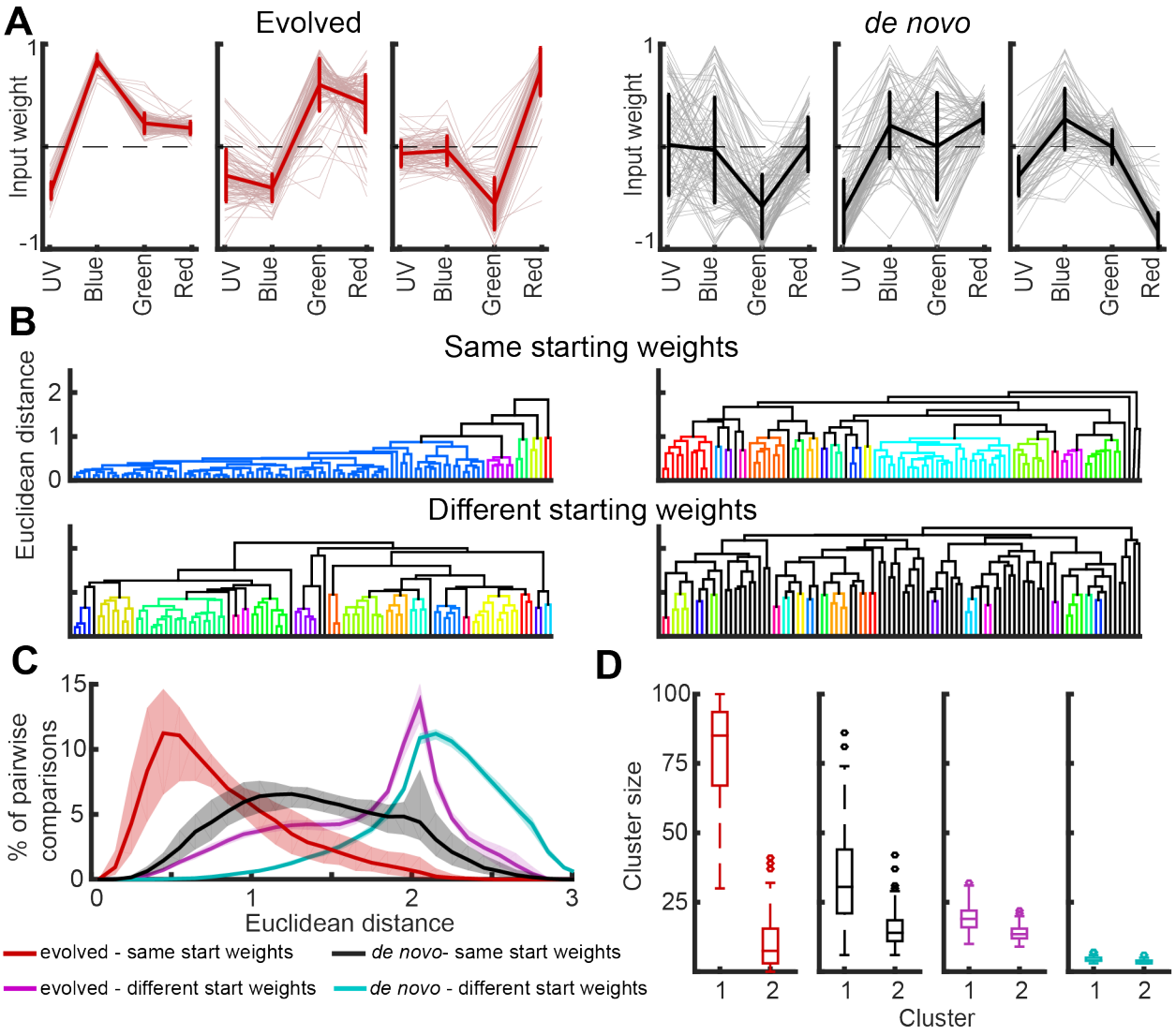

Figure 3.4: Network opponent channels

A. The three opponent channels for all 100 networks independently trained from a single set of starting weights are shown for evolved (left) and *de novo* networks (right).

B. Opponent channels for groups of 100 networks that either shared (top) or did not share (bottom) the same starting weights were compared using hierarchical clustering. Depicted are example dendrograms for evolved and *de novo* networks, with the top row corresponding to the networks in panel A.

C. Euclidean distances were measured between the opponent channels of every pair of networks within a group of 100. Shading shows the 25th and 75th percentile.

D. Cluster sizes are shown for the largest two clusters for each set of 100 networks. Since there are 100 sets of starting weights, there are 100 groups of 100 networks, with the between group variability illustrated by the boxplots. The clustering threshold was set at a Euclidean distance of 1.0, but results did not qualitatively change for different thresholds.

with the largest cluster containing between 3 and 7 networks out of 100 (Fig. 3.4D). I also looked at the distribution of Euclidean distances between every pair of networks in a group, and consistent with small cluster sizes, pairwise distances tended to be large (Fig. 3.4C). Moreover, this distribution of pairwise distances closely matched a null distribution created with opponent channels generated from random numbers (Fig. 3.S3B, Jensen-Shannon Divergence = 0.02). This result suggested that my network design and training protocol were not biased and utilized the full computational state space.

I next compared groups of *de novo* networks sharing the same random starting weights to the baseline computational similarities established from groups with different random starting weights. The distribution of pairwise distances for these groups was shifted substantially towards zero (Fig. 3.4C, JSD = 0.31). These smaller distances led to significantly increased clustering, with the largest cluster containing an average of 33.8 $\pm$ 17.1 networks (Fig. 3.4D, Cohens d = 2.4). Thus, starting weights did constrain and bias network evolution, but *de novo* networks also retained some diversity in how tetrachromatic computations were implemented.

Trichromatic starting weights constrained computations significantly more than random starting weights. Groups of evolved networks sharing the same starting weights typically converged on just a few computational motifs. Pairwise distances were shifted further towards 0 (Fig. 3.4C, JSD = 0.19) and the largest cluster contained 79.2 $\pm$ 17.7 networks (Fig. 3.4D, Cohens d = 1.9). It required only 2.5 $\pm$ 2.1 clusters in order to cluster 90 out of 100 networks, whereas *de novo* networks sharing the same random starting weights needed 12.3 $\pm$ 7.9 clusters (Cohens d = 1.7). Together, these results showed that starting weights constrained network computations, and trichromatic weights impose especially strong constraints that bias a network into a severely restricted region of the available computational state space.

Evolved networks inherit the original opponent channels and consistently add the same novel channel

Finally, I examined groups of evolved networks with different trichromatic starting weights. The largest cluster had 19.4 ± 4.6 networks, and 13.7 ± 2.9 clusters were required to cluster 90 networks. Thus, these groups were most comparable to, but significantly less similar than groups of *de novo* networks with the same random starting weights (Cohens d = 1.2). The pairwise distance distribution was visually consistent with the clustering result (Fig. 3.4C), but the two classes were statistically similar (JSD = 0.05). Interestingly, this pairwise distance distribution matched the distance distribution of the original trichromatic networks visually and statistically (Fig. 3.S3B, JSD = 0.01). This similarity was surprising because the inherently smaller dimensionality of trichromatic networks that have only two opponent channels with three input weights should lead to smaller distances.

To understand how this similarity arose, I analyzed each opponent channel individually rather than as the concatenated group of three (Fig. 3.S3A). I first noticed that the new, third channel for nearly every evolved network had green vs. red opponency regardless of the specific trichromatic starting weights (Fig. 3.4A), and hierarchical clustering of the third channel confirmed this similarity (Fig. 3.S3). In contrast, the first and second channel matched previous results (Fig. 3.4), with groups sharing the same starting weights more similar than groups with different starting weights. Calculating the Euclidean distance between these first two evolved channels and the original two trichromatic channels they evolved from allowed us to ask how much training affected opponent tuning. Evolved network distances (0.33 ± 0.20) were significantly smaller than *de novo* network distances (0.55 ± 0.20, Cohens d = 1.1) or evolved networks with shuffled trichromatic channels (0.66 ± 0.28, Cohens d = 1.3).

Overall, these results indicated that networks evolve tetrachromatic vision by inheriting the original two opponent channels and adding a third, orthogonal channel specifically implementing green vs. red color opponency. This result is consistent with how networks

performed, as limited disruption to short wavelength computations led to limited disruptions in short wavelength performance. Thus, maintenance of this performance may play a causal role in biasing tetrachromatic computations. *De novo* networks, in contrast, were more free to vary and find distinct computational solutions that span the full computational state space.

3.4.3 Hidden layer computations: Hidden unit tuning

Learning targets a specific subset of evolved network hidden units

The opponent channels revealed by PCA describe the combined tuning of a population of individual hidden units. Similar opponent channels between networks sharing the same starting weights could emerge from similar modifications to hidden unit tuning. This would be consistent with an adaptive hotspot hypothesis of evolution that proposes circuit nodes can vary in how evolutionarily flexible they are [12, 14]. Alternatively, evolved networks could exhibit a wide diversity of tuning despite opponent channel similarities. For example, distantly related South American and African electric fish often use similar electro-sensation computations, but the specific anatomical locus of these computations can vary substantially [51].

To distinguish between these options in my networks, I compared the tuning of single hidden units before and after tuning using the cosine distance. This distance metric specifically measures changes in opponent tuning while ignoring changes in overall weight size (Fig. 3.5A). Because each starting network was independently trained 100 times, this analysis generated a distribution of distances for each starting hidden unit (Fig. 3.5B). The hidden units for each starting network were then arranged in order of median distance or distance variability and compared between evolved and *de novo* networks.

In contrast to opponent channel results, evolved network cosine distances were significantly larger (Fig. 3.5E) and more variable (Fig. 3.5F) than *de novo* networks. Large

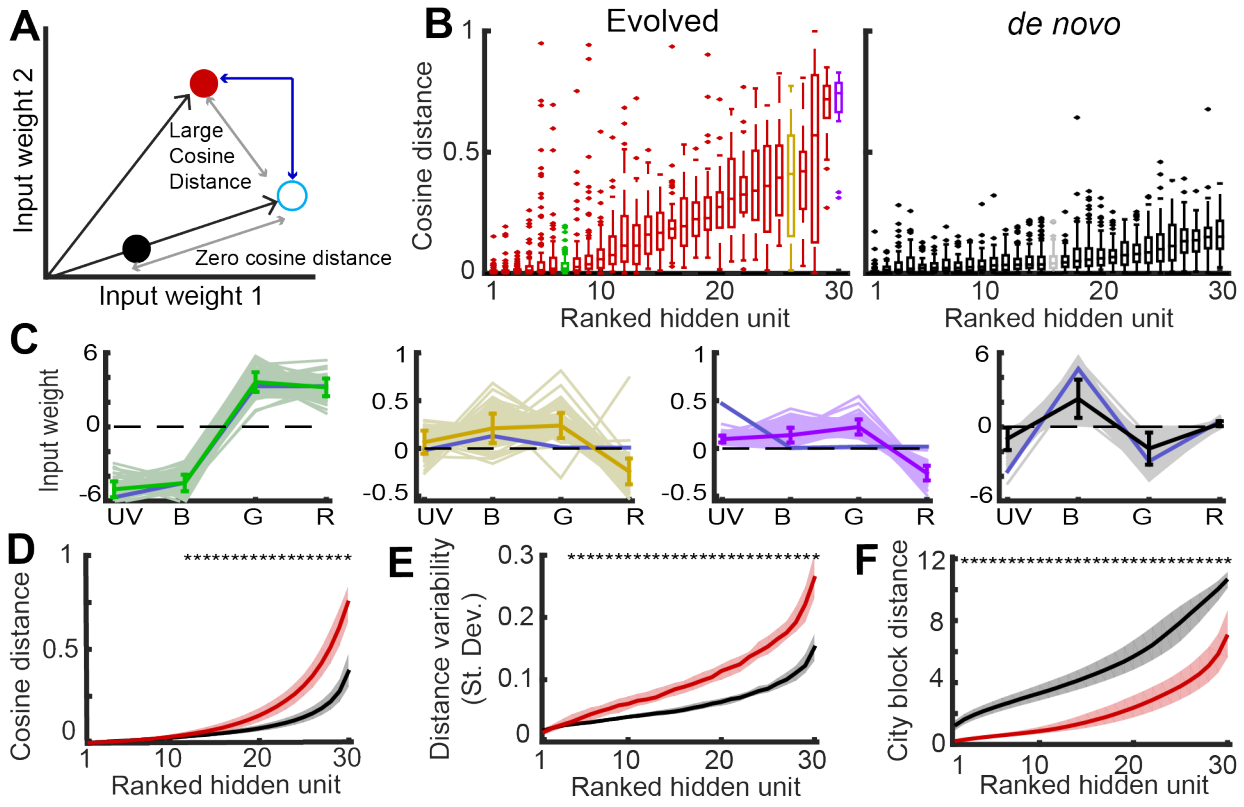

Figure 3.5: Tuning changes in single hidden units
A) Schematic of distance measurements. Length of the blue arrows is the city block distance, and the distance from the open cyan circle to each of the filled circles is the same. Cosine distance measures the change in the vector direction. Cyan and black sit on the same vector so have 0 cosine distance. The cosine distance between cyan and red, in contrast, is large because the vectors from the origin are different.
B) Tuning changes for each hidden unit were measured as the cosine distance between the input weights before training and the input weights after training. Shown are representative examples for a group of networks sharing the same trichromatic or random starting weights. Boxplots show the variability of homologous hidden units ranked by median cosine distance.
C) Shown are the tuning curves of four representative hidden units. The blue line shows the tuning of the original hidden unit. Lightly shaded lines show the tuning for 1 of 100 trained networks. The dark line is the mean ± SEM. Colors of each plot correspond to the colored boxes in panel B. Note the differences in the y-axis.
D) Median cosine distances are compared between evolved and *de novo* networks. The plot is essentially equivalent to panel B, but medians are averaged across each group of 100 networks sharing the same starting weights. Shading shows the 25th and 75th percentile .Asterisks show significance with Cohen's d > 0.50.
E) Rather than ranking hidden units by median cosine distance, they were now ranked by the variance of the cosine distance.
F) Instead cosine distances, this plot shows the city block distances for each hidden unit.

distances for 10-15 hidden units per network were typically associated with the development of green vs. red opponency in hidden units that originally had small weights and weak or no opponency (Fig. 3.5C, yellow and magenta). In contrast, hidden units with the smallest cosine distances always had large input weights and clear opponent tuning (Fig. 3.5C, green). Performing the same analysis on networks with 50 hidden units similarly found 10-15 hidden units with especially large distances (Fig. 3.S4. The extra hidden units compared to 30 hidden unit networks had the smallest distances and varied little between networks. This result is broadly consistent with an adaptive hotspot explanation for network evolution. Many hidden units were rigidly constrained and did not vary, and tuning curves of these hidden units suggest an important role in short wavelength discrimination. A small subset of hidden units, in contrast, were flexible and adapted to expand and improve color vision. As expected, green vs. red opponency appeared in these hidden units, but surprisingly, these computationally flexible hidden units could vary substantially relative to each other.

Hidden unit outputs are robust to input variability

In addition to having large cosine distances, evolved network hidden units also showed high variability (Fig. 3.5B,E). Differences in the specific opponent tuning of homologous hidden units could be an important factor in how different networks function, but the variation could also reflect network computations that are robust to perturbation. To distinguish between these possibilities, I generated tuning curves for the output response of the hidden layer. Previous analyses focused on the input weights from each of the four input layer photoreceptors, biologically analogous to looking at the dendrites of a neuron. Before connecting to the filter bank output layer, however, hidden unit responses are passed through a sigmoid non-linearity that transforms responses to values between 0 and 1. I measured output tuning curves for wavelengths spanning the full visual range and compared the tuning of homologous hidden units using hierarchical clustering (Fig. 3.S5).

The sigmoid non-linearity typically made hidden unit responses robust to differences in

input tuning. In general, hidden unit outputs exhibited binary 0 or 1 responses with relatively sharp transition zones (Fig. 3.S5A,B). Because of this non-linearity, input units could vary substantially with only minor effects on the output. One exception to this, however, is when input responses for two hidden units have positive and negative responses. When this occurs, small differences are magnified and can flip responses between 0 and 1 easily. For evolved network hidden units, these deviations typically occurred at long wavelengths where novel green vs. red computations were developing (Fig. 3.S5). Differences between homologous *de novo* hidden units, in contrast, could exhibit these zero-crossing deviations anywhere along the visual spectrum.

Surprisingly, despite larger and more variable input tuning, output tuning for homologous hidden units in evolved networks were more similar than *de novo* networks. Visual inspection of the pairwise distance distribution suggested that evolved network hidden unit outputs were substantially more similar, but statistically the distributions were relatively similar (JSD = 0.04, Fig. 3.S5C). Combining all hidden units (100 starting networks X 30 hidden units), the largest cluster had an average of 46.4 $\pm$ 23.8 hidden units for evolved networks and 36.6 $\pm$ 24.6 hidden units for *de novo* networks (Fig. refmodeling s5D). Using the stringent significance criterion, this difference was marginally not significant (Cohen's d = 0.41). When ranking hidden units for each trichromatic or random starting network from 1 to 30 by cluster size, however, comparisons were highly significant (Cohen's d $>$ 1.0) for all but the 5 least variable hidden units. Overall, these results broadly mirror the opponent channel analysis and are opposite to the input weight analysis. Importantly, PCA was independent and unaware of the eventual sigmoid non-linearity, suggesting that the opponent channel analysis captured computationally relevant tuning differences.

De novo networks vary connection strength more than evolved networks

In addition to changes in opponent tuning, hidden units could also increase or decrease the overall strength of connection. Proportional changes to input weight sizes appeared to be the

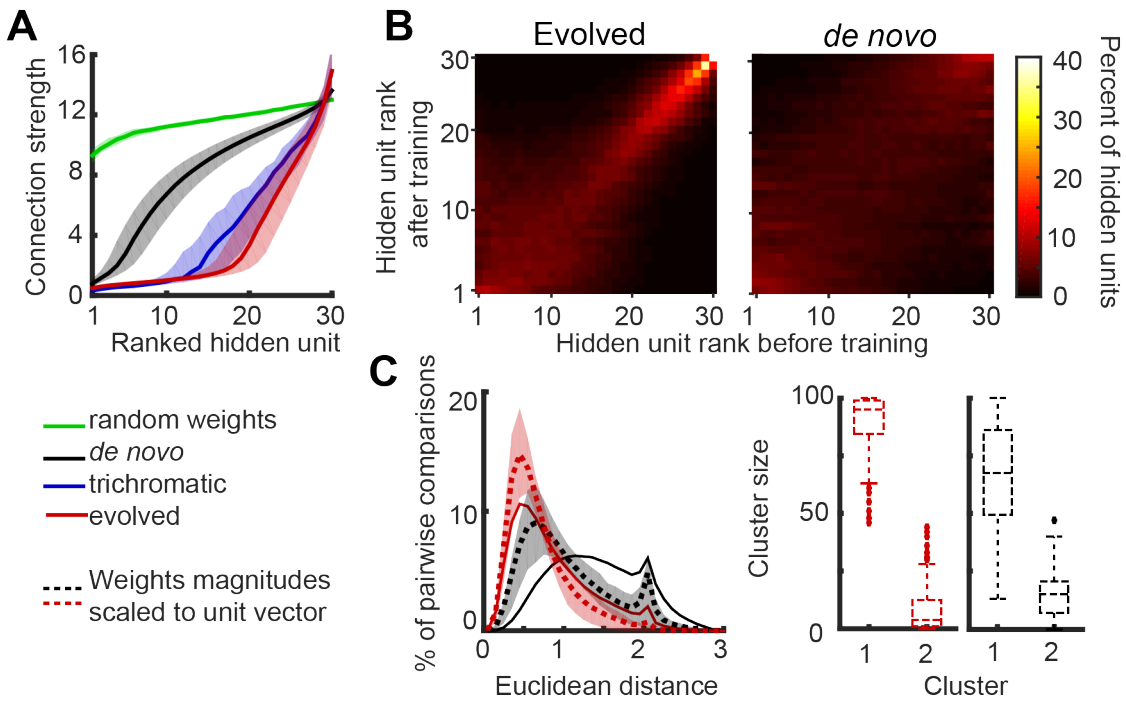

Figure 3.6: Weight magnitudes differ between evolved and *de novo* networks
A. Weight magnitudes were defined as the sum of the absolute value of the four input weights to a hidden unit. Hidden units for each network were then ranked in order of increasing size. B. Hidden units for a network were ranked by weight magnitude before and after training. Heat maps show how the rank of hidden unit changed after training.
C. In order to remove the influence of weight magnitude on opponent channel results (Fig. 3.4), input weights for each hidden unit were proportionally scaled so that the weight magnitudes were equal to 1. The same opponent channel analysis was then completed. Solid lines show the distances without re-scaling the weights and match Fig. 3.4C. Cluster sizes are based on a clustering threshold of 1.0 to match the original analysis. Lowering this threshold increases the difference between evolved and *de novo* networks as it removes ceiling effects (i.e. the largest cluster can only have 100 out of 100 networks in a group).

primary way that *de novo* network hidden units learned. Hidden units for *de novo* networks had small cosine distances, but city block distances were substantially bigger and more variable than evolved network hidden units (Fig. 3.5C, black). To examine this learning difference between evolved and *de novo* networks in greater detail, I quantified connection strength as the sum of the absolute value of the four input weights to a each hidden unit. Connection strength of a hidden unit was then compared before and after training as well as between homologous hidden units (Fig. 3.6A).

For all networks, training almost exclusively led to decreases in the connection strength

of a hidden unit (Fig. 3.6A). Random starting weights were large and varied little between hidden units. Training these random starting weights with a tetrachromatic input layer decreased connection strength, leading to a relatively uniform distribution. Networks with only a trichromatic input layer decreased connection strengths significantly more, with 10-12 out of 30 hidden units having connection strengths close to 0. Evolved networks derived from these trichromatic networks suppressed weights further, with 16-18 hidden units having connection strengths near zero.

This extra decrease in connection strength for trichromatic networks was reminiscent of L2 regularization, which is commonly used in machine learning to prevent over-fitting. This effect was specifically due to trichromatic networks having long wavelength output units that were, by design, unable to successfully learn (Fig. 3.S6). This apparent regularization effect could potentially explain why trichromatic networks outperformed tetrachromatic networks for short and middle wavelength output units (Fig. 3.2). I investigated this by generating a new set of *de novo* tetrachromatic networks with an L2 regularization term explicitly added to the training protocol (Fig. 3.S6). As expected, these networks had smaller connection strengths, but network performance failed to improve beyond networks without L2 regularization.

Hidden unit opponent tuning and connection strength combined give rise to opponent channels

Training decreased connection strengths, but it was unclear whether homologous hidden units consistently converged on similar connection strengths. To investigate connection strength variability, I compared relative connection strength from before and after training. For each starting network, hidden units were ranked from 1 to 30 in order of increasing connection strength. Similarly, I assigned ranks to hidden units for each trained network and asked if starting rank was correlated with trained rank (Fig. 3.6B). For both evolved and *de novo* networks, starting rank was significantly correlated with trained rank ($p < 0.001$). Driven

primarily by hidden units with large connection strengths, the evolved network correlation ($r = 0.72 \pm 0.10$) was significantly stronger than the *de novo* network correlation ($r = 0.43 \pm 0.12$, Cohens $d = 1.9$).

Together with the small cosine distances for *de novo* networks, this result raised the possibility that connection strength rather than opponent tuning were the important factor driving opponent channel similarities. In other words, the observed opponent channels might disproportionately reflect the tuning of a small number of hidden units with large connection strengths rather than real variability in overarching network computation. Since *de novo* network connection strengths varied more, the apparent increase in opponent channel similarities for evolved networks might not be due to constraints on the opponent tuning. To control for this possibility, I removed the influence of connection strength by normalizing the connection strength of each hidden unit to a unit vector. Using these normalized hidden units, I then recalculated the opponent channels and performed the same analyses as seen in Fig. 3.4.

Normalizing hidden unit connection strength led to increases in opponent channel similarities for both evolved and *de novo* networks (Fig. 3.6C). For *de novo* networks, the largest cluster nearly doubled in size, and the distribution of pairwise distances shifted towards 0 to approximately match evolved networks that did not have normalized connection strengths. Normalizing connection strength led to more modest increases in opponent channel similarities for evolved networks, although this may be due to ceiling effects since evolved networks were already highly similar. Regardless, evolved network opponent channels remained significantly more similar than *de novo* networks (Fig. 3.6C, pairwise distance distribution: JSD = 0.10; cluster size: Cohens $d = 1.2$).

Together, these results showed that the opponent channels observed in Fig. 3.4 are created through a combination of connection strength and opponent tuning. Even though *de novo* network hidden units have small cosine distances reflecting small changes in opponent tuning, these small changes in opponent tuning across a network combine to have a large

influence on the opponent channels as well as the output tuning curves. Evolved network computations, in contrast, were constrained by the computations of the ancestral trichromatic network. A subset of hidden units, however, were relatively unconstrained and free to vary. This flexibility may be important for allowing the network to traverse the computational space and lead to the observed differences in learning rate.

3.5 Discussion

In this study, I designed a simple neural network model trained with standard machine learning algorithms to simulate the evolution of tetrachromatic vision from a trichromatic ancestor. Results were consistent with ideas about phylogenetic history constraining and biasing evolution for network performance, the overarching computational structure of a network, and the tuning of single hidden units. Similarities between evolved networks that surpassed the similarity expectations set by *de novo* networks suggest that circuit structures pre-trained for a particular function impose especially strong constraints on how neural circuits compute. Related to biology, these findings broadly suggest that phylogenetic relationships and history are important to consider when attempting to understand the functional organization of circuits underlying behavior.

3.5.1 Constraints on evolution

Evolution does not necessarily prohibit an animal from reaching any particular phenotype. Major evolutionary shifts do occur, with often cited examples including the turtle carapace and bird feathers [4, 171]. However, these innovations appear to be unlikely and rare. For example, insects may benefit from shifting from a compound eye to a simple eye with better resolution, but phylogenetic history and developmental patterns make this unlikely to happen. By simulating convergent evolution both across and within distinct phylogenetic lineages, my simulations were capable of a detailed examination of how these constraints

might influence neural computation.

Expanding the range of color vision necessitates evolving a new photoreceptor. Consistent with ideas about the peripheral nervous system being amenable to evolution [22], mutating the input layer had limited detrimental effects on performance. The MSE performance metric likely overestimated the effect of mutation due to output tuning curves having a long wavelength shift. Thus, they observed tuning curves were poorly matched to the target, but further inspection showed that the output layer maintained regularly spaced, narrowly tuned tuning curves that should allow for trichromatic color vision, although a direct measure color vision impairment was not feasible. If the impairment was as minimal as it appeared, it provides a means for a novel photoreceptor to remain in a population while computational circuits adapt. This result suggests that the initial mutation is not an important aspect for explaining the observed diversity of color vision in butterflies and insects.

Although the novel photoreceptor did not impair color vision, it was also insufficient to improve color vision. Novel, neutral variants present in a population at low frequency are more likely to go extinct than drift to fixation. Thus, an inability for the color vision circuits to adapt to the novel input might be a strong constraint on evolution. Different sets of starting weights learned at different rates, and these differences were significantly larger for evolved networks. Slowly learning networks may be more rigidly locked into a particular computational pattern. In a real biological system, this might mean that the number of mutations with positive effect are smaller and traversing the computational state space is more difficult. If the adaptive phenotype is not readily accessible, it is less likely to evolve.

Accessibility of a new computational phenotype might be related to how flexible the individual hidden units were. The non-linear transformation of hidden unit responses permitted input weights to vary substantially without huge consequences to computation, except for when the sign of an input changed. This combination may have facilitated large changes that allowed for novel computations to be implemented while also limiting deleterious pleiotropic effects on existing computations. Hidden units that have more flexibility could potentially

make more targeted changes to computations and find computational solutions for tetrachromatic inputs more easily.

Although single hidden units were free to vary, opponent channel computations were highly constrained. *De novo* networks with different random starting weights showed agreed with color vision theory, showing that an effectively infinite number of opponent channel combinations can lead to perceptually equivalent color discrimination. Evolved networks, however, were constrained to implement the same computations as the original trichromatic network. In retrospect, this makes sense because these original computations were necessary for short wavelength color vision. Disrupting these computations would likely disrupt that performance, making it a non-viable evolutionary path.

There was no clear relationship between the observed opponent channels and the tuning of individual hidden units. *De novo* network hidden units were largely unchanged in terms of opponent tuning, suggesting that a random wiring scheme is sufficient to implement color vision. Evidence for this type of organization has been found for both vertebrates [172, 173] and invertebrates [162]. Nonetheless, the percent of variance explained for the opponent channels suggested that they described real variability in the overarching computations of the network. This relationship may be due to slight biases towards particular computations in the population of hidden units. Alternatively, hidden unit tuning curves were complex and could potentially encode differing proportions of each opponent channel.

3.5.2 What does an epoch mean

An important aspect for relating these model results to biology is attempting to understand what a training epoch might mean in biological time. This relationship conceivably could be different for different taxa. In particular, vertebrate cortex undergoes substantial activity dependent development that restructures circuits. Thus, for vertebrates, the entirety of training could conceivably occur within a single individual. Experimental data from two mammalian systems supports this idea.

First, new world monkeys have only two opsin encoding genes, with the long wavelength sensitive opsin (green) having multiple alleles with distinct spectral sensitivities (green and red) [39]. Because this is an X-linked gene, males and homozygous females are necessarily dichromatic. Because of X-inactivation, heterozygous females, in contrast, randomly express one of the two opsins in each photoreceptor, and behavioral experiments have conclusively shown that these females exhibit trichromatic vision [174]. Thus, even within a single species and population, mechanisms of cortical development are flexible enough to code for trichromatic vision when the periphery allows for it.

A second example comes from genetic manipulation of dichromatic laboratory mice [175]. Similar to primates, the long wavelength gene is X-linked, but there is no evidence for natural allelic variation. Experiments introduced an allele using genetic methods and created a situation similar to the new world primates. Similarly, heterozygous females were behaviorally trichromatic, although caveats to the conclusions exist [176]. Together, color vision in these two systems suggests that activity dependent plasticity is a powerful developmental mechanism that can enhance the flexibility of cortical circuits.

In contrast to the mammalian cortex, insect nervous systems appear to be more rigidly constrained and genetically specified [177, 178, 179], although a degree of activity dependent development can be observed [180, 181, 182]. For these animals, single epochs may be better thought of as generations. Because the backpropagation algorithm necessarily improves performance each epoch, training epochs could potentially be thought of even as numerous generations between adaptive genetic mutations. Some training epochs have a large effect on network performance, while others have a smaller effect, mirroring the exponential distribution of effect size that different genetic loci often have on behavioral traits.

Some degree of activity dependent development is known in insects, both in the visual [183] and olfactory systems [180, 184], although the extent of flexibility and function remains an open question. Conceivably, small amounts of developmental plasticity could match the first few training epochs, where mutant networks quickly recover trichromatic performance.

These changes entail shifting connection strengths, but don't fundamentally alter the computations. Plasticity that could mediate this has been observed anatomically in the olfactory system [180], but the functional effect of differing numbers of synaptic connections remains untested.

3.5.3 Curriculum learning

Classroom education, pet training, and behavioral experiments in a laboratory environment regularly use training techniques referred to as 'shaping' [185, 186]. Introducing numerous complex features of a task simultaneously can make learning difficult. In contrast, breaking tasks down into smaller, simpler tasks and iteratively adding complexity makes the task simpler overall and increases rates of learning. Implementing analogous methods in machine learning can lead to similar results, with networks performing and generalizing better [169].

My network simulations suggest that curriculum learning may also be valuable on evolutionary time scales. For regions of visual space where tri- and tetrachromatic networks performed well, trichromatic networks were significantly better. It first appeared that this was simply due to networks having the same number of hidden units but a restricted range of learnable stimuli. However, evolved networks inherited this improved performance. Since trichromatic computations require only 2 opponent channels, the dimensionality of the state space is much lower (4 inputs X 3 channels for tetrachromatic computations vs. 3 inputs X 2 channels for trichromatic computations). The stimulus set was identical for the network types, but the lower dimensionality of the feasible computations seems to have allowed for better computational solutions to be found.

3.5.4 Color vision as a special case

The simplicity of the computational state space for color vision was both a benefit and limitation of this study. At least in theory, there is a near infinite number of ways to implement color vision, which is supported by my network results [158, 159]. This means

that there is not necessarily a single globally optimal solution or local minimums. The benefit of this simplicity was that it isolated the effects of phylogenetic constraint. Because there is no single globally optimal solution, I can more confidently attribute my results showing strong similarities between networks sharing the same starting weights to constraints on learning trajectories.

However, this relatively simple computational landscape may not be reflective of the average computation implemented by a neural circuit. Computations for other behaviors and perceptions are conceivably much more complex, with the potential for local minima that vary in performance and barriers of bad performance that vary in how difficult they are to pass. The results presented here clearly show that ancestry constrains learning trajectories, but an important next step is to understand how these constraints might interact with complex computational landscapes. Perhaps networks will be capable of finding globally optimal solutions regardless of starting point. Alternatively, barriers may prevent globally optimal solutions and force a network to find a local optimum or prevent novel computations all together.

One way to address the interaction between constraint and optimality would be to identify a complex computation amenable to models of its evolution. Modifying the color vision circuits presented here is also an option though. For my models, both the input and output layers were symmetrical. Varying output unit widths or the number of output units for select regions of the spectrum could alter the computational state space and make some sets of computations better. This may reflect biology as well, as animals have different ecological needs and colors can vary in behavioral relevance across species and habitats [187]. A multitude of evidence indicates that photoreceptor tuning can adjust rapidly to suit these species specific needs [153]. It is possible, but untested, that the circuits implementing color vision also adapt.

3.5.5 Predictions for experiment

Directly relating simulation results to a real biological system is difficult, but my results do give predictions for future experimental work. Butterflies would be an excellent system for study, as they are a species rich group that heavily rely on color vision for natural behavior. The evolution of red photoreceptors is relatively common as well as numerous examples of species specific photoreceptors [90, 122, 123]. Comparative physiology across these animals could lead to insights about how color computations evolved from the shared trichromatic ancestors.

One prediction from these models is that color vision systems would be highly similar across butterflies. Similar to model hidden units, I would expect most neurons involved in color vision to have largely similar tuning properties across animals. Methods to identify and target homologous neurons would be necessary to test this prediction. One cell type of particular interest may be a large axon tract that directly connects the optic lobes to the mushroom bodies [188] and is known to include color opponent neurons (Michiyo Kinoshita, personal communications). A second prediction is that I might find an abundance of neurons specifically implementing green vs. red opponency. Butterfly anatomy might make the circuit especially amenable to this type of change, as the first optic neuropil exclusively receives input from green and red photoreceptors [103, 104].

3.5.6 Concluding remarks

Overall, my modeling results showed that ancestry constrained the evolution of novel computations. This result largely agrees with conceptual ideas in evolutionary biology as well as experiments on non-neural systems. Observations from the nervous system suggest these constraints are similarly important to the brain and behavior, with data from a limited but growing number of systems supporting this notion. These constraints have the potential to have a big impact on how neural circuits implement behaviorally relevant computations. The field of systems neuroscience often implicitly assumes optimal implementation of com-

putations, but barriers to evolution may make locally optimal solutions more accessible. Further examination and consideration of these constraints, circuit evolution, and phylogenetic history is an important aspect for understanding evolutionary patterns and principles that guide basic brain function.

3.6 Methods

3.6.1 Network design

Color vision networks were designed as 3 layer, feed forward networks that responded to monochromatic light stimuli. Preliminary networks were generated using a broad array of tuning parameters for both the input and output layers. The particular set of tuning parameters used in this study was chosen because it maximized performance differences between tri- and tetrachromatic networks. The input layer, simulating photoreceptors, had Gaussian tuning curves with 35 nm standard deviations centered on 350 (UV), 430 (blue), 520 (green), and 600 nm (red). Responses were scaled by a luminance factor between 1 and 100 and passed through a saturating nonlinearity that capped the response at 50. A total of 34 output units evenly tiled the visual range, from 320 to 650 nm in 10 nm increments. Each output unit had a standard deviation of 7.5 nm. The hidden layer had between 10 and 50 hidden units, with analyses focused on 30 hidden units. Hidden unit responses were passed through a sigmoid nonlinearity.

Networks were trained with the Levenberg-Marquardt backpropagation algorithm, which is the Matlab default. Alternative learning algorithms failed to perform well. Training samples were monochromatic light stimuli paired with a luminance factor. Wavelengths varied from 300 to 670 nm in 5 nm increments, and luminance factors varied continuously from 1 to 100. Each training epoch had 400 novel pairs of wavelength and luminance factor. Using this large training set minimized the influence of training data on learning trajectories and effectively isolated the effect of starting weights. Severely reduced training sets with 10 nm wavelength increments and 6 discrete luminance factors (228 total stimuli) resulted in only minor performance decrements.

Circuit evolution was simulated using a two stage training process. First, I trained trichromatic networks with a UV, blue, and two green input unit units. Starting weights were set with the Nguyen-Widrow initialization algorithm. The two green input units had identical

starting weights, making them function as a single input. After 50 training epochs, one of the green input units was mutated to red, and the network was trained for 100 more epochs. The un-mutated, trichromatic network was also trained for 50 more epochs (100 total), and these networks were used for all analyses. I trained 100 trichromatic networks using different random starting weights. Each trichromatic network was independently evolved 100 times using different sets of training data, for a total of 10,000 networks. In preliminary analyses I compared networks with different starting weights and the same training epochs. Results did not differ from networks with different starting weights and different training data.

As a comparison for evolved networks, I also trained a set of *de novo* networks. These networks were not pre-trained with a trichromatic input layer, but were otherwise identical to the evolved networks. Instead, these networks were directly trained for tetrachromatic vision from random starting weights. Mirroring the evolved networks, I generated 100 sets of random starting weights, again using the Nguyen-Widrow initialization algorithm. Each random network was trained 100 independent times using a tetrachromatic input layer. All analyses on these networks were performed in the same way as the evolved networks.

3.6.2 Network analysis

My goal in analyzing these networks was to compare the effects of starting weight on output layer performance and hidden layer computations. To accomplish this, I regularly separated networks into groups of 100. Four types of group were made: 1) evolved networks with the same trichromatic starting weights, 2) evolved networks with different trichromatic starting weights, 3) *de novo* networks with the same random starting weights, and 4) *de novo* networks with different random starting weights. With 100 unique starting points for evolved and *de novo* networks, this meant that each group type was comprised of 100 groups of 100 networks.

Using network simulations meant that I generated a large sample size. Having 10,000 evolved and *de novo* networks separated into 100 groups meant that nearly every statistical comparison was highly significant. I opted to instead employ a stricter significance criterion

based on effect size. Throughout the paper, rather than report p values, I instead report significance based on Cohens d > 0.50.

3.6.3 Network performance

I measured tuning curves for each of the 34 output units and compared them to the target response. Output unit responses were calculated for stimuli between 300 and 670 nm in 1 nm increments. Tuning curves were made by averaging the response across 10 luminance factors ranging from 10 to 100 in steps of 10. Performance was then defined as the MSE between the observed and expected tuning curve. Results were qualitatively similar when calculating the MSE for any single luminance factor. Overall performance decreased slightly without averaging, but the general shape of the performance figures was unchanged.

I assessed the effect of starting weights on performance by analyzing networks in groups that shared or did not share the same starting weights (see above). Fully trained networks showed little variation across all networks, so I instead analyzed performance after 10 training epochs. Performance was measured both as the average and standard deviation. Looking at average performance, I reduced each group to a single performance value by averaging across all networks and output units in a group. Each group type had 100 groups, and thus each group type resulted in a distribution of average performance. Mean centered distributions were compared between group types using a two tailed Kolmogorov Smirnov test with $\alpha = 0.05$. I also calculated the standard deviation of performance. Unlike average performance, I did not pool across output units for this analysis and instead examined each output unit individually.

3.6.4 Opponent channels

The overarching computational structure of the hidden layer was analyzed by using PCA to extract the opponent channels. For this analysis, each hidden unit was an observation, and the UV, blue, green, and red input weights were the variables. PCA reduced the dimension-

ality to 4 eigenvectors, the first three of which consistently had color opponent interactions. The fourth typically had all positive input weights and was not analyzed further. I used the same grouping scheme described above to compare networks that either shared or did not share the same starting weights. All opponent channels were scaled to unit vectors to make them comparable, but the sign was arbitrary. To account for this, I calculated every pairwise correlation between an opponent channel for one network and all other networks in a group of 100. Opponent channels with at least 50 negative correlations had its sign flipped. I tried several different procedures, and this correlation based method maximized similarities between networks.

Similarities and differences between networks were measured using agglomerative hierarchical clustering. I compared both single channels and the full set of three opponent channels together. I also generated groups of random opponent channels as a null hypothesis. These opponent channels were made with a random number generator, scaled to a unit vector, and sign flipped using the same correlation procedure. There was no prior expectation on how the opponent channels should be ordered, and efforts to maximize similarities found no procedure better than ordering and labeling opponent channels according to percent of variance explained. To examine the full set of channels, I concatenated the three channels into a 12 dimensional vector (3 channels X 4 input weights). I clustered networks using Euclidean distances between networks and a complete linkage algorithm, which maximized cophenetic correlations ($c > 0.85$). The clustering threshold was set at 1.0, but results did not depend on the precise threshold. In addition to cluster size, I also examined the distribution of all pairwise distances within a group of 100 networks. Pairwise distances were binned in distance intervals of 0.1 for visualization purposes and intervals of 0.01 for analysis since this bin size maximized distribution entropy. The distributions of pairwise distances were compared between group types using the Jensen-Shannon divergence, a metric related to the Kullback-Leibler divergence.

Opponent channels emerged through hidden units that varied both in relative opponent

interactions and in overall connection strength. To isolate the effects of relative opponent tuning, the weight magnitudes for each hidden unit were individually scaled to a unit vector. Using these networks with modified weights that preserved opponent tuning, I performed the identical opponent channel analysis.

3.6.5 Hidden unit weight changes

Changes to hidden unit tuning were tracked over training. Each hidden unit was treated as a 4 dimensional vector with a UV, blue, green, and red axis. Hidden units could independently vary in overall connection strength (i.e. vector length) or relative opponent interactions (i.e. vector direction), and I analyzed each using city block and cosine distances, respectively. Distances were calculated between the original, untrained hidden unit and the same hidden unit after training was complete. Since each starting point was independently trained 100 times, this resulted in a distribution of changes.

For each starting network, I calculated the mean distance and the standard deviation for each hidden unit. The hidden units for each network were then arranged in ascending order. Evolved networks were compared to *de novo* networks using Cohens d.

3.7 Supplemental figures

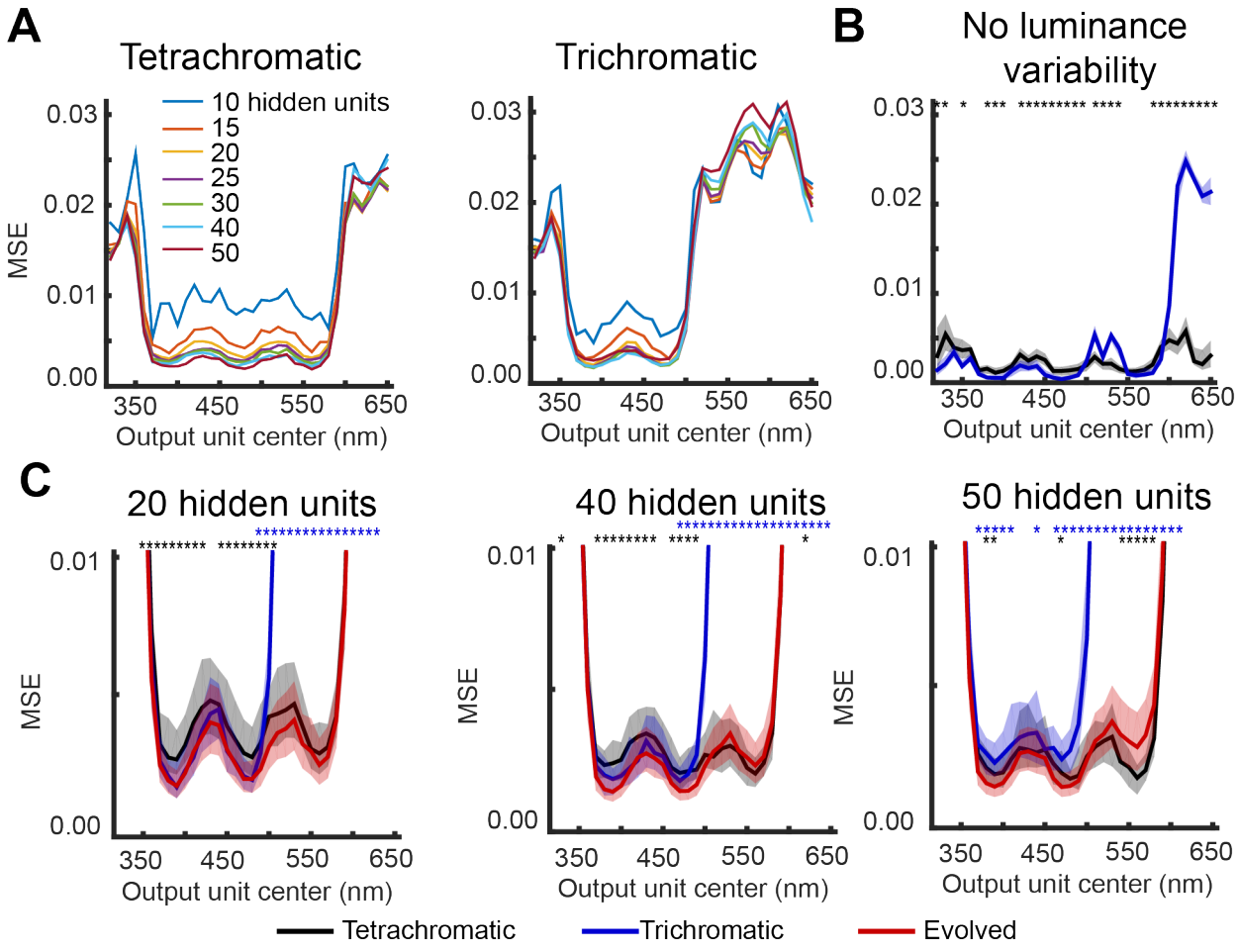

Figure 3.S1: [Effect of hidden layer size on performance
A) Performance is shown for tetrachromatic and trichromatic networks that vary in the size of the hidden layer.
B) Tri- and tetrachromatic networks were trained with stimuli that lacked differences in luminance.
C) Each panel shows the performance of evolved networks with different hidden layer sizes after 100 training epochs.

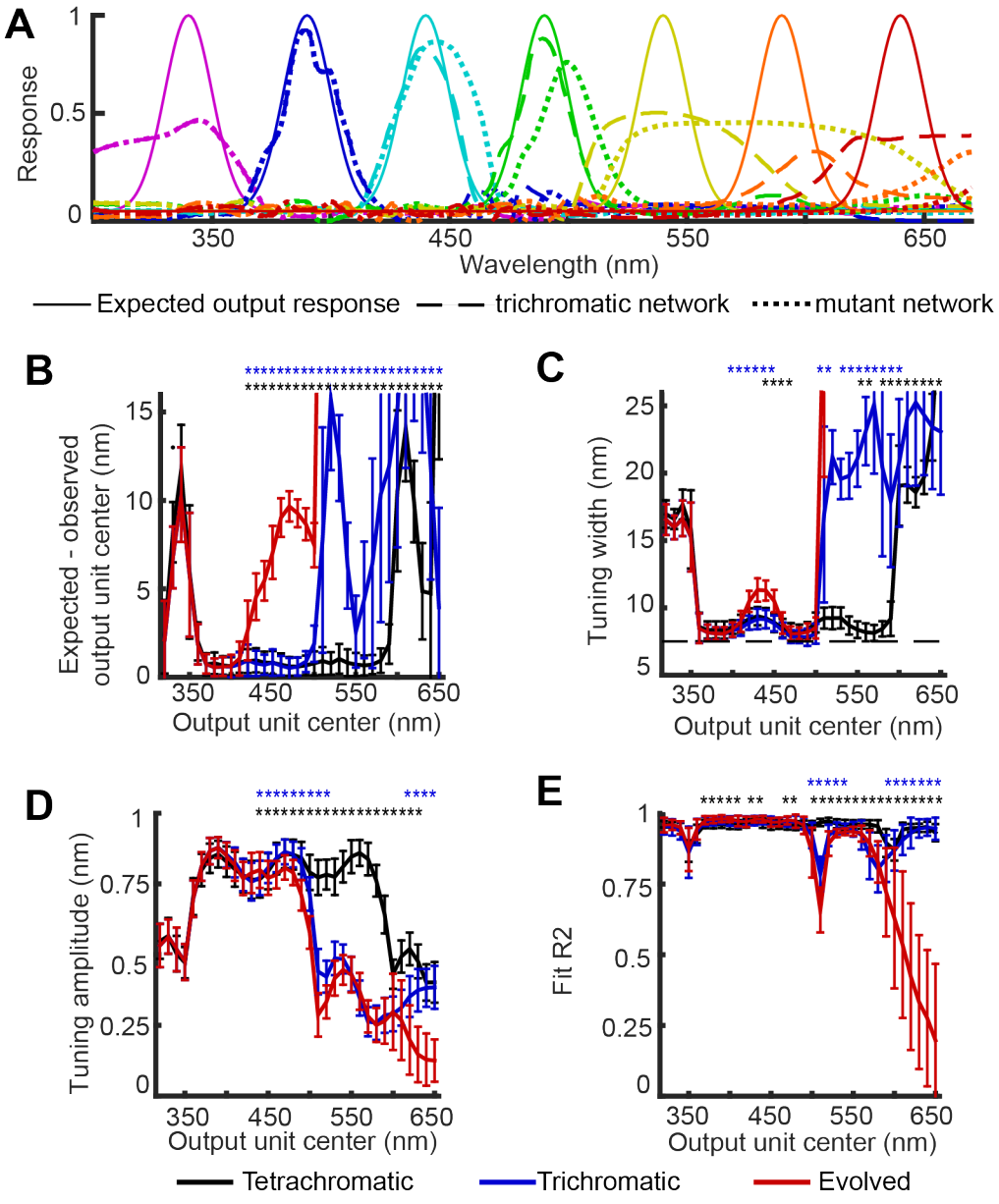

Figure 3.S2: Output unit RFs change little in mutant networks
A) Example output unit tuning curves are shown for a representative example of a network trained for trichromatic vision before and after mutating the input layer.
B, C, D) Rather than calculating the MSE, Gaussian tuning curves were fit to each individual output unit. Plots show the fit parameters of these Gaussians for trichromatic, tetrachromatic, and evolved networks. In panel C, the dotted line shows the tuning width of the target output unit RF. Data is shown as the mean ± SEM, with asterisks denoting significant differences between mutant networks and either tri- or tetrachromatic networks.

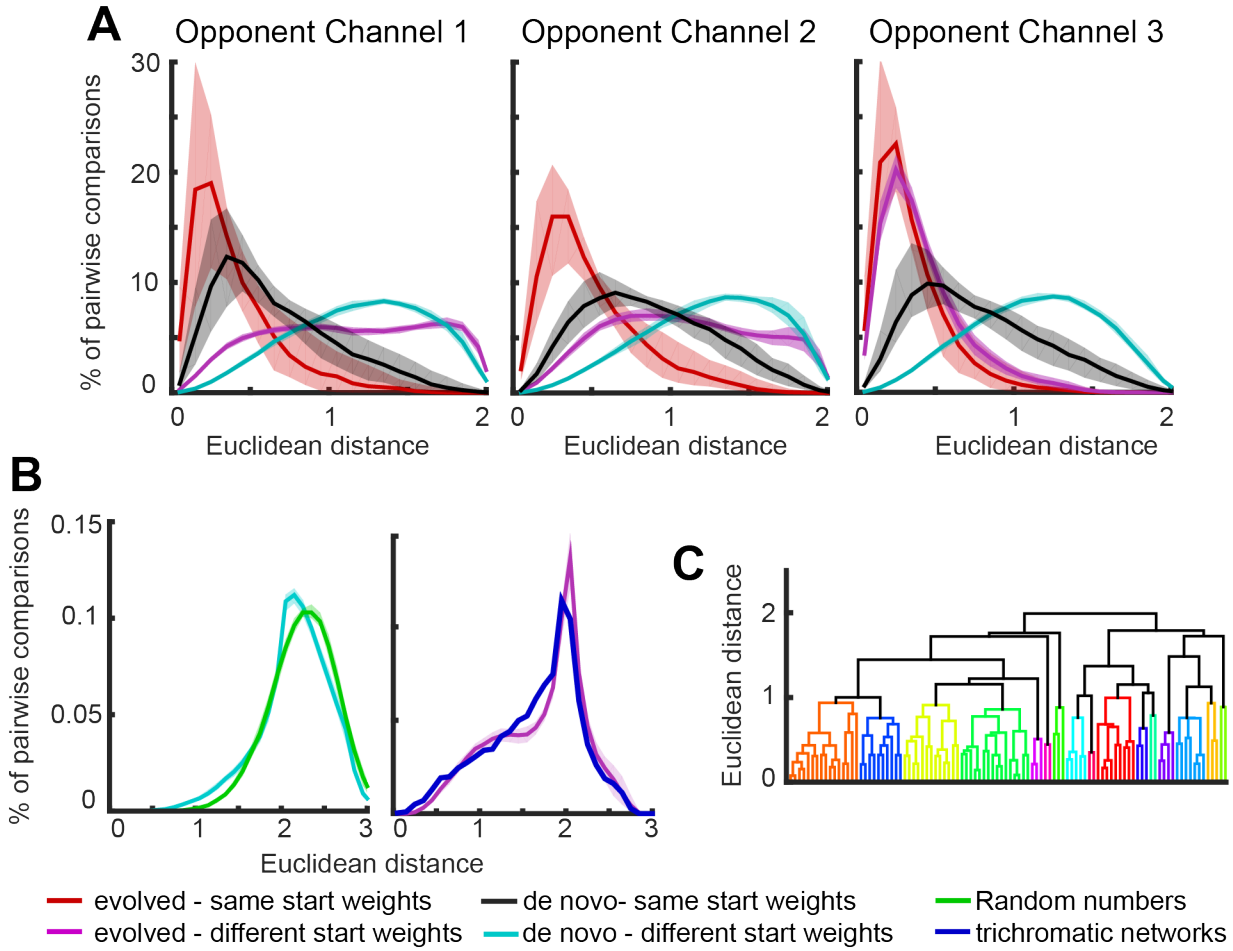

Figure 3.S3: Hierarchical clustering of single opponent channels
A) Each opponent channel was clustered individually, with plots showing the distribution of pairwise distances. Data largely matches results for the combined analysis (Fig. 3.4), except for the shift in the third channel for groups of evolved networks with different starting weights.
B) Distribution of pairwise distances is compared between groups of *de novo* networks with different starting weights and a null distribution made from random numbers (left), and between evolved networks with different starting weights and the original 100 trichromatic networks that were subsequently evolved.
C) Dendrogram shows the similarities in opponent channels for the original 100 trichromatic networks that were evolved into tetrachromatic networks.

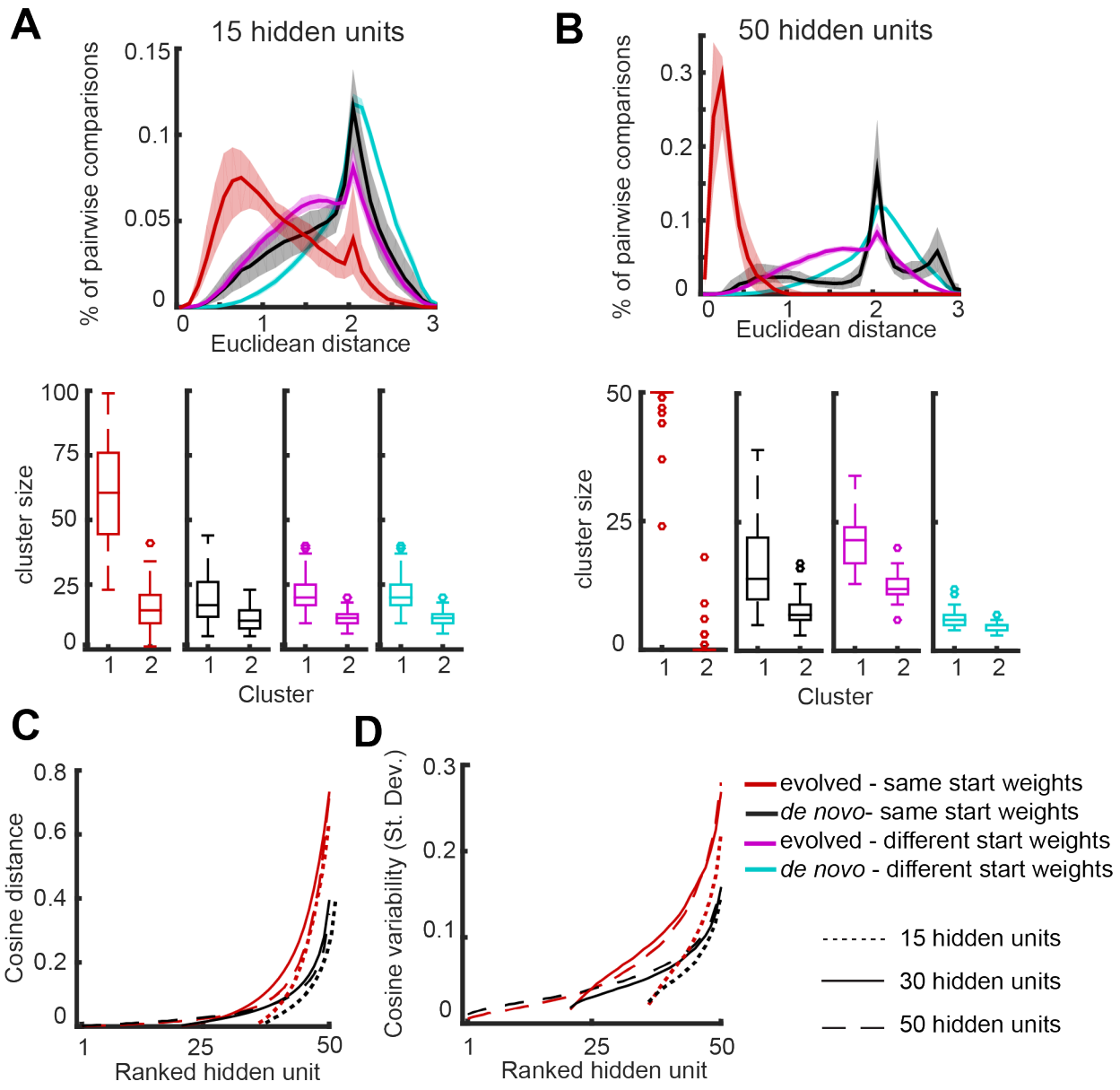

Figure 3.S4: Opponent channels for networks with different hidden layer sizes
A, B) Hierarchical clustering of networks that had 15 or 50 hidden units. The clustering threshold was set at a Euclidean distance 1.0. Note that, due to the slow speed of training, only 50 trichromatic networks with 50 hidden units were generated, with each evolved 50 times.
C, D) Cosine distances were calculated for hidden units before and after training for networks with different hidden layer sizes. Plots show hidden units ranked by median distance (C) and distance variability (D). Ranked hidden units are aligned to hidden unit 50, such that the 15 hidden layer networks are plotted as ranked hidden units 36 to 50 on the x-axis.

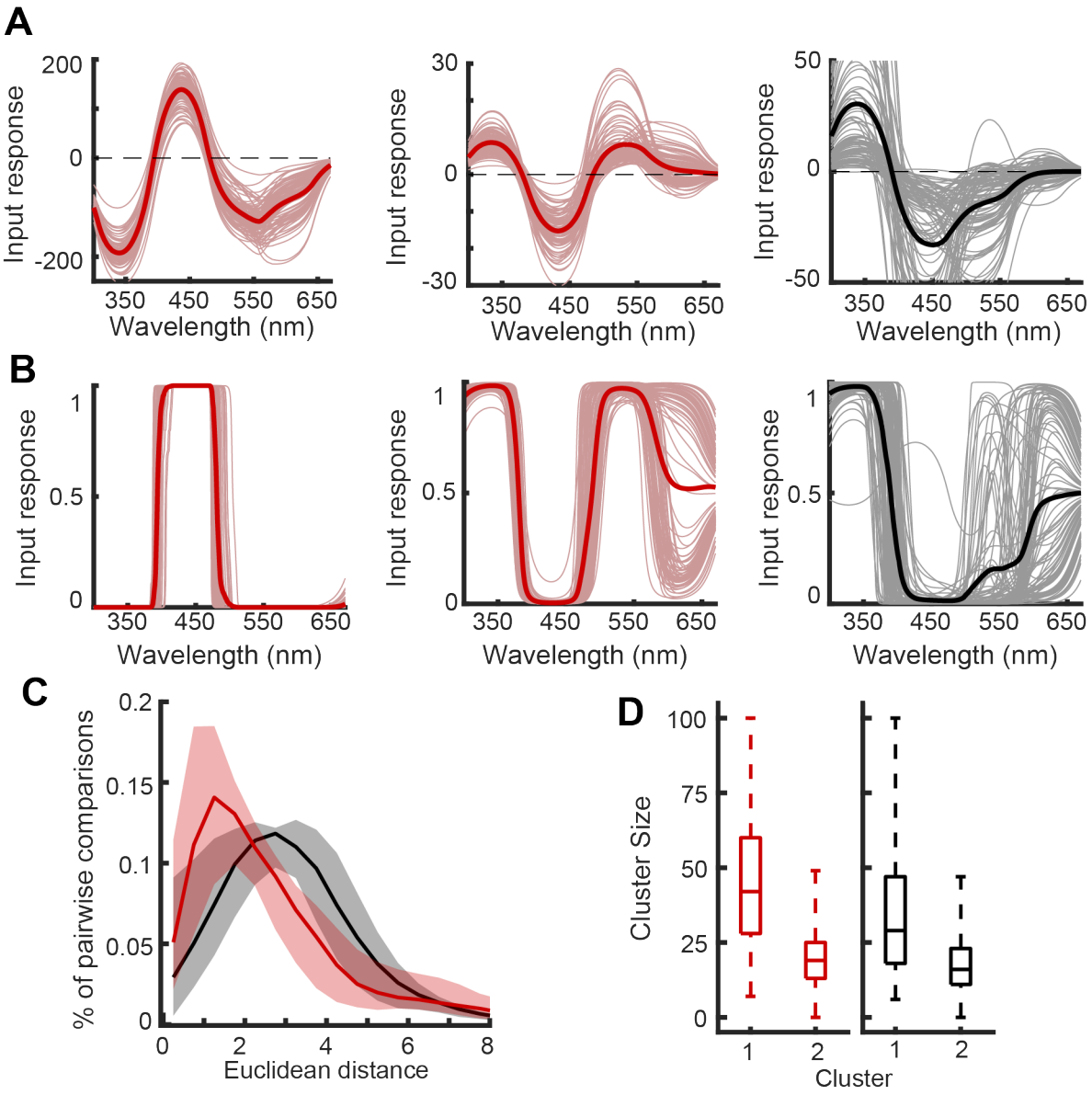

Figure 3.S5: Hidden unit output responses
A) Each plot shows the input tuning of homologous hidden units trained from the same starting weights. Each point represents the response of the input layer photoreceptors to a monochromatic stimulus convolved with the input weights.
B) Input responses of a hidden unit are passed through a sigmoid non-linearity that scales responses to values between 0 and 1. Notice that variability is primarily observed for regions where input tuning curves are on both sides of the 0 line.
C, D) Homologous output units were analyzed using hierarchical clustering. Even though cosine distances for the input weights are larger and more variable for evolved networks, output tuning curves are more similar than *de novo* networks.

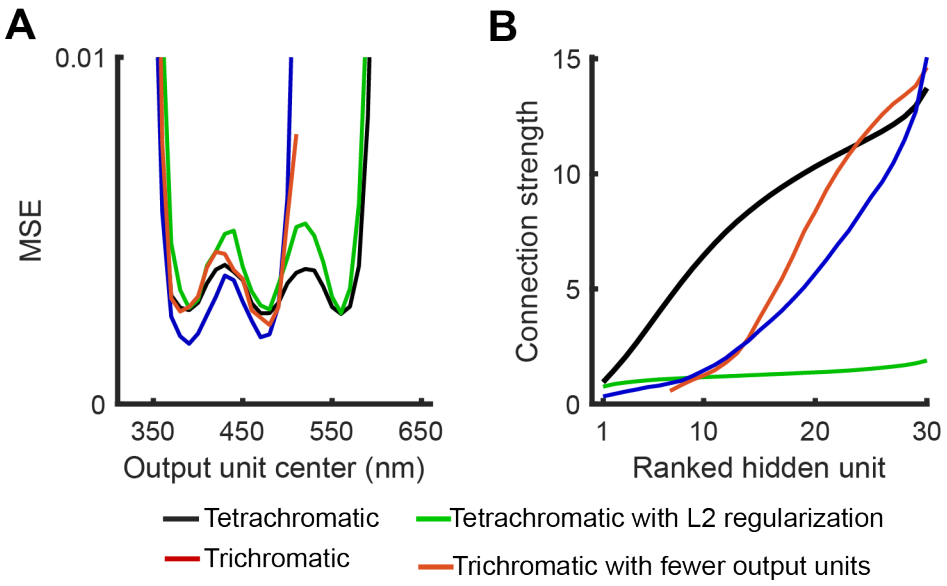

Figure 3.S6: Alternative training protocols
Trichromatic networks were generated without long wavelength output units. Tetrachromatic networks were generated using an L2 regularization term explicitly added to the training protocol. Figures show the performance (A) and connection strength (B) for these networks. Combined, these two sets of networks suggest that the performance enhancement of trichromatic networks is specifically due to output units that are unable to learn by design.

CHAPTER 4

CONCLUSIONS

4.1 Summary of results

For my thesis work, I completed two projects that used complementary approaches to examine the evolution of neural computation in circuits related to color vision. Color vision was a good model system as the computations associated with color perception are relatively simple, well-understood, and tractable relative to other sensory systems [158, 189]. These aspects of color vision make it accessible for comparative studies across different neural circuits. My projects represent a first step in understanding the evolution of color vision computation and neural circuits and lay the foundation for future experimental work that has the potential to uncover broad patterns of neural circuit evolution.

The experimental portion of my thesis examined the neural basis of courtship preferences in *Heliconius* butterflies. Although the project was specifically focused on studying a complex behavioral decision of which females to court, this decision is primarily mediated through color vision. Males preferentially court white or yellow females (or both), and this was shown to have a genetic origin associated with a single genetic locus. Characterizing the functional organization of the eye revealed a surprising amount of diversity across species and sex. One feature in particular that represented a signature of synaptic connectivity and color opponent computations between photoreceptors correlated well with male mate preference. Males preferring yellow females had UV photoreceptors that usually had inhibition from LW photoreceptors, while males preferring white females lacked these connections. Future investigations into how central brain circuits process information could lead to greater insights into how this difference in peripheral connectivity influences male preference. Experiments could also be extended to other *Heliconius* species, a genus where male preference for conspecific wing patterns that have a Mendelian genetic origin is common [71]. With convergence and divergence of wing patterns in these mimetic butterflies, this diversity could potentially

reveal patterns of how and why particular circuit modifications are made to change behavior.

My second project took a theoretical approach to the evolution of color vision using neural networks trained with standard machine learning algorithms. This project was particularly interested in asking how phylogenetic history might constrain the evolution of new perceptions and the underlying computations. Multiple networks were trained for trichromatic vision to simulate distinct phylogenetic lineages. Convergent and parallel evolution was then simulated by repeatedly mutating the 'eye' of these networks to tetrachromatic and observing how the performance and computations responded. Results were broadly consistent with conceptual ideas in evolutionary biology about how evolutionary constraints bias but do not prohibit evolutionary trajectories [4]. An obvious next step continuing the modeling approach would be to add complexity to the computation, making the adaptive landscape more rugged and less symmetrical. This added complexity would add optimality into the equation, asking how optimal solutions interact with the constraints I observed. The modeling results also generated predictions for future experimental studies. A real nervous system is significantly more complex than my three layer neural networks, but my results would predict that butterflies with independent origins of tetrachromatic vision would nonetheless have optic lobe circuits and computations that are highly similar because they share a similar trichromatic ancestor.

4.2 Evolution of peripheral sensory systems

The peripheral nervous system is thought to be particularly amenable to evolutionary modification. Because the periphery is relatively, feed-forward and modular, modifications can occur with limited pleiotropic effects. Changes in sensitivity or a new receptor type can enhance the detectability of behaviorally relevant sensory cues, but neural processing of these novel peripheral responses can potentially proceed without substantial alterations. Sensory receptors for vision [35], audition [34], and chemosensation [33] can rapidly diversify, and tuning changes can occur with a limited number of genetic mutations. These changes often

appear related to adaptation to the statistics of the natural environment, but have also been shown to be capable of enacting large behavioral changes [37, 38, 39]. The peripheral motor system seems similarly capable of modification, with research often focusing on homologous neurons comprising central pattern generators [190].

Both of my projects examined how evolution of the peripheral visual system might contribute to the evolution of color vision behaviors and perceptions. Results from each project were broadly consistent with peripheral sensory systems being evolutionarily labile. The *Heliconius* butterflies I studied are very closely related, yet eye organization varied substantially between species and with sex. Most of these differences likely require few or no changes to how the central brain processes in the incoming sensory information. For example, UV2 is thought to be useful for increasing the discriminability of the genus specific 3-OHK yellow pigment from other yellow pigments. This enhanced discrimination does not require circuit changes, but instead simply emerges for free from the shifted spectral sensitivity. For the theory project, the first step in network evolution was the mutation of the input layer from tri- to tetrachromatic by the addition of a novel red photoreceptor. This mutation impaired network performance slightly, but the networks retained trichromatic color vision to a large degree. This lack of deleterious effects showed that central circuits might be robust to changes of the periphery.

Results from my project also highlighted the potentially limited capacity of simple peripheral changes alone to enact large changes in behavior. In my butterfly experiments, the difference in eye organization that was related to mate preference was not a simple change in spectral sensitivity but rather a signature of differences in photoreceptor synaptic connectivity. Simple models further showed that simple, linear changes would be unable to lead to a radical shift in preference for wings that differ primarily in presence or absence of UV reflectance. Synaptic connectivity differences could have large, non-linear effects on processing that enables this big shift in perception and behavioral preference. Despite the complexity of this modification compared to shifts in spectral sensitivity, a potential neural

correlate of male preference was still observed in the peripheral visual system. Overall, this result suggests that both peripheral circuits and receptors may be especially amenable to evolutionary change.

Similarly for my theory project, a novel photoreceptor alone was insufficient to confer improved and expanded color vision. Gaining the capacity for green vs. red discrimination instead required retraining the networks so that it could develop a new set of computations. This result in particular highlights the limitations in the evolution of sensory receptors. Changes in peripheral sensing can adapt an animal to the statistics of the natural environment, but they cannot necessarily lead to novel computations. Large shifts in perception such as adding a novel color dimension to color vision, however, does require a shift in how sensory information is processed.

4.3 Constraints on evolution

Evolutionary processes are constrained and biased by phylogenetic history [4]. Evolutionary trajectories can be biased into paths that are more accessible while preventing evolution of a phenotype that may be optimal. Throughout biology, consideration of evolutionary constraints and the mechanisms of evolution has been an important aspect of understanding broader evolutionary patterns [6]. Due to the inherently complex and highly integrated organization of neural circuits, these constraints may be especially strong for evolution of the brain and behavior [14]. Thus, evolutionary constraints may play an important role in how neural circuits and the computations they implement are organized to mediate adaptive, observable behaviors.

Direct tests of phylogenetic constraint were not feasible for my experimental study focused on eye organization in a small group of closely related butterflies. However, my results as well as genus-wide preferences for conspecific wing patterns make this system an excellent model for future investigations into this issue. First, the possibility of gaining genetic access to a courtship specific circuit through the transcription factor fruitless would allow for in-

depth studies of neural computation evolution. Circuit differences between butterflies with different preferences could then be understood in the context of how the circuit functions as a whole, and potentially lead to intuitions into why photoreceptor synaptic connectivity is the locus for evolutionary change. The power of this well-defined circuit has already been illustrated through the study of two *Drosophila* species with different pheromone preferences [13]. Second, diversity across the genus in Mendelian wing patterns could allow for wide spread comparative studies of the neural basis for courtship. Combining in-depth circuit studies related to genetic variability with comparative studies across the genus would allow for these complementary bottom-up and top-down approaches to be combined into a single model system that could reveal patterns of how neural circuits evolve.

The effect of phylogenetic history on evolution was the focus of my theoretical project. This project combined parallel evolution of tetrachromatic vision within a lineage as well as convergent evolution across lineages. Every network was capable of learning the novel computation, which is consistent with evolution not strictly prohibiting any evolutionary trajectories. Further, phylogenetic history did in fact constrain the evolution of novel computations. If I was to examine just a single evolution from different lineages, I might conclude that color vision is not constrained since networks used a variety of computational mechanisms. However, the precise evolutionary trajectories were contingent on the specific trichromatic starting points. Parallel evolution within a lineage consistently converged on a severely limited number of computations even though the potential computational space was effectively infinite. Overall, these modeling results suggest that phylogenetic history is an important aspect to consider when trying to understand how neural circuits implement behaviorally relevant computations.

4.4 Final remarks

Evolution in the fundamental concept and theory that unites and underlies all of biology. Within neuroscience, an evolutionary perspective has the capacity to bridge gaps between

different levels of analysis including genetics, cellular biology, and systems neuroscience. Ultimately all of these aspects of nervous system combine, converge, and interact at the level of neural circuits and the computations they implement to mediate adaptive behaviors. Exploring how evolutionary processes and constraints affect nervous system organization has not only intrinsic value, but can also lead to insights into the basic principles underlying the functional organization of the brain.

REFERENCES

[1] Tim W. Fawcett, Steven Hamblin, and Luc-Alain Giraldeau. Exposing the behavioral gambit: the evolution of learning and decision rules. *Behavioral Ecology*, 24(1):2–11, January 2013.

[2] G. A. Parker and J. Maynard Smith. Optimality theory in evolutionary biology. *Nature*, 348(6296):27–33, November 1990.

[3] MelinaE. Hale. Mapping Circuits beyond the Models: Integrating Connectomics and Comparative Neuroscience. *Neuron*, 83(6):1256–1258, September 2014.

[4] J. Maynard Smith, R. Burian, S. Kauffman, P. Alberch, J. Campbell, B. Goodwin, R. Lande, D. Raup, and L. Wolpert. Developmental Constraints and Evolution: A Perspective from the Mountain Lake Conference on Development and Evolution. *The Quarterly Review of Biology*, 60(3):265–287, September 1985.

[5] Gnter P. Wagner and Lee Altenberg. Perspective: Complex Adaptations and the Evolution of Evolvability. *Evolution*, 50(3):967–976, 1996.

[6] Paul M. Brakefield. Evo-devo and accounting for Darwin's endless forms. *Philosophical Transactions of the Royal Society B: Biological Sciences*, 366(1574):2069–2075, July 2011.

[7] Jay F. Storz. Causes of molecular convergence and parallelism in protein evolution. *Nature Reviews Genetics*, 17(4):239–250, April 2016.

[8] David L. Stern. The genetic causes of convergent evolution. *Nature Reviews Genetics*, 14(11):751–764, November 2013.

[9] Maria Antonietta Tosches. Developmental and genetic mechanisms of neural circuit evolution. *Developmental Biology*, 431(1):16–25, November 2017.

[10] Paul S Katz. Evolution and development of neural circuits in invertebrates. *Current Opinion in Neurobiology*, 17(1):59–64, February 2007.

[11] Paul S Katz and Phoenix D Quinlan. The importance of identified neurons in gastropod molluscs to neuroscience. *Current Opinion in Neurobiology*, 56:1–7, June 2019.

[12] Yun Ding, Joshua L. Lillvis, Jessica Cande, Gordon J. Berman, Benjamin J. Arthur, Xi Long, Min Xu, Barry J. Dickson, and David L. Stern. Neural Evolution of Context-Dependent Fly Song. *Current Biology*, 29(7):1089–1099.e7, April 2019.

[13] Laura F. Seeholzer, Max Seppo, David L. Stern, and Vanessa Ruta. Evolution of a central neural circuit underlies Drosophila mate preferences. *Nature*, 559(7715):564–569, July 2018.

[14] Paul S. Katz. Neural mechanisms underlying the evolvability of behaviour. *Philosophical Transactions of the Royal Society B: Biological Sciences*, 366(1574):2086–2099, July 2011.

[15] James P. C. Dumont and R. Meldrum Robertson. Neuronal Circuits: An Evolutionary Perspective. *Science*, 233(4766):849–853, August 1986.

[16] A. J. Tierney. Evolutionary implications of neural circuit structure and function. *Behavioural Processes*, 35(1):173–182, December 1995.

[17] T. Bullock and G.A. Horridge. *Structure and function in the nervous systems of invertebrates*. Structure and function in the nervous systems of invertebrates. San Francisco, Freeman, 1965.

[18] Rafael Yuste. From the neuron doctrine to neural networks. *Nature Reviews Neuroscience*, 16(8):487–497, August 2015.

[19] Kiisa C Nishikawa, Curtis W Anderson, Stephen M Deban, and James C O'Reilly. The evolution of neural circuits controlling feeding behavior in frogs. *Brain, behavior and evolution*, 40(2-3):125–140, 1992.

[20] J. Lee Kavanau. Conservative behavioural evolution, the neural substrate. *Animal Behaviour*, 39(4):758–767, April 1990.

[21] Sean Psujek and Randall D. Beer. Developmental bias in evolution: evolutionary accessibility of phenotypes in a model evo-devo system. *Evolution & Development*, 10(3):375–390, 2008.

[22] Andres Bendesky and Cornelia I. Bargmann. Genetic contributions to behavioural diversity at the geneenvironment interface. *Nature Reviews Genetics*, 12(12):809–820, December 2011.

[23] John Irwin Johnson, John A. W. Kirsch, Roger L. Reep, and Robert C. Switzer Iii. Phylogeny through Brain Traits: More Characters for the Analysis of Mammalian Evolution. *Brain, Behavior and Evolution*, 43(6):319–347, 1994.

[24] I. Sinakevitch, J. K. Douglass, G. Scholtz, R. Loesel, and N. J. Strausfeld. Conserved and convergent organization in the optic lobes of insects and isopods, with reference to other crustacean taxa. *Journal of Comparative Neurology*, 467(2):150–172, 2003.

[25] Elke K. Buschbeck and Nicholas J. Strausfeld. The relevance of neural architecture to visual performance: Phylogenetic conservation and variation in dipteran visual systems. *Journal of Comparative Neurology*, 383(3):282–304, 1997.

[26] Sarah M. Farris and Nathan S. Roberts. Coevolution of generalist feeding ecologies and gyrencephalic mushroom bodies in insects. *Proceedings of the National Academy of Sciences*, 102(48):17394–17399, November 2005.

[27] S. R. Shaw and D. Moore. Evolutionary remodeling in a visual system through extensive changes in the synaptic connectivity of homologous neurons. *Visual Neuroscience*, 3(5):405–410, November 1989.

[28] Jennifer Dugas-Ford, Joanna J. Rowell, and Clifton W. Ragsdale. Cell-type homologies and the origins of the neocortex. *Proceedings of the National Academy of Sciences*, 109(42):16974–16979, October 2012.

[29] Walter J Gehring and Kazuho Ikeo. Pax 6: mastering eye morphogenesis and eye evolution. *Trends in Genetics*, 15(9):371–377, September 1999.

[30] Trevor D. Lamb. Evolution of phototransduction, vertebrate photoreceptors and retina. *Progress in Retinal and Eye Research*, 36:52–119, September 2013.

[31] James M Newcomb and Paul S Katz. Different functions for homologous serotonergic interneurons and serotonin in species-specific rhythmic behaviours. *Proceedings of the Royal Society B: Biological Sciences*, 276(1654):99–108, January 2009.

[32] Larry J. Young and Zuoxin Wang. The neurobiology of pair bonding. *Nature Neuroscience*, 7(10):1048–1054, October 2004.

[33] Atsushi Matsui, Yasuhiro Go, and Yoshihito Niimura. Degeneration of Olfactory Receptor Gene Repertories in Primates: No Direct Link to Full Trichromatic Vision. *Molecular Biology and Evolution*, 27(5):1192–1200, May 2010.

[34] Robert R. Capranica and Anne J. M. Moffat. Neurobehavioral Correlates of Sound Communication in Anurans. In Jrg-Peter Ewert, Robert R. Capranica, and David J. Ingle, editors, *Advances in Vertebrate Neuroethology*, NATO Advanced Science Institutes Series, pages 701–730. Springer US, Boston, MA, 1983.

[35] Julin Torres-Dowdall, Michele E. R. Pierotti, Andreas Hrer, Nidal Karagic, Joost M. Woltering, Frederico Henning, Kathryn R. Elmer, and Axel Meyer. Rapid and Parallel Adaptive Evolution of the Visual System of Neotropical Midas Cichlid Fishes. *Molecular Biology and Evolution*, 34(10):2469–2485, October 2017.

[36] Jack W. Bradbury and Sandra L. Vehrencamp. *Principles of animal communication, 2nd ed.* Principles of animal communication, 2nd ed. Sinauer Associates, Sunderland, MA, US, 2011.

[37] Patrick T. McGrath, Yifan Xu, Michael Ailion, Jennifer L. Garrison, Rebecca A. Butcher, and Cornelia I. Bargmann. Parallel evolution of domesticated Caenorhabditis species targets pheromone receptor genes. *Nature*, 477(7364):321–325, September 2011.

[38] Lucia L. Prieto-Godino, Raphael Rytz, Steeve Cruchet, Benote Bargeton, Liliane Abuin, Ana F. Silbering, Vanessa Ruta, Matteo Dal Peraro, and Richard Benton. Evolution of Acid-Sensing Olfactory Circuits in Drosophilids. *Neuron*, 93(3):661–676.e6, February 2017.

[39] Gerald H. Jacobs. Evolution of colour vision in mammals. *Philosophical Transactions of the Royal Society B: Biological Sciences*, 364(1531):2957–2967, October 2009.

[40] Chelsea A. Weitekamp and Laurent Keller. Genes and Behaviour. In *Genes and Behaviour*, pages 93–109. John Wiley & Sons, Ltd, 2019.

[41] J. Roman Arguello and Richard Benton. Open questions: Tackling Darwins instincts: the genetic basis of behavioral evolution. *BMC Biology*, 15(1):26, April 2017.

[42] Jesse N. Weber, Brant K. Peterson, and Hopi E. Hoekstra. Discrete genetic modules are responsible for complex burrow evolution in Peromyscus mice. *Nature*, 493(7432):402–405, January 2013.

[43] Caroline K. Hu and Hopi E. Hoekstra. Peromyscus burrowing: A model system for behavioral evolution. *Seminars in Cell & Developmental Biology*, 61:107–114, January 2017.

[44] Jennifer Dugas-Ford and Clifton W. Ragsdale. Levels of Homology and the Problem of Neocortex. *Annual Review of Neuroscience*, 38(1):351–368, July 2015.

[45] Detlev Arendt, Jacob M. Musser, Clare V. H. Baker, Aviv Bergman, Connie Cepko, Douglas H. Erwin, Mihaela Pavlicev, Gerhard Schlosser, Stefanie Widder, Manfred D. Laubichler, and Gnter P. Wagner. The origin and evolution of cell types. *Nature Reviews Genetics*, 17(12):744–757, December 2016.

[46] Alexandru S. Denes, Gspr Jkely, Patrick R. H. Steinmetz, Florian Raible, Heidi Snyman, Benjamin Prud'homme, David E. K. Ferrier, Guillaume Balavoine, and Detlev Arendt. Molecular Architecture of Annelid Nerve Cord Supports Common Origin of Nervous System Centralization in Bilateria. *Cell*, 129(2):277–288, April 2007.

[47] Linda Z. Holland, Joo E. Carvalho, Hector Escriva, Vincent Laudet, Michael Schubert, Sebastian M. Shimeld, and Jr-Kai Yu. Evolution of bilaterian central nervous systems: a single origin? *EvoDevo*, 4(1):27, October 2013.

[48] Joshua R. Sanes and S. Lawrence Zipursky. Design Principles of Insect and Vertebrate Visual Systems. *Neuron*, 66(1):15–36, April 2010.

[49] Gilles Laurent. Olfactory network dynamics and the coding of multidimensional signals. *Nature Reviews Neuroscience*, 3(11):884–895, November 2002.

[50] David J. Anderson. Circuit modules linking internal states and social behaviour in flies and mice. *Nature Reviews Neuroscience*, 17(11):692–704, November 2016.

[51] Gary J. Rose. Insights into neural mechanisms and evolution of behaviour from electric fish. *Nature Reviews Neuroscience*, 5(12):943–951, December 2004.

[52] Henry Walter Bates. Contributions to an Insect Fauna of the Amazon Valley. Lepidoptera: Heliconid. *Transactions of the Linnean Society of London*, 23(3):495–566, 1862.

[53] K S Brown. The Biology of Heliconius and Related Genera. *Annual Review of Entomology*, 26(1):427–457, 1981.

[54] Carlos F. Arias, Camilo Salazar, Claudia Rosales, Marcus R. Kronforst, Mauricio Linares, Eldredge Bermingham, and W. Owen McMillan. Phylogeography of Heliconius cydno and its closest relatives: disentangling their origin and diversification. *Molecular Ecology*, 23(16):4137–4152, 2014.

[55] James Mallet and Mathieu Joron. Evolution of Diversity in Warning Color and Mimicry: Polymorphisms, Shifting Balance, and Speciation. *Annual Review of Ecology and Systematics*, 30(1):201–233, 1999.

[56] N. S. Flanagan, A. Tobler, A. Davison, O. G. Pybus, D. D. Kapan, S. Planas, M. Linares, D. Heckel, and W. O. McMillan. Historical demography of Mllerian mimicry in the neotropical Heliconius butterflies. *Proceedings of the National Academy of Sciences*, 101(26):9704–9709, June 2004.

[57] Nicola L. Chamberlain, Ryan I. Hill, Durrell D. Kapan, Lawrence E. Gilbert, and Marcus R. Kronforst. Polymorphic Butterfly Reveals the Missing Link in Ecological Speciation. *Science*, 326(5954):847–850, November 2009.

[58] Durrell D. Kapan. Three-butterfly system provides a field test of mllerian mimicry. *Nature*, 409(6818):338–340, January 2001.

[59] Richard M. Merrill, Richard W. R. Wallbank, Vanessa Bull, Patricio C. A. Salazar, James Mallet, Martin Stevens, and Chris D. Jiggins. Disruptive ecological selection on a mating cue. *Proceedings of the Royal Society B: Biological Sciences*, 279(1749):4907–4913, December 2012.

[60] Marcus R. Kronforst and Riccardo Papa. The Functional Basis of Wing Patterning in Heliconius Butterflies: The Molecules Behind Mimicry. *Genetics*, 200(1):1–19, May 2015.

[61] Ryan A. York and Russell D. Fernald. The Repeated Evolution of Behavior. *Frontiers in Ecology and Evolution*, 4, 2017.

[62] Riccardo Papa, Durrell D. Kapan, Brian A. Counterman, Karla Maldonado, Daniel P. Lindstrom, Robert D. Reed, H. Frederik Nijhout, Tomas Hrbek, and W. Owen McMillan. Multi-Allelic Major Effect Genes Interact with Minor Effect QTLs to Control Adaptive Color Pattern Variation in Heliconius erato. *PLOS ONE*, 8(3):e57033, March 2013.

[63] Marcus R. Kronforst, Laura G. Young, Durrell D. Kapan, Camille McNeely, Rachel J. O'Neill, and Lawrence E. Gilbert. Linkage of butterfly mate preference and wing color preference cue at the genomic location of wingless. *Proceedings of the National Academy of Sciences*, 103(17):6575–6580, April 2006.

[64] H. Frederik Nijhout, Gregory A. Wray, and Lawrence E. Gilbert. An analysis of the phenotypic effects of certain colour pattern genes in Heliconius (Lepidoptera: Nymphalidae). *Biological Journal of the Linnean Society*, 40(4):357–372, August 1990.

[65] H. Alejandro Merchn, Chris D. Jiggins, and Mauricio Linares. A Narrow Heliconius cydno (Nymphalidae; Heliconiini) Hybrid Zone With Differences in Morph Sex Ratios1. *Biotropica*, 37(1):119–128, 2005.

[66] LE Gilbert. Adaptive novelty through introgression in Heliconius wing patterns: evidence for shared genetic tool box from synthetic hybrid zones and a theory of diversification. *Ecology and evolution taking flight: butterflies as model systems*, pages 281–318, 2003.

[67] Marcus R. Kronforst, Durrell D. Kapan, and Lawrence E. Gilbert. Parallel Genetic Architecture of Parallel Adaptive Radiations in Mimetic Heliconius Butterflies. *Genetics*, 174(1):535–539, September 2006.

[68] Robert D. Reed, Riccardo Papa, Arnaud Martin, Heather M. Hines, Brian A. Counterman, Carolina Pardo-Diaz, Chris D. Jiggins, Nicola L. Chamberlain, Marcus R. Kronforst, Rui Chen, Georg Halder, H. Frederik Nijhout, and W. Owen McMillan. optix Drives the Repeated Convergent Evolution of Butterfly Wing Pattern Mimicry. *Science*, 333(6046):1137–1141, August 2011.

[69] Arnaud Martin, Riccardo Papa, Nicola J. Nadeau, Ryan I. Hill, Brian A. Counterman, Georg Halder, Chris D. Jiggins, Marcus R. Kronforst, Anthony D. Long, W. Owen McMillan, and Robert D. Reed. Diversification of complex butterfly wing patterns by repeated regulatory evolution of a Wnt ligand. *Proceedings of the National Academy of Sciences*, 109(31):12632–12637, July 2012.

[70] Anyi Mazo-Vargas, Carolina Concha, Luca Livraghi, Darli Massardo, Richard W. R. Wallbank, Linlin Zhang, Joseph D. Papador, Daniel Martinez-Najera, Chris D. Jiggins, Marcus R. Kronforst, Casper J. Breuker, Robert D. Reed, Nipam H. Patel, W. Owen McMillan, and Arnaud Martin. Macroevolutionary shifts of WntA function potentiate butterfly wing-pattern diversity. *Proceedings of the National Academy of Sciences*, 114(40):10701–10706, October 2017.

[71] Chris D. Jiggins. Ecological Speciation in Mimetic Butterflies. *BioScience*, 58(6):541–548, June 2008.

[72] James Mallet. What does Drosophila genetics tell us about speciation? *Trends in Ecology & Evolution*, 21(7):386–393, July 2006.

[73] Chris D. Jiggins, Russell E. Naisbit, Rebecca L. Coe, and James Mallet. Reproductive isolation caused by colour pattern mimicry. *Nature*, 411(6835):302–305, May 2001.

[74] Jess Mavrez, Camilo A. Salazar, Eldredge Bermingham, Christian Salcedo, Chris D. Jiggins, and Mauricio Linares. Speciation by hybridization in Heliconius butterflies. *Nature*, 441(7095):868–871, June 2006.

[75] Claire Mrot, Brigitte Frrot, Ene Leppik, and Mathieu Joron. Beyond magic traits: Multimodal mating cues in Heliconius butterflies. *Evolution*, 69(11):2891–2904, 2015.

[76] Kathy Darragh, Sohini Vanjari, Florian Mann, Maria F. Gonzalez-R, Colin R. Morrison, Camilo Salazar, Carolina Pardo-Diaz, Richard M. Merrill, W. Owen McMillan, Stefan Schulz, and Chris D. Jiggins. Male sex pheromone components in Heliconius butterflies released by the androconia affect female choice. *bioRxiv*, page 033506, May 2017.

[77] Chris D. Jiggins, Mauricio Linares, Russell E. Naisbit, Camilo Salazar, Ziheng H. Yang, and James Mallet. Sex-Linked Hybrid Sterility in a Butterfly. *Evolution*, 55(8):1631–1638, August 2001.

[78] Russell E. Naisbit, Chris D. Jiggins, Mauricio Linares, Camilo Salazar, and James Mallet. Hybrid Sterility, Haldane's Rule and Speciation in Heliconius cydno and H. melpomene. *Genetics*, 161(4):1517–1526, August 2002.

[79] Richard M. Merrill, Audrey Chia, and Nicola J. Nadeau. Divergent warning patterns contribute to assortative mating between incipient Heliconius species. *Ecology and Evolution*, 4(7):911–917, 2014.

[80] Richard M. Merrill, Bas Van Schooten, Janet A. Scott, and Chris D. Jiggins. Pervasive genetic associations between traits causing reproductive isolation in Heliconius butterflies. *Proceedings of the Royal Society B: Biological Sciences*, 278(1705):511–518, February 2011.

[81] Richard M. Merrill, Pasi Rastas, Simon H. Martin, Maria C. Melo, Sarah Barker, John Davey, W. Owen McMillan, and Chris D. Jiggins. Genetic dissection of assortative mating behavior. *PLOS Biology*, 17(2):e2005902, February 2019.

[82] Bart Boerjan, Julie Tobback, Arnold De Loof, Liliane Schoofs, and Roger Huybrechts. Fruitless RNAi knockdown in males interferes with copulation success in Schistocerca gregaria. *Insect Biochemistry and Molecular Biology*, 41(5):340–347, May 2011.

[83] Barry J. Dickson. Wired for Sex: The Neurobiology of Drosophila Mating Decisions. *Science*, 322(5903):904–909, November 2008.

[84] Erica L. Westerman, Nicholas W. VanKuren, Darli Massardo, Aye Tenger-Trolander, Wei Zhang, Ryan I. Hill, Michael Perry, Erick Bayala, Kenneth Barr, Nicola Chamberlain, Tracy E. Douglas, Nathan Buerkle, Stephanie E. Palmer, and Marcus R. Kronforst. Aristaless Controls Butterfly Wing Color Variation Used in Mimicry and Mate Choice. *Current Biology*, 28(21):3469–3474.e4, November 2018.

[85] M. R. Kronforst, L. G. Young, and L. E. Gilbert. Reinforcement of mate preference among hybridizing Heliconius butterflies. *Journal of Evolutionary Biology*, 20(1):278–285, January 2007.

[86] Riitta Nolo, Lois A Abbott, and Hugo J Bellen. Senseless, a Zn Finger Transcription Factor, Is Necessary and Sufficient for Sensory Organ Development in Drosophila. *Cell*, 102(3):349–362, August 2000.

[87] Benjamin J. Frankfort, Riitta Nolo, Zhihuan Zhang, Hugo Bellen, and Graeme Mardon. senseless Repression of rough Is Required for R8 Photoreceptor Differentiation in the Developing Drosophila Eye. *Neuron*, 32(3):403–414, November 2001.

[88] Baotong Xie, Mark Charlton-Perkins, Elizabeth McDonald, Brian Gebelein, and Tiffany Cook. Senseless functions as a molecular switch for color photoreceptor differentiation in Drosophila. *Development*, 134(23):4243–4253, December 2007.

[89] Liesbeth Zwarts, Lies Vanden Broeck, Elisa Cappuyns, Julien F. Ayroles, Michael M. Magwire, Veerle Vulsteke, Jason Clements, Trudy F. C. Mackay, and Patrick Callaerts. The genetic basis of natural variation in mushroom body size in Drosophila melanogaster. *Nature Communications*, 6(1):1–11, December 2015.

[90] Adriana D. Briscoe. Reconstructing the ancestral butterfly eye: focus on the opsins. *Journal of Experimental Biology*, 211(11):1805–1813, June 2008.

[91] Michael F. Land. Variations in the Structure and Design of Compound Eyes. In Doekele Gerben Stavenga and Roger Clayton Hardie, editors, *Facets of Vision*, pages 90–111. Springer Berlin Heidelberg, 1989.

[92] Yuichi Takeuchi, Kentaro Arikawa, and Michiyo Kinoshita. Color discrimination at the spatial resolution limit in a swallowtail butterfly, Papilio xuthus. *Journal of Experimental Biology*, 209(15):2873–2879, August 2006.

[93] Brett M Seymoure, W Owen Mcmillan, and Ronald Rutowski. Peripheral eye dimensions in Longwing (Heliconius) butteries vary with body size and sex but not light environment nor mimicry ring. *The Journal of Research on the Lepidoptera*, 48:10, 2015.

[94] D.-E. Nilsson, M. F. Land, and J. Howard. Afocal apposition optics in butterfly eyes. *Nature*, 312(5994):561–563, December 1984.

[95] Dan-Eric Nilsson. Optics and Evolution of the Compound Eye. In Dr Doekele Gerben Stavenga and Dr Roger Clayton Hardie, editors, *Facets of Vision*, pages 30–73. Springer Berlin Heidelberg, January 1989.

[96] Michael F. Land. Visual Acuity in Insects. *Annual Review of Entomology*, 42(1):147–177, 1997.

[97] Willi A. Ribi. Structural Differences in the Tracheal Tapetum of Diurnal Butterflies. *Zeitschrift fr Naturforschung C*, 34(3-4):284–287, 1979.

[98] Gordon L. Fain, Roger Hardie, and Simon B. Laughlin. Phototransduction and the Evolution of Photoreceptors. *Current Biology*, 20(3):R114–R124, September 2010.

[99] R. C. Hardie. Is histamine a neurotransmitter in insect photoreceptors? *Journal of Comparative Physiology A*, 161(2):201–213, March 1987.

[100] Markus Friedrich, Emily J. Wood, and Meng Wu. Developmental evolution of the insect retina: insights from standardized numbering of homologous photoreceptors. *Journal of Experimental Zoology Part B: Molecular and Developmental Evolution*, 316B(7):484–499, November 2011.

[101] Ivo Sauman, Adriana D. Briscoe, Haisun Zhu, Dingding Shi, Oren Froy, Julia Stalleicken, Quan Yuan, Amy Casselman, and Steven M. Reppert. Connecting the Navigational Clock to Sun Compass Input in Monarch Butterfly Brain. *Neuron*, 46(3):457–467, May 2005.

[102] Doekele G. Stavenga and Kentaro Arikawa. Evolution of color and vision of butterflies. *Arthropod Structure & Development*, 35(4):307–318, December 2006.

[103] Shin-Ya Takemura and Kentaro Arikawa. Ommatidial type-specific interphotoreceptor connections in the lamina of the swallowtail butterfly, Papilio xuthus. *The Journal of Comparative Neurology*, 494(4):663–672, February 2006.

[104] Shin-Ya Takemura, Michiyo Kinoshita, and Kentaro Arikawa. Photoreceptor projection reveals heterogeneity of lamina cartridges in the visual system of the Japanese yellow swallowtail butterfly, Papilio xuthus. *The Journal of Comparative Neurology*, 483(3):341–350, March 2005.

[105] Michael Perry, Michiyo Kinoshita, Giuseppe Saldi, Lucy Huo, Kentaro Arikawa, and Claude Desplan. Molecular logic behind the three-way stochastic choices that expand butterfly colour vision. *Nature*, 535(7611):280–284, July 2016.

[106] Doekele G. Stavenga. Reflections on colourful ommatidia of butterfly eyes. *Journal of Experimental Biology*, 205(8):1077–1085, April 2002.

[107] Mathias F. Wernet, Michael W. Perry, and Claude Desplan. The evolutionary diversity of insect retinal mosaics: common design principles and emerging molecular logic. *Trends in Genetics*, 31(6):316–328, June 2015.

[108] Yoshitaka Hamanaka, Michiyo Kinoshita, Uwe Homberg, and Kentaro Arikawa. Immunocytochemical Localization of Amines and GABA in the Optic Lobe of the Butterfly, Papilio xuthus. *PLoS ONE*, 7(7):e41109, July 2012.

[109] Yoshitaka Hamanaka, Hiromichi Shibasaki, Michiyo Kinoshita, and Kentaro Arikawa. Neurons innervating the lamina in the butterfly, Papilio xuthus. *Journal of Comparative Physiology A*, 199(5):341–351, May 2013.

[110] H. Langer and G. Struwe. Spectral absorption by screening pigment granules in the compound eye of butterflies (Heliconius). *Journal of comparative physiology*, 79(2):203–212, June 1972.

[111] K. Arikawa, S. Mizuno, D. G. W. Scholten, M. Kinoshita, T. Seki, J. Kitamoto, and D. G. Stavenga. An ultraviolet absorbing pigment causes a narrow-band violet receptor and a single-peaked green receptor in the eye of the butterfly Papilio. *Vision Research*, 39(1):1–8, January 1999.

[112] Kentaro Arikawa, Dick G. W. Scholten, Michiyo Kinoshita, and Doekele G. Stavenga. Tuning of Photoreceptor Spectral Sensitivities by Red and Yellow Pigments in the Butterfly Papilio xuthus. *Zoological Science*, 16(1):17–24, February 1999.

[113] Kentaro Arikawa, Primoz Pirih, and Doekele G. Stavenga. Rhabdom constriction enhances filtering by the red screening pigment in the eye of the Eastern Pale Clouded yellow butterfly, Colias erate (Pieridae). *Journal of Experimental Biology*, 212(13):2057–2064, July 2009.

[114] D. Stavenga, M. Kinoshita, E.-C. Yang, and K. Arikawa. Retinal regionalization and heterogeneity of butterfly eyes. *Naturwissenschaften*, 88(11):477–481, October 2001.

[115] Guillermo Zaccardi, Almut Kelber, Marilou P. Sison-Mangus, and Adriana D. Briscoe. Color discrimination in the red range with only one long-wavelength sensitive opsin. *Journal of Experimental Biology*, 209(10):1944–1955, May 2006.

[116] Douglas Blackiston, Adriana D. Briscoe, and Martha R. Weiss. Color vision and learning in the monarch butterfly, Danaus plexippus (Nymphalidae). *Journal of Experimental Biology*, 214(3):509–520, February 2011.

[117] K. Arikawa. Spectral organization of the eye of a butterfly, Papilio. *Journal of Comparative Physiology A*, 189(11):791–800, November 2003.

[118] Primo Pirih, Kentaro Arikawa, and Doekele G. Stavenga. An expanded set of photoreceptors in the Eastern Pale Clouded Yellow butterfly, Colias erate. *Journal of Comparative Physiology A*, 196(7):501–517, June 2010.

[119] Pei-Ju Chen, Hiroko Awata, Atsuko Matsushita, En-Cheng Yang, and Kentaro Arikawa. Extreme Spectral Richness in the Eye of the Common Bluebottle Butterfly, Graphium sarpedon. *Behavioral and Evolutionary Ecology*, page 18, 2016.

[120] Pei-Ju Chen, Kentaro Arikawa, and En-Cheng Yang. Diversity of the Photoreceptors and Spectral Opponency in the Compound Eye of the Golden Birdwing, Troides aeacus formosanus. *PLoS ONE*, 8(4):e62240, April 2013.

[121] Kentaro Arikawa. The eyes and vision of butterflies. *The Journal of Physiology*, 595(16):5457–5464, 2017.

[122] Francesca D. Frentiu, Gary D. Bernard, Marilou P. Sison-Mangus, Andrew Van Zandt Brower, and Adriana D. Briscoe. Gene Duplication Is an Evolutionary Mechanism for Expanding Spectral Diversity in the Long-Wavelength Photopigments of Butterflies. *Molecular Biology and Evolution*, 24(9):2016–2028, September 2007.

[123] Marilou P. Sison-Mangus, Gary D. Bernard, Jochen Lampel, and Adriana D. Briscoe. Beauty in the eye of the beholder: the two blue opsins of lycaenid butterflies and the opsin gene-driven evolution of sexually dimorphic eyes. *The Journal of Experimental Biology*, 209(16):3079–3090, August 2006.

[124] Hiroko Awata, Motohiro Wakakuwa, and Kentaro Arikawa. Evolution of color vision in pierid butterflies: blue opsin duplication, ommatidial heterogeneity and eye regionalization in Colias erate. *Journal of Comparative Physiology A*, 195(4):401–408, April 2009.

[125] Adriana D. Briscoe, Seth M. Bybee, Gary D. Bernard, Furong Yuan, Marilou P. Sison-Mangus, Robert D. Reed, Andrew D. Warren, Jorge Llorente-Bousquets, and Chuan-Chin Chiao. Positive selection of a duplicated UV-sensitive visual pigment coincides with wing pigment evolution in Heliconius butterflies. *Proceedings of the National Academy of Sciences*, 107(8):3628–3633, February 2010.

[126] Kyle J. McCulloch, Daniel Osorio, and Adriana D. Briscoe. Sexual dimorphism in the compound eye of Heliconius erato: a nymphalid butterfly with at least five spectral classes of photoreceptor. *Journal of Experimental Biology*, page jeb.136523, May 2016.

[127] Kyle J. McCulloch, Furong Yuan, Ying Zhen, Matthew L. Aardema, Gilbert Smith, Jorge Llorente-Bousquets, Peter Andolfatto, and Adriana D. Briscoe. Sexual Dimorphism and Retinal Mosaic Diversification following the Evolution of a Violet Receptor in Butterflies. *Molecular Biology and Evolution*, 34(9):2271–2284, September 2017.

[128] Seth M. Bybee, Furong Yuan, Monica D. Ramstetter, Jorge Llorente-Bousquets, Robert D. Reed, Daniel Osorio, and Adriana D. Briscoe. UV Photoreceptors and UV-Yellow Wing Pigments in Heliconius Butterflies Allow a Color Signal to Serve both Mimicry and Intraspecific Communication. *The American Naturalist*, 179(1):38–51, January 2012.

[129] Kyle J. McCulloch, Daniel Osorio, and Adriana D. Briscoe. Determination of Photoreceptor Cell Spectral Sensitivity in an Insect Model from In Vivo Intracellular Recordings. *JoVE (Journal of Visualized Experiments)*, 108:e53829, February 2016.

[130] Doekele G. Stavenga. On visual pigment templates and the spectral shape of invertebrate rhodopsins and metarhodopsins. *Journal of Comparative Physiology A*, 196(11):869–878, November 2010.

[131] Victor I. Govardovskii, Nanna Fyhrquist, Tom Reuter, Dmitry G. Kuzmin, and Kristian Donner. In search of the visual pigment template. *Visual Neuroscience*, 17(4):509–528, July 2000.

[132] Witold Filipowicz, Suvendra N. Bhattacharyya, and Nahum Sonenberg. Mechanisms of post-transcriptional regulation by microRNAs: are the answers in sight? *Nature Reviews Genetics*, 9(2):102–114, February 2008.

[133] Kentaro Arikawa, Shin Mizuno, Michiyo Kinoshita, and Doekele G. Stavenga. Coexpression of Two Visual Pigments in a Photoreceptor Causes an Abnormally Broad Spectral Sensitivity in the Eye of the Butterfly Papilio xuthus. *The Journal of Neuroscience*, 23(11):4527–4532, June 2003.

[134] Caitlin Anderson, India Reiss, Cyrus Zhou, Annie Cho, Haziq Siddiqi, Benjamin Mormann, Cameron M Avelis, Peter Deford, Alan Bergland, Elijah Roberts, James Taylor, Daniel Vasiliauskas, and Robert J Johnston. Natural variation in stochastic photoreceptor specification and color preference in Drosophila. *eLife*, 6:e29593, December 2017.

[135] Natasha I. Bloch. Evolution of opsin expression in birds driven by sexual selection and habitat. *Proceedings of the Royal Society B: Biological Sciences*, 282(1798):20142321, January 2015.

[136] Nathan S. Hart. Variations in cone photoreceptor abundance and the visual ecology of birds. *Journal of Comparative Physiology A*, 187(9):685–697, November 2001.

[137] Xudong Qiu, Kurt A.J. Vanhoutte, Doekele G. Stavenga, and Kentaro Arikawa. Ommatidial heterogeneity in the compound eye of the male small white butterfly, Pieris rapae crucivora. *Cell and Tissue Research*, 307(3):371–379, March 2002.

[138] Kentaro Arikawa, Motohiro Wakakuwa, Xudong Qiu, Masumi Kurasawa, and Doekele G. Stavenga. Sexual Dimorphism of Short-Wavelength Photoreceptors in the Small White Butterfly, Pieris rapae crucivora. *The Journal of Neuroscience*, 25(25):5935–5942, June 2005.

[139] Roger C. Hardie and Padinjat Raghu. Visual transduction in Drosophila. *Nature*, 413(6852):186–193, September 2001.

[140] Pei-Ju Chen, Atsuko Matsushita, Motohiro Wakakuwa, and Kentaro Arikawa. Immunolocalization suggests a role of the histamine-gated chloride channel PxHCLB in spectral opponent processing in butterfly photoreceptors. *Journal of Comparative Neurology*, 527(4):753–766, March 2019.

[141] Yuri Ogawa, Hiroko Awata, Motohiro Wakakuwa, Michiyo Kinoshita, Doekele G. Stavenga, and Kentaro Arikawa. Coexpression of three middle wavelength-absorbing visual pigments in sexually dimorphic photoreceptors of the butterfly Colias erate. *Journal of Comparative Physiology A*, 198(12):857–867, December 2012.

[142] Susan D. Finkbeiner, Dmitry A. Fishman, Daniel Osorio, and Adriana D. Briscoe. Ultraviolet and yellow reflectance but not fluorescence is important for visual discrimination of conspecifics by Heliconius erato. *Journal of Experimental Biology*, 220(7):1267–1276, April 2017.

[143] Allan W. Snyder, Randolf Menzel, and Simon B. Laughlin. Structure and function of the fused rhabdom. *Journal of comparative physiology*, 87(2):99–135, June 1973.

[144] B. Minke and K. Kirschfeld. The contribution of a sensitizing pigment to the photosensitivity spectra of fly rhodopsin and metarhodopsin. *The Journal of General Physiology*, 73(5):517–540, May 1979.

[145] K. Vogt and K. Kirschfeld. Sensitizing pigment in the fly. *Biophysics of structure and mechanism*, 9(4):319–328, December 1983.

[146] G. A. Horridge, L. Marelja, R. Jahnke, and T. Mati. Single electrode studies on the retina of the butterflyPapilio. *Journal of Comparative Physiology A*, 150(3):271–294, September 1983.

[147] S. H. Montgomery and R. M. Merrill. Divergence in brain composition during the early stages of ecological specialization in Heliconius butterflies. *Journal of Evolutionary Biology*, 30(3):571–582, 2017.

[148] Stephen H. Montgomery, Richard M. Merrill, and Swidbert R. Ott. Brain composition in Heliconius butterflies, posteclosion growth and experience-dependent neuropil plasticity. *Journal of Comparative Neurology*, 524(9):1747–1769, 2016.

[149] Daisuke Yamamoto, Kosei Sato, and Masayuki Koganezawa. Neuroethology of male courtship in Drosophila: from the gene to behavior. *Journal of Comparative Physiology A*, 200(4):251–264, February 2014.

[150] Johannes Schindelin, Ignacio Arganda-Carreras, Erwin Frise, Verena Kaynig, Mark Longair, Tobias Pietzsch, Stephan Preibisch, Curtis Rueden, Stephan Saalfeld, Benjamin Schmid, Jean-Yves Tinevez, Daniel James White, Volker Hartenstein, Kevin Eliceiri, Pavel Tomancak, and Albert Cardona. Fiji: an open-source platform for biological-image analysis. *Nature Methods*, 9(7):676–682, July 2012.

[151] Chrisantha Thomas Fernando, Eors Szathmary, and Phil Husbands. Selectionist and Evolutionary Approaches to Brain Function: A Critical Appraisal. *Frontiers in Computational Neuroscience*, 6, 2012.

[152] Walter Helligenberg and Gary Rose. Neural correlates of the jamming avoidance response (JAR) in the weakly electric fish Eigenmannia. *Trends in Neurosciences*, 8:442–449, 1985.

[153] Adriana D Briscoe and Lars Chittka. The evolution of color vision in insects. *Annual review of entomology*, 46(1):471–510, 2001.

[154] Hisaharu Koshitaka, Michiyo Kinoshita, Misha Vorobyev, and Kentaro Arikawa. Tetrachromacy in a butterfly that has eight varieties of spectral receptors. *Proceedings of the Royal Society B: Biological Sciences*, 275(1637):947–954, April 2008.

[155] Adriana D. Briscoe. Homology Modeling Suggests a Functional Role for Parallel Amino Acid Substitutions Between Bee and Butterfly Red- and Green-Sensitive Opsins. *Molecular Biology and Evolution*, 19(6):983–986, June 2002.

[156] B. B. Lee, P. R. Martin, and A. Valberg. Sensitivity of macaque retinal ganglion cells to chromatic and luminance flicker. *The Journal of Physiology*, 414(1):223–243, 1989.

[157] Angelique C. Paulk, Andrew M. Dacks, and Wulfila Gronenberg. Color processing in the medulla of the bumblebee (Apidae: Bombus impatiens). *The Journal of Comparative Neurology*, 513(5):441–456, April 2009.

[158] M. Vorobyev and D. Osorio. Receptor noise as a determinant of colour thresholds. *Proceedings of the Royal Society of London B: Biological Sciences*, 265(1394):351–358, March 1998.

[159] Lars Chittka. The colour hexagon: a chromaticity diagram based on photoreceptor excitations as a generalized representation of colour opponency. *Journal of Comparative Physiology A*, 170(5):533–543, June 1992.

[160] Leo M Hurvich and Dorothea Jameson. An opponent-process theory of color vision. *Psychological Review*, 64(6), 1957.

[161] Adrian G. Dyer, Angelique C. Paulk, and David H. Reser. Colour processing in complex environments: insights from the visual system of bees. *Proceedings of the Royal Society B: Biological Sciences*, page rspb20102412, December 2010.

[162] Vera Vasas, Fei Peng, HaDi MaBouDi, and Lars Chittka. Randomly weighted receptor inputs can explain the large diversity of colour-coding neurons in the bee visual system. *Scientific Reports*, 9(1):8330, December 2019.

[163] Akira Sakurai, JamesM. Newcomb, JoshuaL. Lillvis, and PaulS. Katz. Different Roles for Homologous Interneurons in Species Exhibiting Similar Rhythmic Behaviors. *Current Biology*, 21(12):1036–1043, June 2011.

[164] J. Kien and R. Menzel. Chromatic properties of interneurons in the optic lobes of the bee. *Journal of comparative physiology*, 113(1):17–34, January 1977.

[165] S. L Swihart. The neural basis of colour vision in the butterfly, Heliconius erato. *Journal of Insect Physiology*, 18(5):1015–1025, May 1972.

[166] S. Zeki. The representation of colours in the cerebral cortex. *Nature*, 284(5755):412–418, April 1980.

[167] S. J. Schein and R. Desimone. Spectral properties of V4 neurons in the macaque. *Journal of Neuroscience*, 10(10):3369–3389, October 1990.

[168] Francismeire J. Telles, Almut Kelber, and Miguel A. Rodrguez-Girons. Wavelength discrimination in the hummingbird hawkmoth Macroglossum stellatarum. *Journal of Experimental Biology*, 219(4):553–560, February 2016.

[169] Yoshua Bengio, Jrme Louradour, Ronan Collobert, and Jason Weston. Curriculum Learning. In *Proceedings of the 26th Annual International Conference on Machine Learning*, ICML '09, pages 41–48, New York, NY, USA, 2009. ACM.

[170] Dorothea Jameson and Leo M. Hurvich. Some Quantitative Aspects of an Opponent-Colors Theory I Chromatic Responses and Spectral Saturation. *Journal of the Optical Society of America*, 45(7):546, July 1955.

[171] Massimo Pigliucci. Do We Need an Extended Evolutionary Synthesis? *Evolution*, 61(12):2743–2749, 2007.

[172] Patricia R. Jusuf, Paul R. Martin, and Ulrike Grnert. Random Wiring in the Midget Pathway of Primate Retina. *Journal of Neuroscience*, 26(15):3908–3917, April 2006.

[173] Lauren E. Wool, Joanna D. Crook, John B. Troy, Orin S. Packer, Qasim Zaidi, and Dennis M. Dacey. Nonselective Wiring Accounts for Red-Green Opponency in Midget Ganglion Cells of the Primate Retina. *Journal of Neuroscience*, 38(6):1520–1540, February 2018.

[174] Gerald H. Jacobs. Within-species variations in visual capacity among squirrel monkeys (Saimiri Sciureus): Color vision. *Vision Research*, 24(10):1267–1277, 1984.

[175] Gerald H. Jacobs, Gary A. Williams, Hugh Cahill, and Jeremy Nathans. Emergence of Novel Color Vision in Mice Engineered to Express a Human Cone Photopigment. *Science*, 315(5819):1723–1725, March 2007.

[176] Walter Makous. Comment on "Emergence of Novel Color Vision in Mice Engineered to Express a Human Cone Photopigment". *Science*, 318(5848):196–196, October 2007.

[177] P. Robin Hiesinger, R. Grace Zhai, Yi Zhou, Tong-Wey Koh, Sunil Q. Mehta, Karen L. Schulze, Yu Cao, Patrik Verstreken, Thomas R. Clandinin, Karl-Friedrich Fischbach, Ian A. Meinertzhagen, and Hugo J. Bellen. Activity-Independent Prespecification of Synaptic Partners in the Visual Map of Drosophila. *Current Biology*, 16(18):1835–1843, September 2006.

[178] Anna Brochtrup and Thomas Hummel. Olfactory map formation in the Drosophila brain: genetic specificity and neuronal variability. *Current Opinion in Neurobiology*, 21(1):85–92, February 2011.

[179] Mattias C. Larsson, Ana I. Domingos, Walton D. Jones, M. Eugenia Chiappe, Hubert Amrein, and Leslie B. Vosshall. Or83b Encodes a Broadly Expressed Odorant Receptor Essential for Drosophila Olfaction. *Neuron*, 43(5):703–714, September 2004.

[180] Randall M. Golovin, Jacob Vest, Dominic J. Vita, and Kendal Broadie. Activity-Dependent Remodeling of Drosophila Olfactory Sensory Neuron Brain Innervation during an Early-Life Critical Period. *Journal of Neuroscience*, 39(16):2995–3012, April 2019.

[181] Takuya Kaneko, Ann Marie Macara, Ruonan Li, Yujia Hu, Kenichi Iwasaki, Zane Dunnings, Ethan Firestone, Shawn Horvatic, Ananya Guntur, Orie T. Shafer, Chung-Hui Yang, Jie Zhou, and Bing Ye. Serotonergic Modulation Enables Pathway-Specific Plasticity in a Developing Sensory Circuit in Drosophila. *Neuron*, 95(3):623–638.e4, August 2017.

[182] Fernando Vonhoff and Haig Keshishian. Activity-Dependent Synaptic Refinement: New Insights from Drosophila. *Frontiers in Systems Neuroscience*, 11, 2017.

[183] Martin Barth, Helmut V. B. Hirsch, Ian A. Meinertzhagen, and Martin Heisenberg. Experience-Dependent Developmental Plasticity in the Optic Lobe of Drosophila melanogaster. *Journal of Neuroscience*, 17(4):1493–1504, February 1997.

[184] Jean-Marc Devaud, Angel Acebes, and Alberto Ferrs. Odor Exposure Causes Central Adaptation and Morphological Changes in Selected Olfactory Glomeruli in Drosophila. *Journal of Neuroscience*, 21(16):6274–6282, August 2001.

[185] B. F. Skinner. The Shaping of Phylogenic Behavior. *Journal of the Experimental Analysis of Behavior*, 24(1):117–120, 1975.

[186] Kai A. Krueger and Peter Dayan. Flexible shaping: How learning in small steps helps. *Cognition*, 110(3):380–394, March 2009.

[187] Lars Chittka. Optimal Sets of Color Receptors and Color Opponent Systems for Coding of Natural Objects in Insect Vision. *Journal of Theoretical Biology*, 181(2):179–196, July 1996.

[188] Michiyo Kinoshita, Miki Shimohigasshi, Yoshiya Tominaga, Kentaro Arikawa, and Uwe Homberg. Topographically distinct visual and olfactory inputs to the mushroom body in the Swallowtail butterfly, Papilio xuthus. *Journal of Comparative Neurology*, 523(1):162–182, January 2015.

[189] Lars Chittka, Willy Beier, Horst Hertel, Erwin Steinmann, and Randolf Menzel. Opponent colour coding is a universal strategy to evaluate the photoreceptor inputs in Hymenoptera. *Journal of Comparative Physiology A*, 170(5):545–563, June 1992.

[190] Paul S. Katz and Melina E. Hale. Evolution of Motor Systems. In Scott L. Hooper and Ansgar Bschges, editors, *Neurobiology of Motor Control*, pages 135–176. John Wiley & Sons, Inc., Hoboken, NJ, USA, June 2017.